OBSERVATION AND ANALYSIS ON THE CHARACTERISTICS

OF STRAIN INDUCED BY FROST HEAVE FOR

A FULL-SCALE BURIED, CHILLED GAS PIPELINE

by

Kun Yang

RECOMMENDED:

Dr. Gang Chen

Dr. Margaret M. Darrow

Dr. Scott Huang, Advisory Committee Chair

Dr. Rajive Ganguli
Chair, Department of Mining and Geological Engineering

APPROVED:

Dr. Douglas J. Goering
Dean, College of Engineering and Mines

Dr. John C. Eichelberger
Dean of the Graduate School

11/28/13

Date

OBSERVATION AND ANALYSIS ON THE CHARACTERISTICS OF STRAIN INDUCED BY FROST HEAVE FOR A FULL-SCALE BURIED, CHILLED GAS PIPELINE

A

THESIS

Presented to the Faculty

of the University of Alaska Fairbanks

in Partial Fulfillment of the Requirements

for the Degree of

MASTER OF SCIENCE

By

Kun Yang, B.S.

Fairbanks, Alaska

December 2013

Abstract

This thesis examines the strain characteristics of a large-scale, buried chilled gas pipeline in the discontinuous permafrost region. A full-scale chilled pipeline gas experiment was conducted in Fairbanks, Alaska. The test pipeline had a length of 105 m and a diameter of 0.9 m. One-third of the pipeline was located in permafrost and the rest was in non-permafrost. The monitoring data were collected from December 1999 to January 2005 including both freezing and thawing phases. In the transition zone between frozen and unfrozen soil, the foundation experienced a vertical movement caused by differential frost heave. The test results indicated that the bending action was the main factor for the pipeline for the circumferential and longitudinal strain distribution of the pipeline. Moreover, linear relationships were developed between frost heave and the longitudinal strain at the top and the bottom (i.e., 0^o and 180^o) of the pipe. The developed equations can be used to predict the strain of the pipe caused by differential frost heave for future tests with similar site conditions.

Table of Contents

List of Figures

List of Tables

Page

Acknowledgements

I would like to express my sincere gratitude to my advisor, Professor Scott L. Huang, for his indispensable guidance and continued support, for his reviewing of the thesis, and for providing the experimental data of the chilled gas pipeline in Fairbanks, Alaska.

I would like to extend my thanks to Professor Gang Chen and Professor Margaret M. Darrow for their useful suggestions and comments throughout the course of the study. My thanks also go to Dr. Satoshi Akagawa, who gave me valuable help on the data of the steel pipeline.

In addition, I would like to thank the Department of Mining and Geological Engineering for providing financial support during my study.

Finally, I would like to express my gratitude to my parents for their constant encouragement, support, and assistance.

CHAPTER 1. INTRODUCTION

1.1 Overview

According to the data provided by the State of Alaska's Division of Geological & Geophysical Surveys in 1974 (Klein et al., 1974), the total discovered recoverable gas in Alaska is 31 trillion cubic feet. Of that, the Prudhoe Bay Field contains 26 trillion cubic feet, which is more than the entire annual consumption of the United States. It is, therefore, of great importance to develop this significant natural gas resource and transport it to market.

Compared to other modes of transportation like truck or ship, pipelines have a variety of advantages. For example, pipelines have a lower shipping cost with higher capacity than most other methods. They have a long and continuous service life. With these advantages, a pipeline is a favored mode of natural gas transport. Transporting natural gas from Alaska to the lower 48 states, however, will have its unique challenges. Figure 1.1 shows the permafrost map of Alaska. It can be seen that a pipeline will encounter occurrence of continuous and discontinuous permafrost transporting natural gas from northern energy fields to market. There are some important concerns for design, construction, and operation of gas pipelines in cold regions, which will be detailed below.

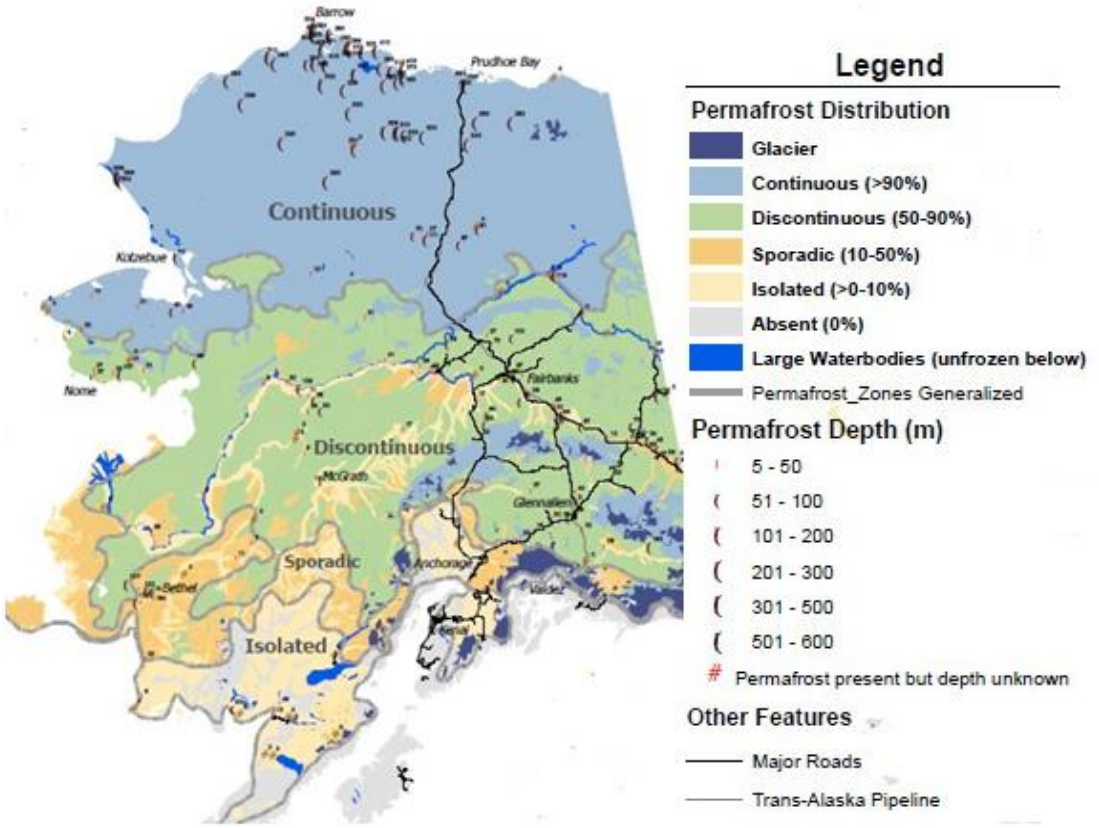

Figure 1.1 Permafrost Map of Alaska (Jorgenson et al., 2008)

Generally speaking, there are mainly two types of pipelines used in arctic regions, namely warm and chilled pipelines. When the temperature of the gas in the pipeline is higher than the surrounding ground (i.e., warm pipeline), ice-rich permafrost will be subject to thaw settlement (see Figure 1.2). A chilled pipeline with gas temperatures below 0^{o}C, on the other hand, will prevent the ground subsidence in ice-rich permafrost terrain, but the neighboring unfrozen soil will become frozen, since the gas temperature is lower than the soil. The chilled pipeline may suffer damage due to frost heave in the surrounding soil. The problem will be even more severe at the transition zone between two types of soil with different frost heave susceptibilities (see Figure 1.3). One of the significant concerns happens when there are spatial differences in frost heave along the

pipeline route. This will result in large deformation of the pipe virtually throughout the whole operation life of several decades.

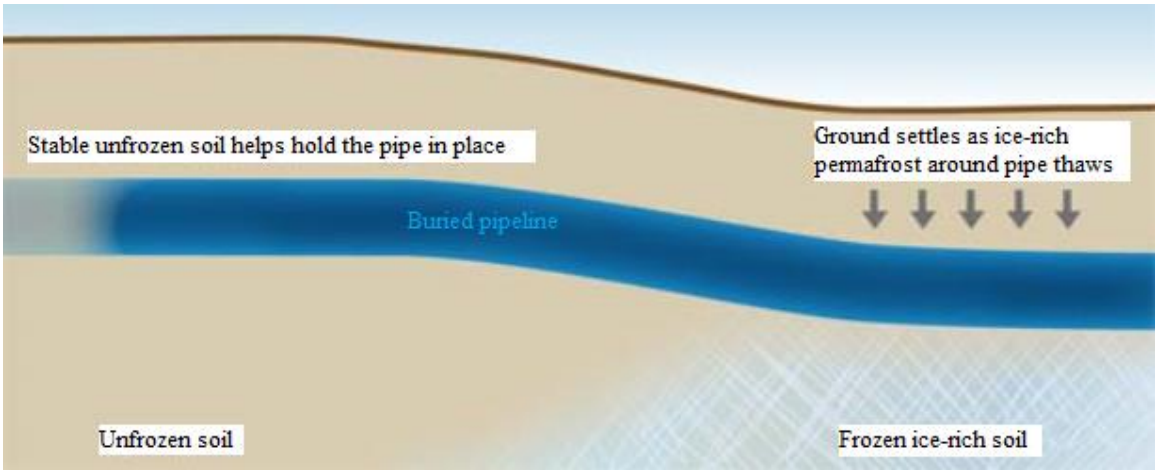

Figure 1.2 Settlement due to Thawing of Ice-rich Permafrost
(National Energy Board, 2011)

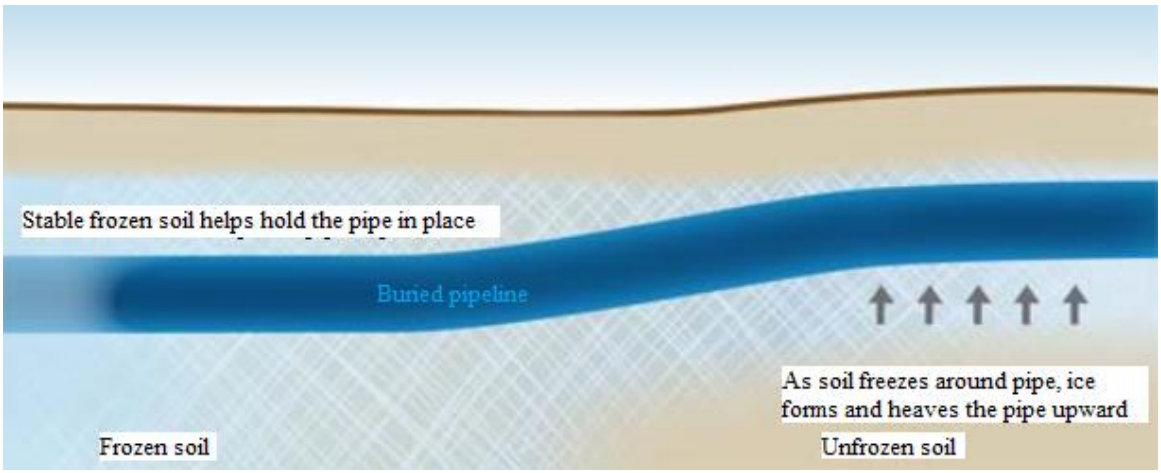

Figure 1.3 Frost Heave due to Freezing of Surrounding Soil
(National Energy Board, 2011)

1.2 Objective of the research

This research studies a full-scale experiment dealing with a large-diameter steel pipeline located at a boundary between permafrost and non-permafrost near Fairbanks, Alaska.

According to Huang et al. (2004), the experiment of the pipeline system was conducted to evaluate the pipeline characteristics caused by differential frost heave and the induced pipe strain. In December 1999, a buried gas pipeline, 105-m long with a 0.9 m diameter and 8.5 mm wall thickness was constructed. The test facility was located at 3.8 km along Chena Hot Springs Road, Fairbanks, Alaska (Huang et al., 2004). During the freezing phase, the initial temperature of chilled air was set at -10^{o}C, and the chilled air system was stopped at the end of July 2003, but the monitoring system continued until the end of May 2005. Table 1.1 summarizes the pipe specifications for the experiment.

Table 1.1 Pipe Specifications for UAF-Hokkaido University Experiment (Akagawa et al., 2012)

Grade		API X-65
Material		Steel
Diameter	cm	91.4
Wall thickness	cm	0.85
Yield stress	kg/cm^2	4920
Tensile strength	kg/cm^2	5760
A (Cross section area of the steel)	cm^2	255.9
I (Geometrical moment of inertia)	cm^4	261994
E (Young's modulus)	kg/cm^3	2100000
Z (Modulus of section)	cm^2	5733

The objective of this thesis is to observe and analyze the strain characteristics of the buried chilled pipeline at the aforementioned test site. The tasks to be achieved are listed below:

(1) Process and classify the strain data set gathered from forty strain gauges welded on the outside surface of the pipe;

(2) Analyze the pipe strain over time resulting from differential frost heave; and

(3) Investigate the relationship between strain and differential frost heave.

1.3 Literature review

The scope of this research is to analyze the strain characteristics of a buried pipeline induced by frost heave. The literature review, therefore, focuses on frost heave, pipeline strain and deformation caused by differential frost heave, as well as the interaction between a buried pipeline and the surrounding soil.

1.3.1 Frost heave mechanism

The mechanism for frost heave has been studied for years by numerous researchers (Taber, 1929; Beskow, 1935; Taylor and Luthin, 1978; O'Neill and Miller, 1982). As indicated by Tsytovich (1975), frost heave is caused by water migration toward the freezing front and accumulation of segregation ice. Generally speaking, frost heave is a complex phenomenon which requires three conditions to occur: freezing temperature, a sufficient water supply, and frost-susceptible soil. Basically, fine-grained soil is more sensitive to frost heave. For example, silt is considered as highly susceptible soil, while sand is not.

1.3.2 Soil-pipeline interaction

Various studies have been carried out in the last century to understand and explain the phenomenon of soil-pipe interaction (Nixon, 1983; Dallimore and Williams, 1984; Konrad and Morgenstern, 1984; Shah, 1990). The basic concepts of soil-pipe interaction are reviewed in the following section.

As indicated by Selvadurai and Shinde (1993), unlike above-ground pipelines, a buried pipeline is strongly affected by the geotechnical nature of the ground. Design and construction of a buried pipeline should take into consideration the interaction between the pipeline and the surrounding soil, which can be induced from the following: (1)

deformation of the pipeline: thermal expansion or contraction of the pipeline due to temperature changes; (2) loading of geotechnical nature: soil consolidation, frost heave, thaw settlement, and ground subsidence; and (3) external loading: road traffic loads, landslides, and earthquake loads.

White (2006) summarized the detailed process and issues dealing with the cold pipeline buried in frost-susceptible soils. When the soil freezes, the volume of water will expand by 9% as it changes to ice. Moreover, free water migrates from unfrozen soil because of a pressure gradient to form ice lenses. At the same time, adhesion of the frozen soil to the pipe and cohesion of the frozen soil mass will anchor the pipe in the freezing ground. Buried chilled pipelines are subjected to stresses imposed by the freezing process wherever spatial differences in frost heave exist. Generally, variations in frost heave depend on differences in the properties of the soil or differences in the thermal transition between frozen and seasonally frozen soil and hydrological conditions (White, 2006).

Shah and Razaqpur (1993) used a two-dimensional frost heave model to analyze the stresses and deformation for buried chilled pipelines. In their study, the finite element method was used to calculate the soil-pipeline interaction process.

Kanie et al. (2010) studied the adfreeze behavior between a chilled gas pipeline and surrounding soil. They presented an axially-symmetric freezing apparatus used to investigate the interactive stress between the frost bulb and the pipe. They also recommended that the pipe flexural properties and the frost bulb should be considered as a composite structure in chilled pipeline designs.

1.3.3 Prior buried chilled pipeline experiments

Several field and lab experiments have been conducted that dealt with chilled pipelines. The Caen-France experiment is summarized and briefly discussed in this section.

As indicated by Dallimore (1985), the Caen-France experiment was conducted on a full-scale chilled pipeline buried in freezing ground. The experiment was a multi-disciplinary test that studied frost heave, pipeline deformation, and induced stresses in the pipeline. For the test facility of the Caen-France experiment, about half of the pipeline was buried in frost-susceptible silt and the rest was buried in non-frost-susceptible sand. The diameter of the pipe was 273 mm with a wall thickness of 5 mm. The Young's modulus of the steel pipeline was 210 GPa, and its yield stress was 230 MPa. Figure 1.4 illustrates that the facility of the Caen-France experiment consisted of an 18-m long, 8-m wide and 5-m high refrigerated hall, which was used to observe the pipeline parameters due to thermal and physical variation.

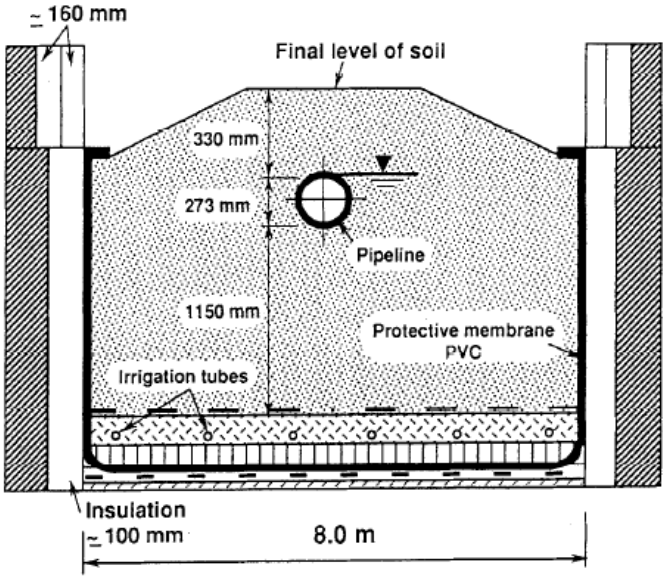

Figure 1.4 Cross Section View of Refrigerated Hall and Pipeline (Dallimore, 1985)

Selvadurai et al. (1999a and 1999b) developed a computational model to examine the pipeline behavior in the Caen-France experiment. They evaluated the interaction between a buried pipeline and surrounding soil affected by differential frost heave. The computational model was coupled with heat conduction and moisture transport within the soil mass. After calculating the one-dimensional, two-dimensional, and three-dimensional

problems and comparing with the lab test, they found that the computational modeling adequately simulated the test.

According to Razaqpur and Wang (1996), the soil-pipe interaction was a time-dependent thermo-mechanical process. The pipeline had the most frost heave-related phenomena that occurred along its length since it suffered damage due to soils of different frost susceptibilities. In this case, they used one-dimensional beam model to simulate the Caen-France pipeline. A computer program was also developed to calculate frost-induced stress within the pipe.

CHAPTER 2. TEST FACILITY OF A FIELD EXPERIMENT

In 2004, Huang et al. published a paper detailing the field experiment conducted jointly by the University of Alaska Fairbanks and Hokkaido University. In the subsequent years, several papers (Kim et al., 2008; Darrow, 2009; Akagawa et al., 2012) were published by the same group of researchers discussing some of the results obtained from the field experiment. This chapter summarizes the discussions from Huang et al. (2004) and Akagawa et al. (2012).

2.1 General layout of the test facility

Huang et al. (2004) and Akagawa et al. (2012) detailed the monitoring parameters and instrumentation plan of the field experiment. As indicated in their papers, the primary goal of the field experiment was to study the frost heave characteristics of the chilled gas pipeline resulting from differential heave across the transition zone between permafrost and non-permafrost soil (i.e., talik) (Huang et al., 2004).

In order to determine the boundary of the non-permafrost and permafrost zones, 26 boreholes were drilled in the test ground. The results showed that about 30% of the pipeline was located in permafrost and 70% in non-permafrost (see Figure 2.1). The observed data of the chilled pipeline was obtained from December 1999 to July 2003. Then circulation of the chilled air was stopped, but the monitoring program continued until May 2005.

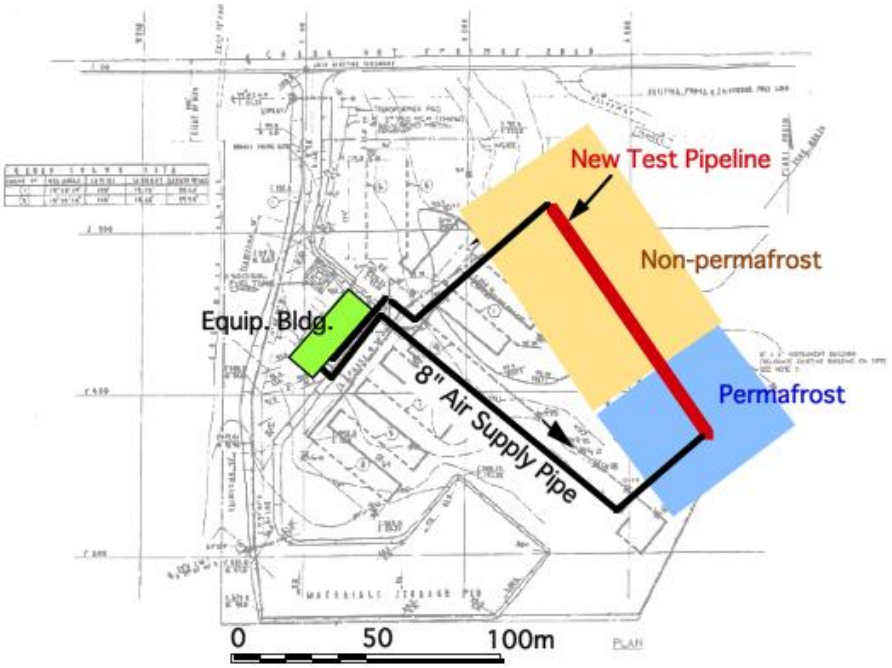

Figure 2.1 General Layout of Test Pipeline (Akagawa et al., 2012)

2.2 Monitoring parameters and instrumentation

As indicated by Huang et al. (2004), the main parameters monitored in the project included air and ground temperatures, strain of pipeline exterior surface, pipeline vertical deformation, and frost heave and thaw settlement of the top 1 meter of soil beneath the pipeline. The total instrumentation included 150 thermistors, 40 strain gauges, 5 heave gauges, 28 heave rods, 8 heave plates, 11 surface settlement points, and 3 water wells.

2.2.1 Air and ground temperatures

The temperatures of the air and ground surrounding the pipeline were obtained by 150 thermistors. One thermistor was installed to monitor the air temperature. The pipeline temperature was measured by 9 thermistors installed on the exterior surface of the pipe. The remaining 140 thermistors were placed on both sides of the pipe to monitor the ground temperature changes. Three thermal fences A, B, and C (i.e., TFA, TFB, and TFC) were installed to monitor changes in the thermal regime of the soil. The locations of

the thermistor strings and the depth of each thermistor are shown in Figure 2.2. From the figure, it can be seen that TFA and TFB were located in the non-permafrost area, and TFC was in the permafrost zone. Moreover, as indicated by Huang et al. (2004), TFA, TFB, and TFC were placed 58 m, 36.5 m, and 13 m from the inlet riser, respectively. TFA consisted of six thermistor strings with thermistors located from 0.14 m to 8.14 m beneath the ground surface. TFB had three thermistor strings, and the thermistors were placed from 0.09 m to 7.76 m beneath the ground surface. There were four thermistor strings for TFC with thermistors at depths ranging from 0.04 m to 7 m.

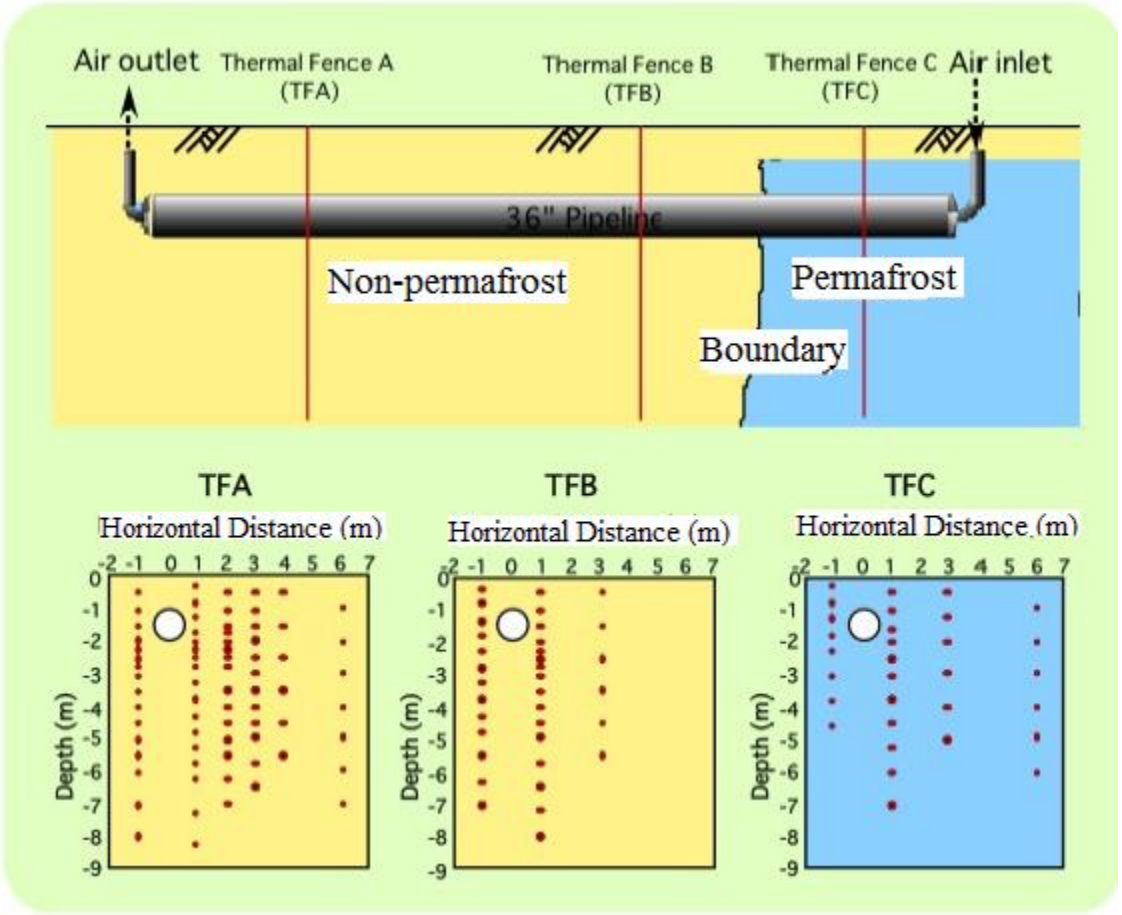

Figure 2.2 Locations and Configurations of the Thermistor Strings (Akagawa et al., 2012)

2.2.2 Pipe strain

The induced strain of the pipeline was an important parameter which needed to be monitored for this project. Forty electric weldable strain gauges (SG) were installed on the exterior surface of the pipe at 11 locations with different orientations. Figure 2.3 shows the locations of the strain gauges. Since the pipeline would bend most in the vicinity of the permafrost-non-permafrost boundary, the majority of the strain gauges were clustered around the transition zone. From the inlet riser, 11 stations were located at 5.32 m, 18.53 m, 22.1 m, 24 m, 26.24 m, 30.68 m, 32.16 m, 33.51 m, 36.8 m, 42.75 m, and 65.52 m. At each station, the strain gauges were welded longitudinally or circumferentially on the outer surface of the pipe to monitor the axial or hoop strain. For the longitudinal direction, there were a total of 32 strain gauges installed at 11 stations at different orientations around the circumference of the pipe (Figure 2.3). For example, the strain gauges were installed longitudinally at 0° (i.e., on the top of the pipe) for all 11 stations. The 180° strain gauges (i.e., at the bottom of the pipe) were welded at all stations except SG-1 and SG-11. The circumferential strain gauges were used to measure the hoop strain of the pipe. Only SG-4 and SG-7 were installed with circumferential strain gauges at 0°, 90°, 180°, and 270°. The orientations were viewed towards the inlet riser, and measured in the clockwise direction.

According to the report written by the engineers at Weir-Jones Engineering Consultants Ltd., the company responsible for installation of the strain gauges (Chong, 1999), the nominal resistance of the strain gauges was 350 ohms, and the gauge factor was 2.09. After all strain gauges were placed at their corresponding locations and the resistance of each gauge verified, a layer of polymer coating and vinyl-backed mastic pads were placed over the gauged surfaces to provide adequate environmental protection. In addition to the forty gauges welded to the pipe, three strain gauges for temperature compensation were also included.

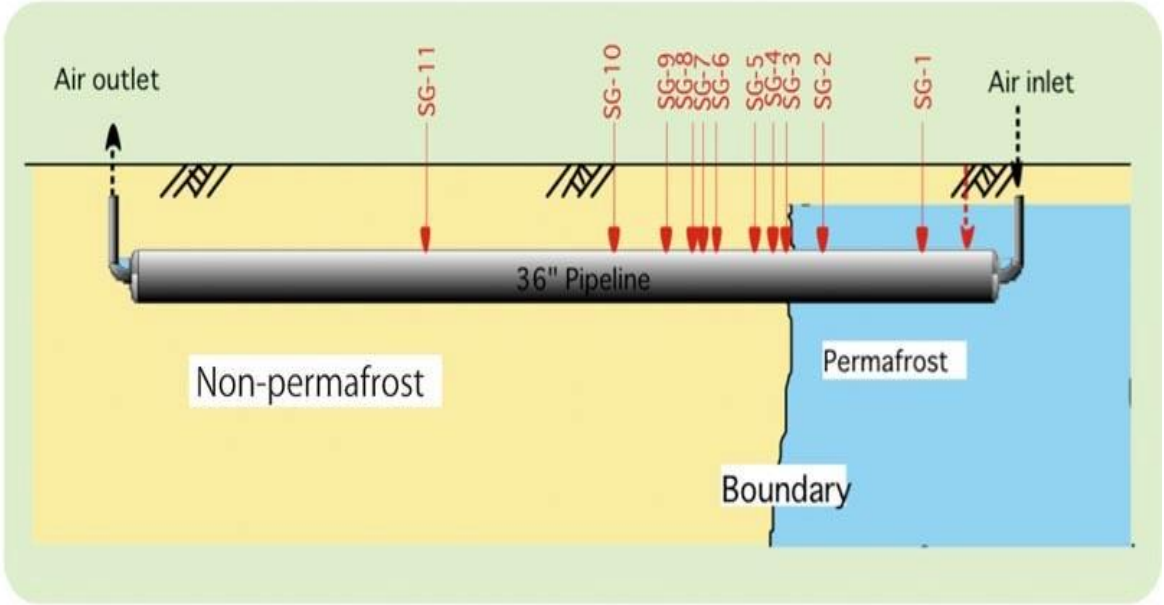

Station (SG)	Distance from inlet riser (m)	Longitudinal	Circumferential
1	5.32	0, 120, 240	--
2	18.53	0, 180	--
3	22.10	0, 90, 180	--
4	24.00	0, 90, 180, 270	0, 90, 180, 270
5	26.24	0, 90, 180	--
6	30.68	0, 90, 180	--
7	32.16	0, 90, 180, 270	0, 90, 180, 270
8	33.51	0, 90, 180	--
9	36.80	0, 180	--
10	42.75	0, 180	--
11	65.52	0, 120, 240	--

Figure 2.3 Locations and Configurations of Strain Gauges (Akagawa et al., 2012)

2.2.3 Pipe movement

The pipeline movement was another important parameter for this project in addition to the strain of the pipeline. In order to monitor the pipeline movement, 28 heave rods (HR) were welded to the top surface of the pipeline as shown in Figure 2.4, and placement of the heave rods was similar to the strain gauges, as they were concentrated around the boundary between non-permafrost and permafrost.

Since the main cause of the vertical movement of the test pipeline was the frost heave of the soil surrounding the pipe, 5 heave gauges (HG) were placed at 1 m beneath the pipeline. They were located at 27.85 m, 30.96 m, 32.33 m, 37.04 m, and 68.85 m from the inlet riser. Figure 2.5 shows the locations of the heave gauges.

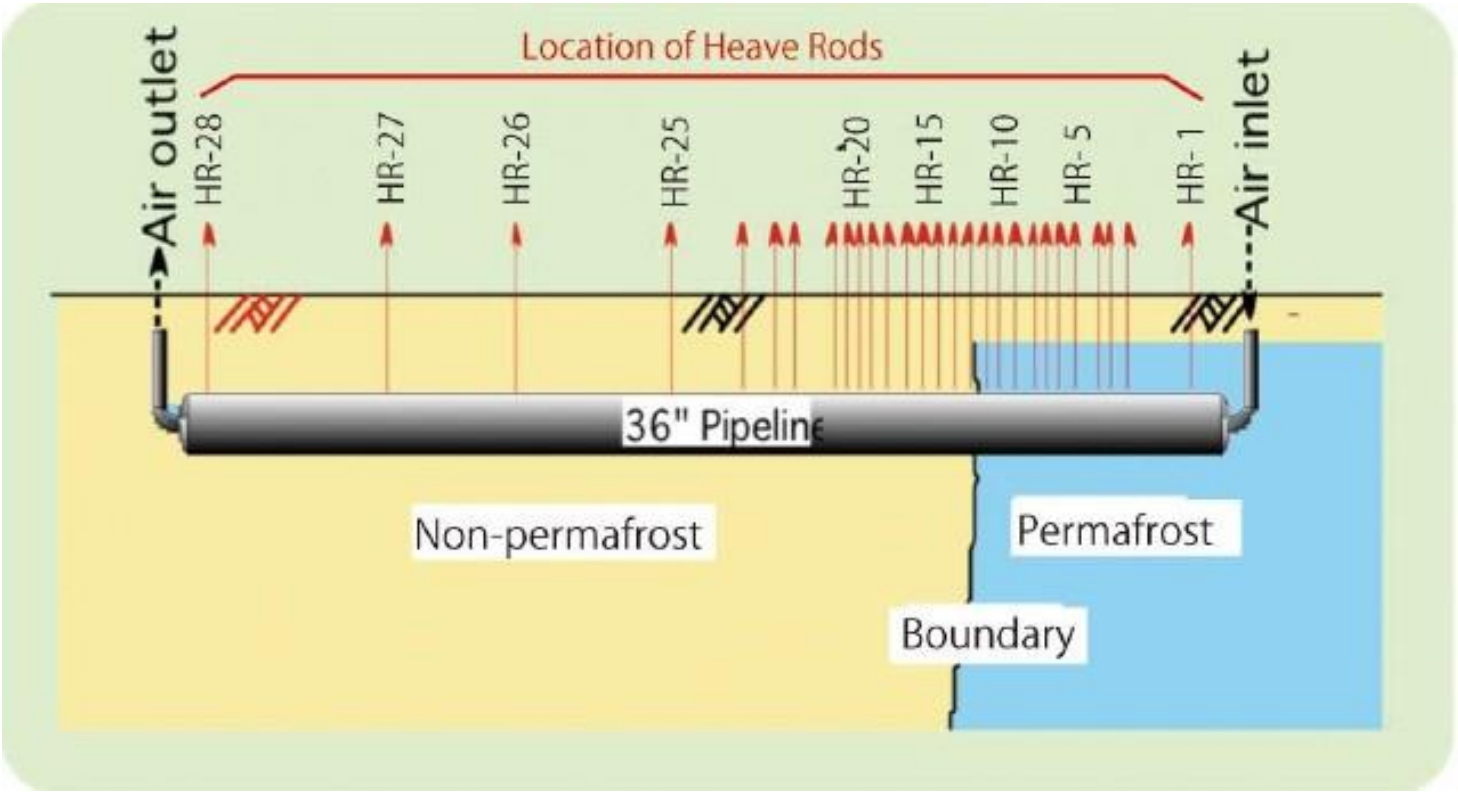

Figure 2.4 Locations and Configurations of Heave Rods (Akagawa et al., 2012)

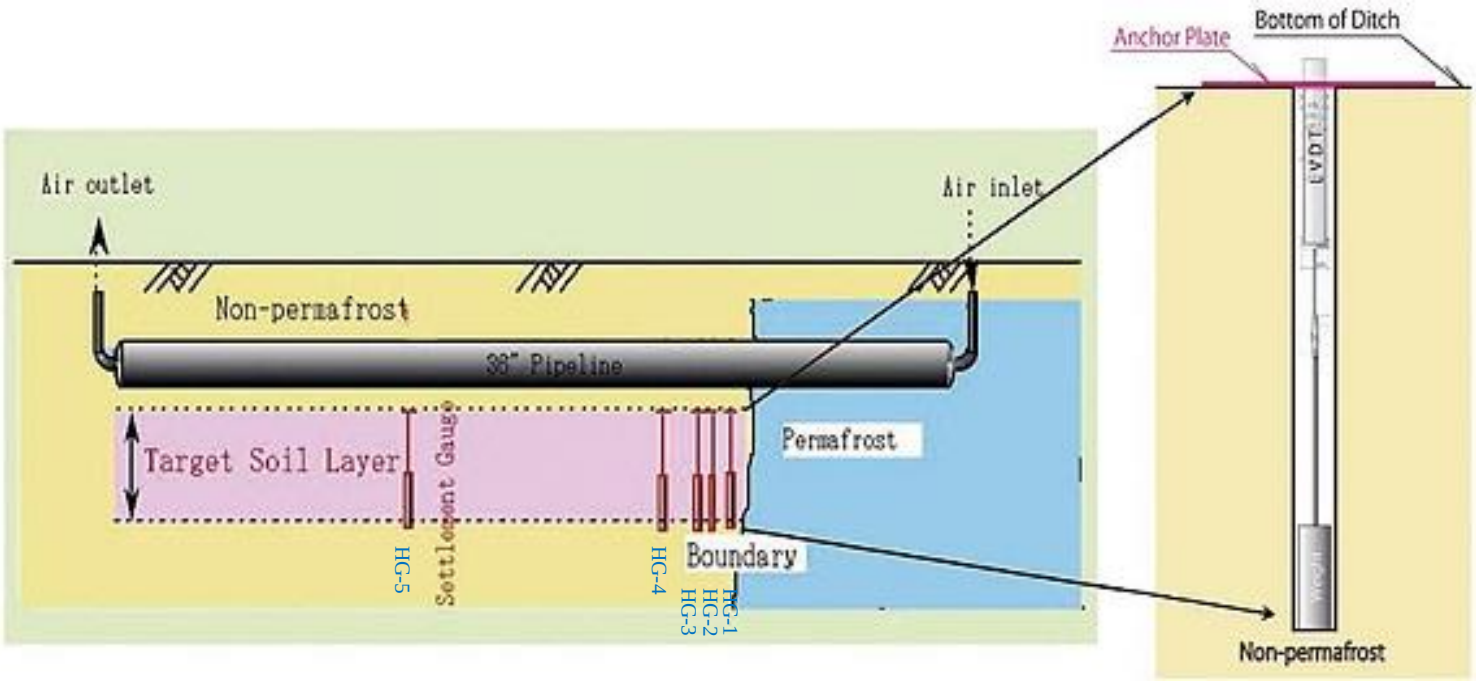

Figure 2.5 Locations and Configurations of Heave Gauges (Akagawa et al., 2012)

CHAPTER 3. FROST HEAVE DATA ANALYSIS

This chapter summarizes the pipeline movement and foundation heave beneath the pipe discussed in the previous publications by Bray (2003), Huang et al. (2004), Kim et al. (2008), and Akagawa et al. (2012). In addition, analysis of the monthly pipe heave measurements for this study is included.

3.1 Heave rod data

As mentioned in Chapter 2, 28 heave rods were installed along the top exterior surface of the pipeline to monitor the vertical movement of the pipe. The measurements were collected manually every two weeks from December 1999 to September 2003. The monthly heave rod movement was calculated in reference to the values surveyed on December 11, 1999 to show the pipe behavior, where positive movement indicated heave and negative movement meant settlement of the pipe. Figure 3.1 to Figure 3.3 show the monthly pipeline movement from December 1999 to September 2003.

Compared to the heave rod locations in Figure 2.4, it can be seen that the amount of pipeline heave, in general, increased with distance away from the inlet riser. However, the portion of the pipeline buried in the permafrost zone also experienced slight vertical movement with thaw settlement before June 2001 and frost heave throughout the remaining cooling stage. In June 2001, the entire pipeline, including the section in permafrost, experienced heaving, and it continued until the end of September 2003. Moreover, the cumulative pipe movement increased as time went on, while after September 2000, the movement between about 20 m and 70 m from the inlet riser accelerated. The pipe experienced the largest movement beyond the transition zone (i.e., 35 m to 55 m from the inlet riser). The maximum pipeline movement was observed in November 2002. The results discussed above also correspond to the analysis in the paper by Huang et al. (2004).

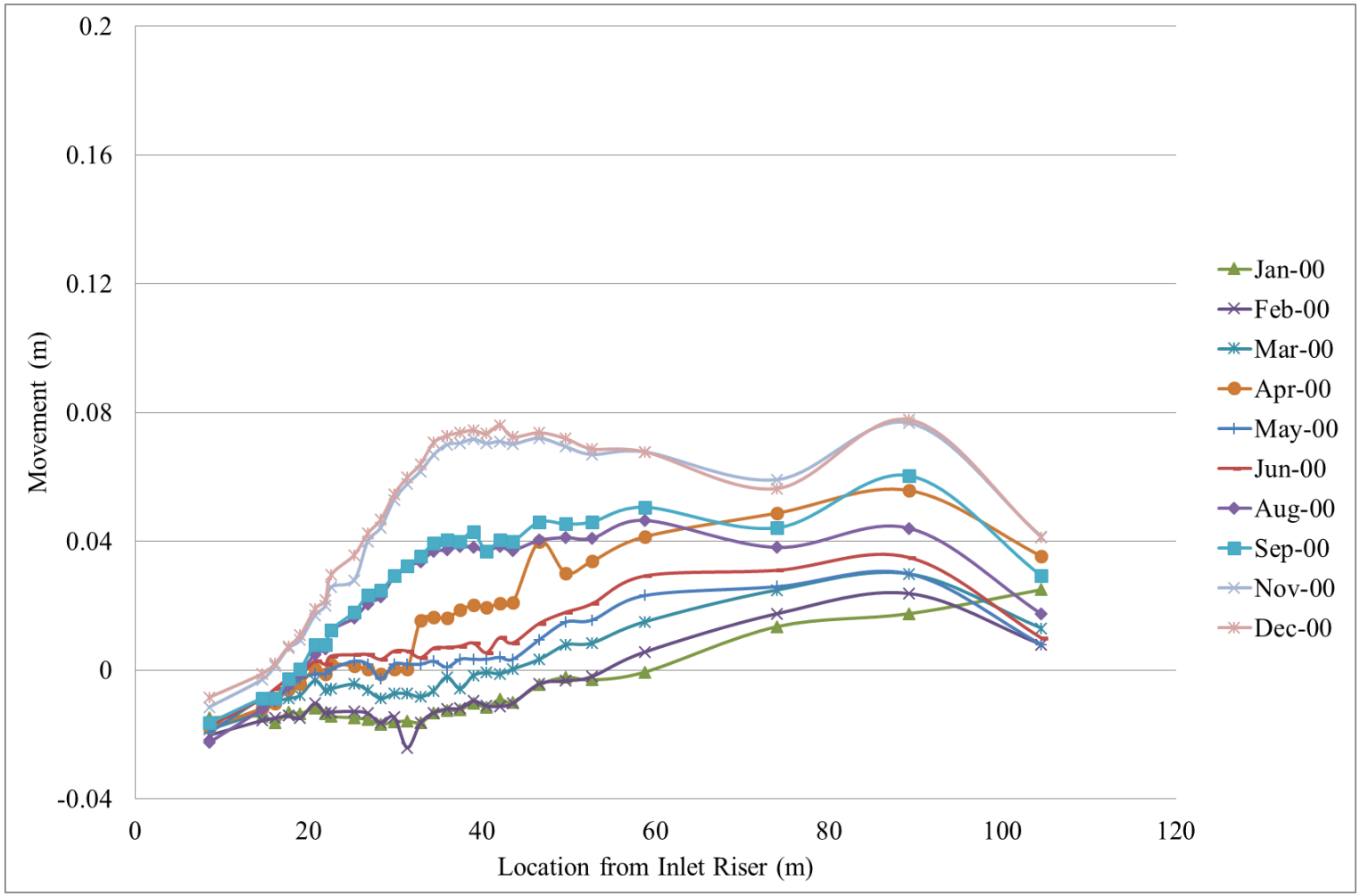

Figure 3.1 Monthly Heave Rod Movement along the Pipeline in 2000

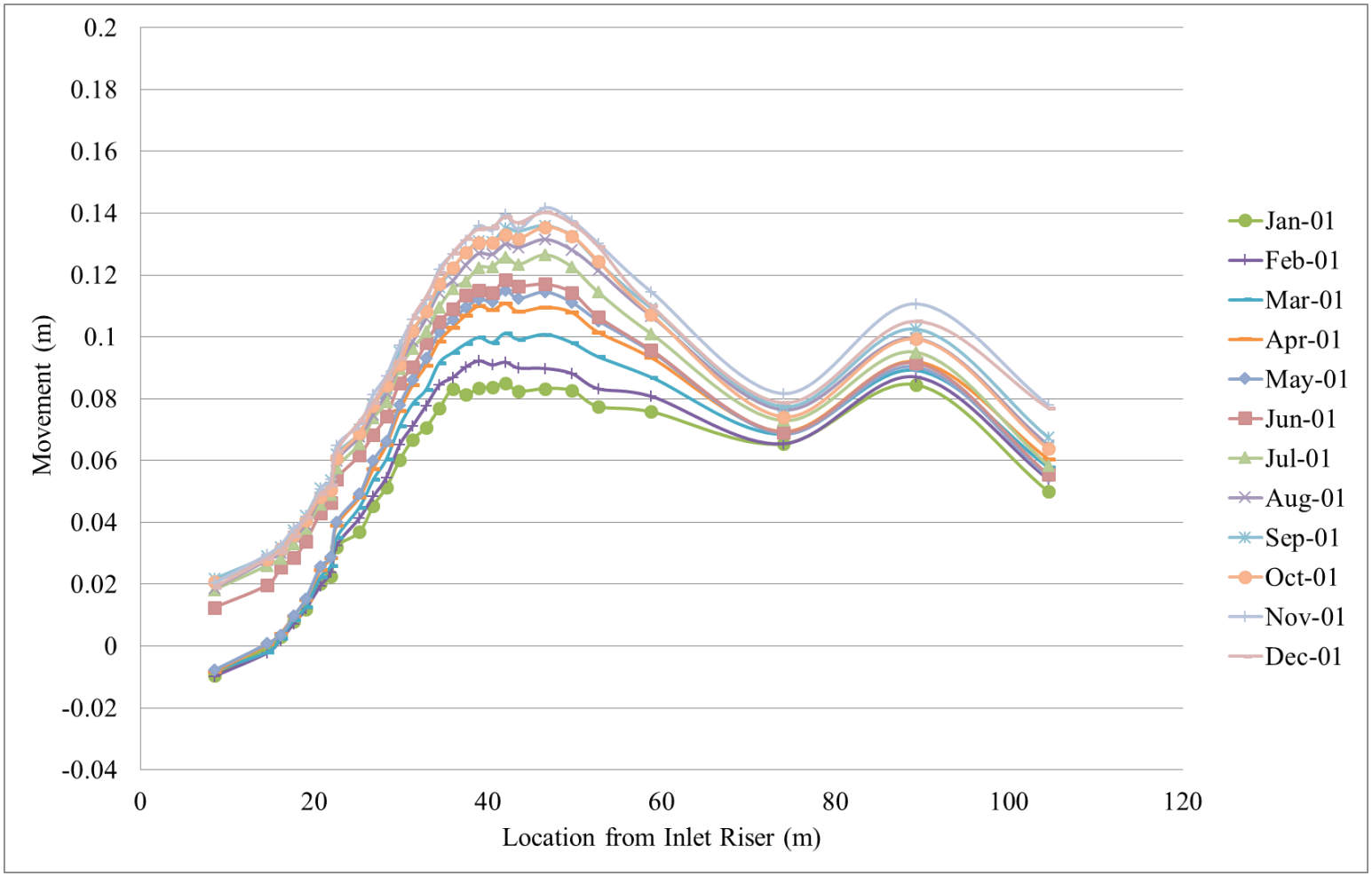

Figure 3.2 Monthly Heave Rod Movement along the Pipeline in 2001

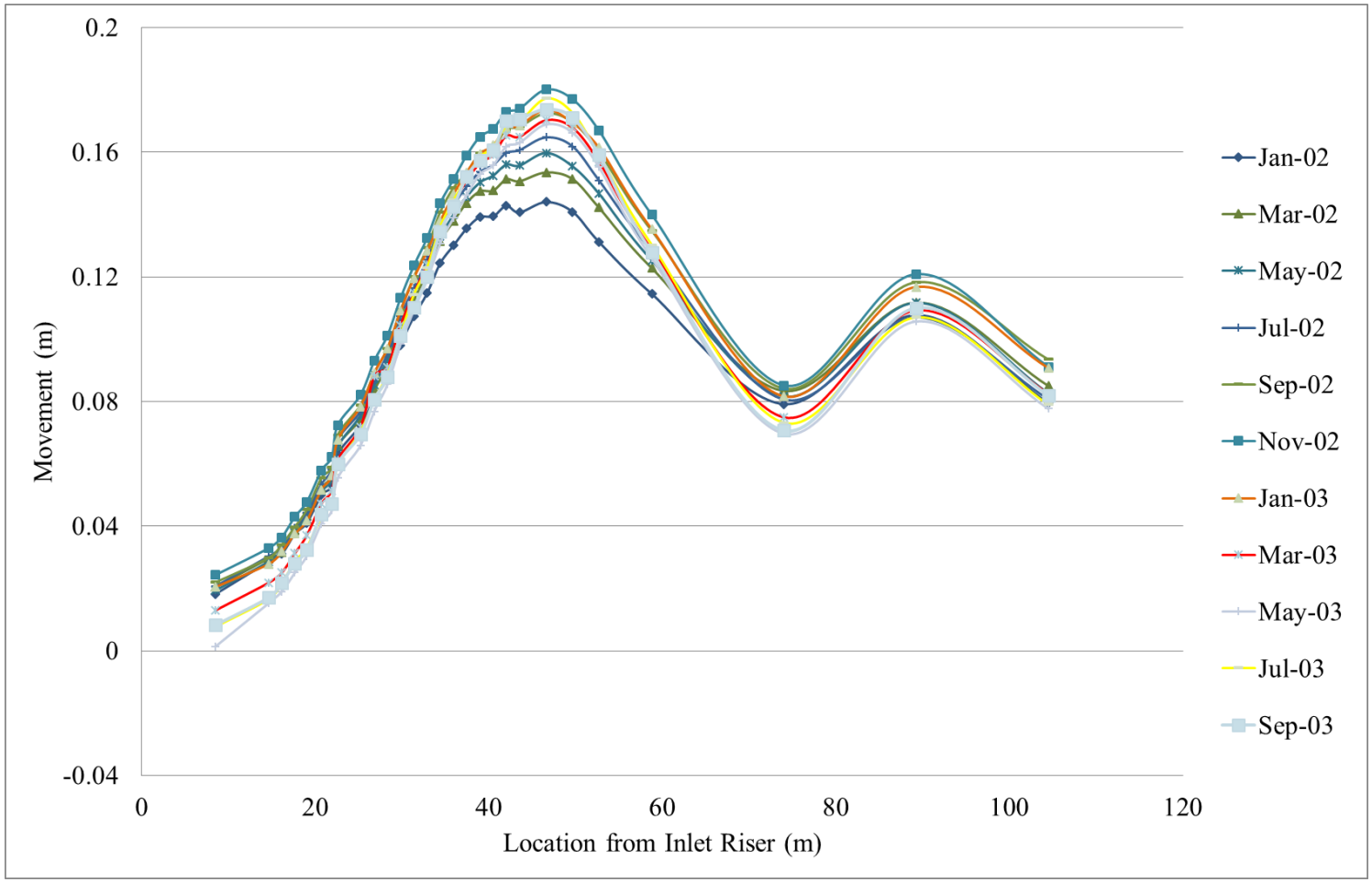

Figure 3.3 Bi-monthly Heave Rod Movement along the Pipeline for 2002 and 2003

3.2 Heave gauge data

Five heave gauges (HG-1 to HG-5) were installed underneath the pipeline as shown in Figure 2.5. Although the heave gauges were monitored from December 11, 1999 to January 14, 2005, they only functioned in the very early stage of freezing and the late stage of thawing. The target depth of foundation soil was 1 m. The gauges were placed at 27.85 m, 30.96 m, 32.33 m, 37.04 m, and 68.85 m from the inlet riser. HG-1 through HG-4 were located near the transition zone, and HG-5 was installed around the middle section of the non-permafrost area.

Figure 3.4 shows heave gauge movement versus pipeline operation time from the beginning of operation to January 2005. Monitoring of heave gauges was performed twice daily from December 11, 1999 to January 14, 2005. With the activation of the chilled air in the pipe, the ground beneath the pipe experienced abrupt increases in frost heave. After May 2000, the gauges could no longer register any differential heave between the anchor and the LVDT plate until July 2004. They then recorded an abrupt downwards movement. The downwards movement was due to the cessation of the pipeline chilling at the end of July 2003. Figure 3.5 shows the portion of the heave pattern from December 1999 to March 2000. All five heave gauges underwent a linear increase from December 1999 to early March 2000, with between 30 to almost 50 mm of total movement. After that jump, the heave gauge movement remained stable until HG-1 to HG-4 went through the second jump near late April 2000. Most notably, the movement of HG-4 changed from approximately 30 to 48 mm. Finally, the heave gauges stabilized around the middle of May 2000. Figure 3.6 shows the settlement pattern after the operation of the chilled pipe system ceased. It can be seen that the five gauges decreased slowly until July 2004. After that, the gauges experienced a sharp drop until the end of operation. HG-1, HG-3, and HG-5 moved the most dropping from approximately 40 mm to -10 mm, which indicated that the soil at each of the gauge locations underwent thaw settlement and a small degree of consolidation. For HG-2 and HG-4, the gauges

decreased about 15 mm and remained at about the same value until the end of the operation.

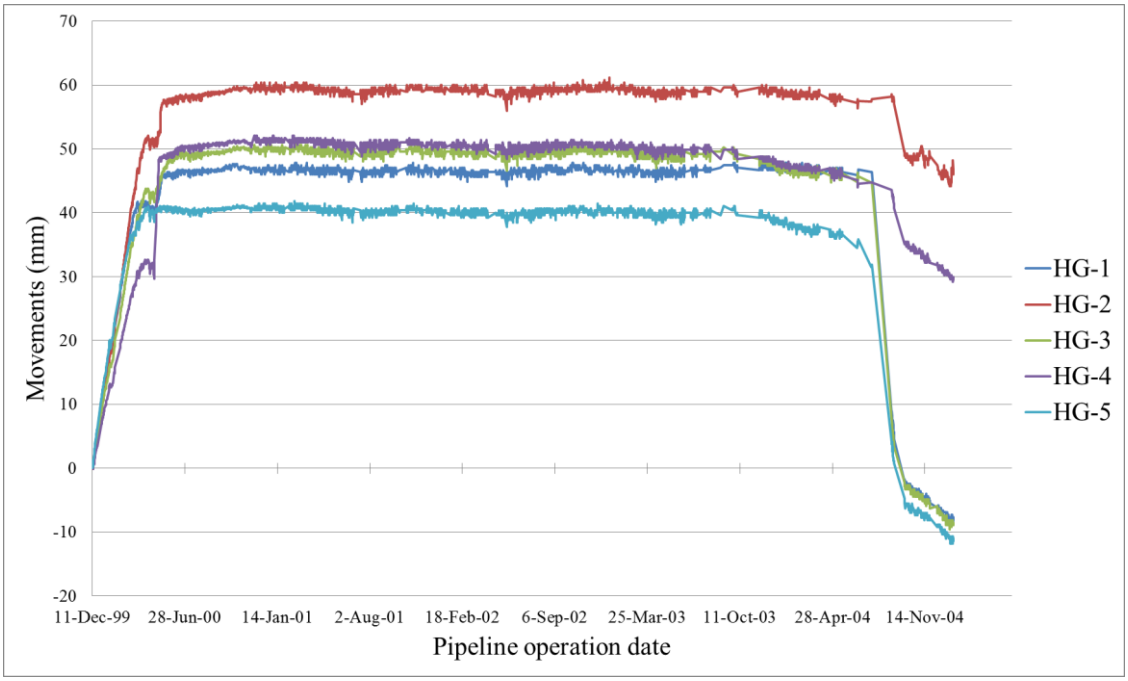

Figure 3.4 Heave Gauge Movements within 1 m beneath the Pipeline from Dec. 1999 to Jan. 2005

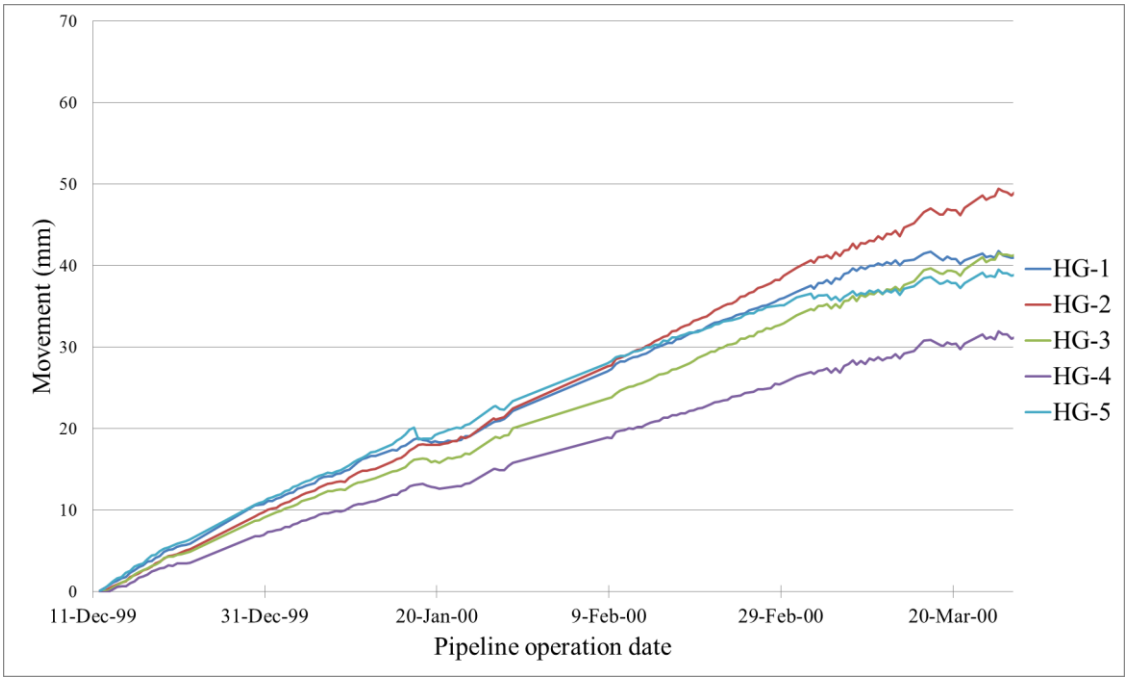

Figure 3.5 Heave Gauge Movements within 1 m beneath the Pipeline for the First Four Months of Operation (Dec. 1999 – Mar. 2000)

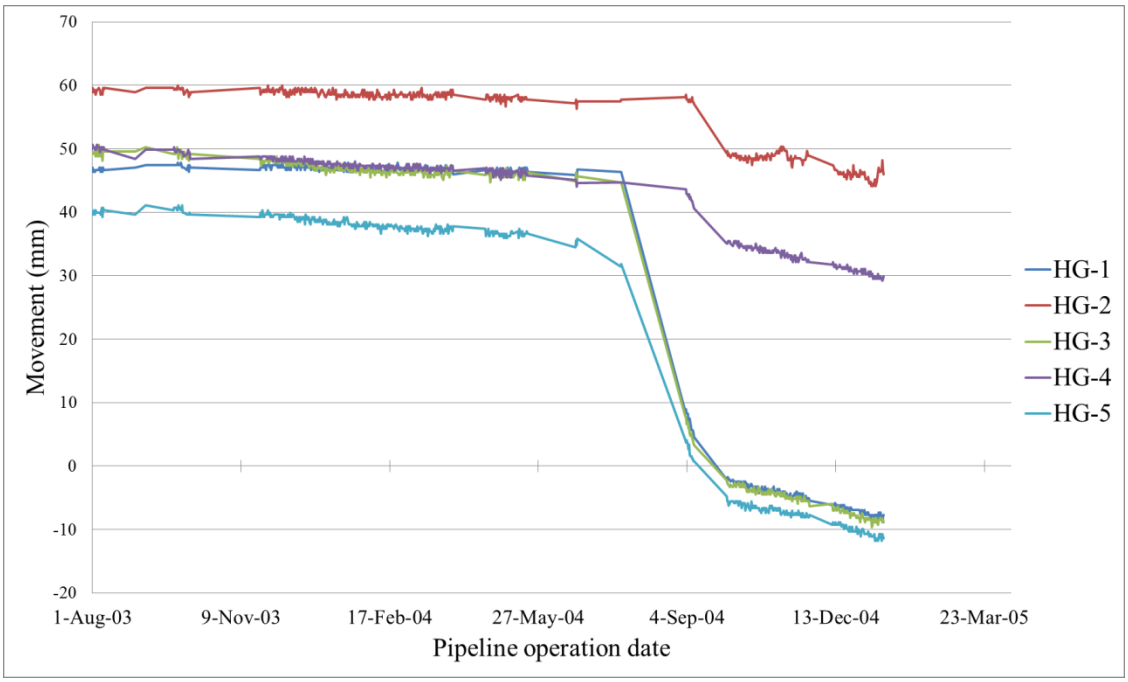

Figure 3.6 Heave Gauge Movements within 1 m beneath the Pipeline after Chilled Air Ceased (Aug. 2003 – Jan. 2005)

CHAPTER 4. ANALYSIS OF FROST HEAVE INDUCED STRAIN

The raw strain data were processed to firstly remove the temperature effects on pipe steel and strain gauges, as well as random noise from measurements. The general trends were analyzed for longitudinal strain and circumferential strain. In the discussion below, the positive strain values represent tensile strain, while negative ones are compressive strain.

4.1 Data processing

The strain of the pipeline was induced from two sources: heave of soil as well as thermal expansion and contraction of pipe steel. Since this study was mainly focused on heave-induced strain, the strain caused by thermal expansion/contraction of pipeline was removed. According to the properties of the pipeline steel used (i.e., API X65), the coefficient of thermal expansion was 12.5 microstrain/^{o}C (με/^{o}C). As mentioned in Chapter 2, the locations of thermistors along the pipeline and strain gauges were not the same. Therefore, the temperature at the location of each strain gauge was interpolated using temperature measurements between two adjacent thermistor locations:

$$T_{HG} = T_a + (D_{HG} - D_a)\frac{T_b - T_a}{D_b - D_a} \tag{4.1}$$

where

T_{HG} = temperature at location of strain gauge (^{o}C),

T_a and T_b = temperatures of thermistors adjacent to strain gauge (^{o}C),

D_{HG} = distance between strain gauge and the inlet riser of pipeline (m), and

D_a and D_b = distances between thermistors and the inlet riser of pipeline (m).

Figure 4.1a shows the history of interpolated temperatures at SG-4. During the operation of the test facility from December 1999 to May 2003, the pipe temperature fluctuated around -10^{o}C and an annually repetitive pattern can be observed. In each cycle, the

highest temperature appeared between June and September, and the lowest temperature appeared between December and March. However, rapid changes in temperature were observed, which is illustrated by the vertical jumps in the figure. The temperature jumps could possibly be caused by the interruption of pipeline operation, which led to the rapid temperature rise. In addition, after the operation of the facility ceased (starting August 2003), the jumps in temperature disappeared, which also indicates that temperature jumps were closely related to the operation of the test facility.

Figure 4.1b shows the history of raw longitudinal strain measured twice daily by the strain gauge placed at 0° at SG-4 (i.e., SG-4-0deg-L). Generally, the strain was in the range between 200 to -100με. Visual inspection indicates that a nearly inverse sawtooth pattern in this data set. The jumps in strain that can be observed might be related to the effect of localized pipe curvature changes. However, there is no direct evidence to support this hypothesis. As mentioned before, temperature also had an effect on the strain gauges. Three dummy strain gauges at 5.32, 27.8, and 65.52 m from the inlet riser were buried with the pipeline to compensate for such effects. The adjustment factor was calculated as the slope of the strain recorded by dummy gauges vs. the corresponding temperatures, as shown in Figure 4.2. The final adjustment factor was the average of these data, with a value of 4.46 με/^{o}C. The effect of temperature on strain gauges was removed and the processed strain data is presented in Figure 4.1c. The processed final strain data is presented in Figure 4.1d. Both the thermal expansion/contraction of the pipeline (12.5 με /^{o}C) and the effect of temperature on the strain gauge (4.46 με /^{o}C) were removed. Although the general trend of strain distribution is discernible in the diagram, noise is amplified and the data demonstrated more compression. However, the exact source of such noise could not be identified. It might be related to air pressure fluctuation inside the pipe and mechanical vibration caused by compressor. The strain discussed hereafter is adjusted strain, in which the thermal expansion/contraction of pipeline and effect of temperature on strain have been removed following the steps mentioned above.

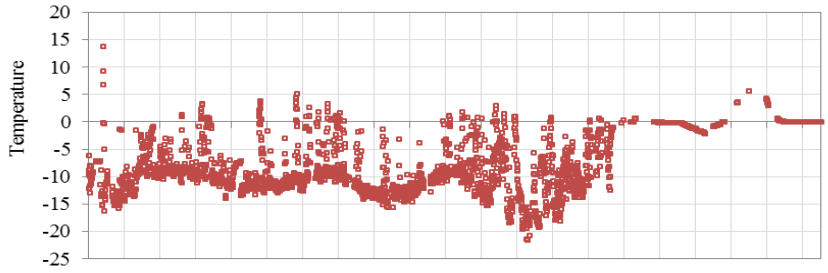

(a) Pipe temperature data in ^{o}C

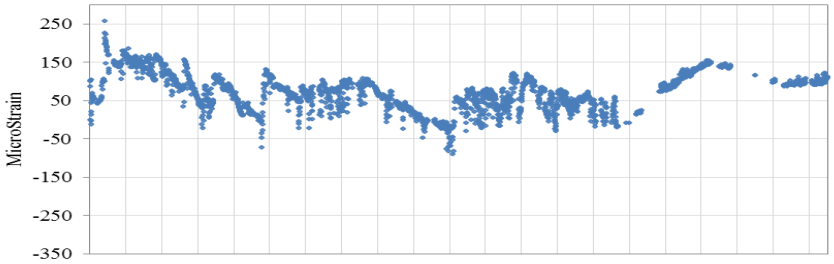

(b) Raw strain data

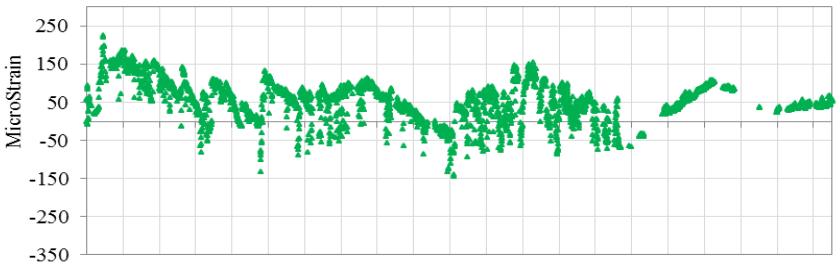

(c) Removal of the effect of temperature on strain gauge

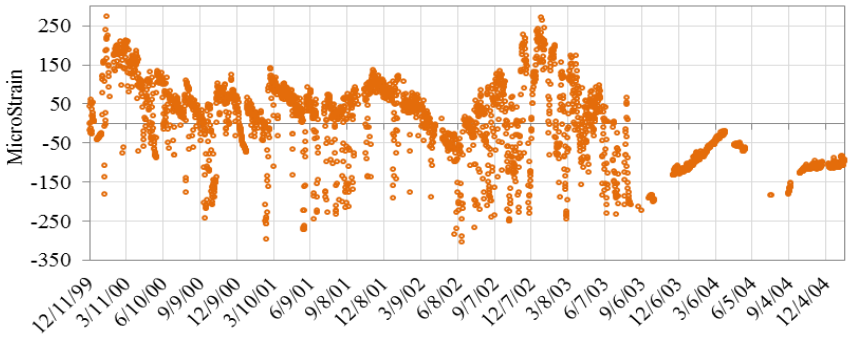

(d) Removal of thermal expansion/contraction of the pipeline and effect of temperature on strain gauge

Figure 4.1 Longitudinal Strain Measurements before and after Temperature Corrections (SG-4-0deg-L)

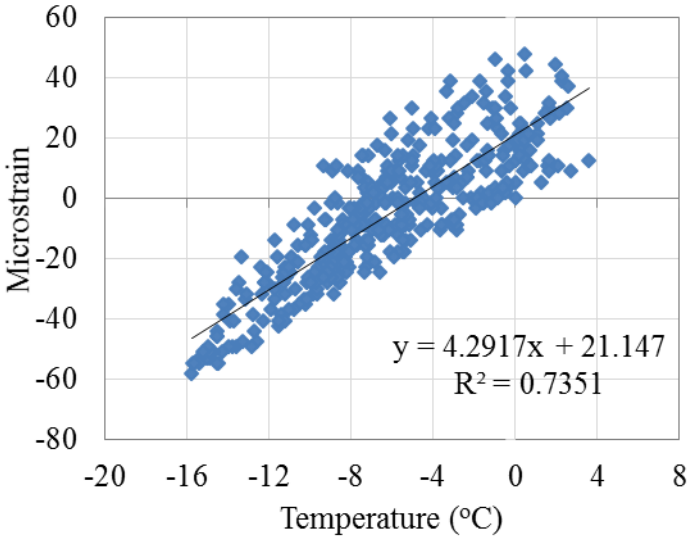

Figure 4.2 Determination of Adjustment Factor to Remove Temperature Effect on Strain Gauges

4.2 Strain development over time

The strain of a chilled gas pipeline is mainly caused by interaction between the pipe and the surrounding soil. Such interaction is driven by the differential frost heave at the boundary between permafrost soil and frost-susceptible soil due to the freezing action of the chilled gas, as described in Chapter 1. Frost heave is developed over time after the chilled gas is circulated through the pipeline, and the induced strain is subsequently developed.

4.2.1 Circumferential strain

In this study, at SG-4 and SG-7, both longitudinal and circumferential strain gauges were installed at 0^o, 90^o, 180^o, and 270^o to investigate strain distribution on the cross section of the pipeline. Figure 4.3 shows the measured circumferential strain of SG-4 over the entire duration of operation. The circumferential strain varied between -200 and 600 με while the facility was in operation. However, right after the chilled air stopped, the

circumferential strain decreased sharply. Such change in induced strain was much quicker than the response of measured heave. By the end of August 2003, the circumferential strain at all positions dropped below 0 με, while the decrease of heave was not observed until August 2004 (see Figure 3.4). After June 2004 changes in circumferential strain at different positions were not consistent. Strain at 270^o started to increase, while strain at 180^o decreased sharply and then increased. At the end of the entire test (i.e., December 2004), the circumferential strain at 0^o, 90^o, and 180^o were all approximately -200 με. In theory, a bent pipeline is symmetrical to the vertical plane along the longitudinal direction. If this is true, then the measured strain along the centerline (i.e., 0^o and 180^o) and the springline (i.e., 90^o and 270^o) should be almost identical to each other. As indicated in Figure 4.3, the circumferential strain at 0^o and 180^o, 90^o and 270^o were nearly identical to each other before the cessation of chilled air.

Figure 4.4 shows the circumferential strain of SG-4 during the first year. At the beginning of the operation, more significant strain changes occurred. For example, two peaks were observed in December 12, 1999 and January 14, 2000, with their values of 1102 and 895 με, respectively. Starting from May 2000, the strain became relatively stable.

Figure 4.5 shows the circumferential strain at SG-7. Generally speaking, the trend was similar to the one obtained from SG-4, but with a wider range of strain between -400 and 900 με. At the beginning of operation, more significant strain changes occurred and after 10 months, the strain became relatively stable. After chilled air was stopped in August 2003, the circumferential strain decreased dramatically. From the beginning of pipe operation to September 2002, the measured strain at 90^o and 270^o were nearly identical to each other. As compared to SG-4, the difference of measured strain between 0^o and 180^o was greater for SG-7. For example, from the same time period (December 2001 to June 2002), the difference between 0^o and 180^o changed 230με for SG-7; however, strain at these locations was nearly identical for SG-4.

Figure 4.6 shows the circumferential strain of SG-7 in the first year. Similar to SG-4, two peaks were observed on December 12, 1999 with the value of 1225 με and on January 23, 2000 with the value of 1026 με. The trends of strain distribution at different orientations were almost parallel to each other. However, the strain at 0^o and 180^o exhibited larger deviations from each other than the strain at 90^o and 270^o.

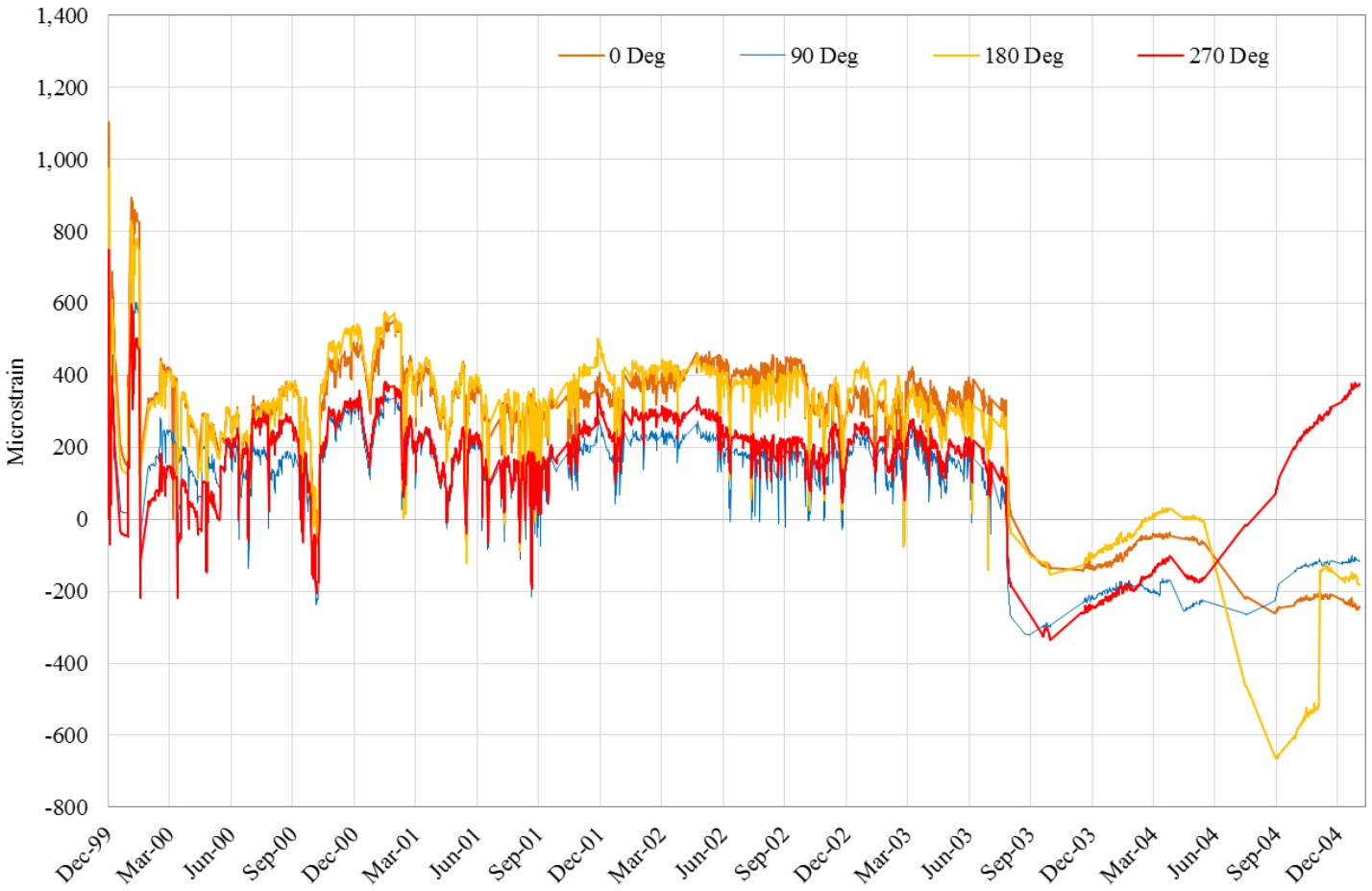

Figure 4.3 Circumferential Strain at SG-4 throughout Pipeline Operation

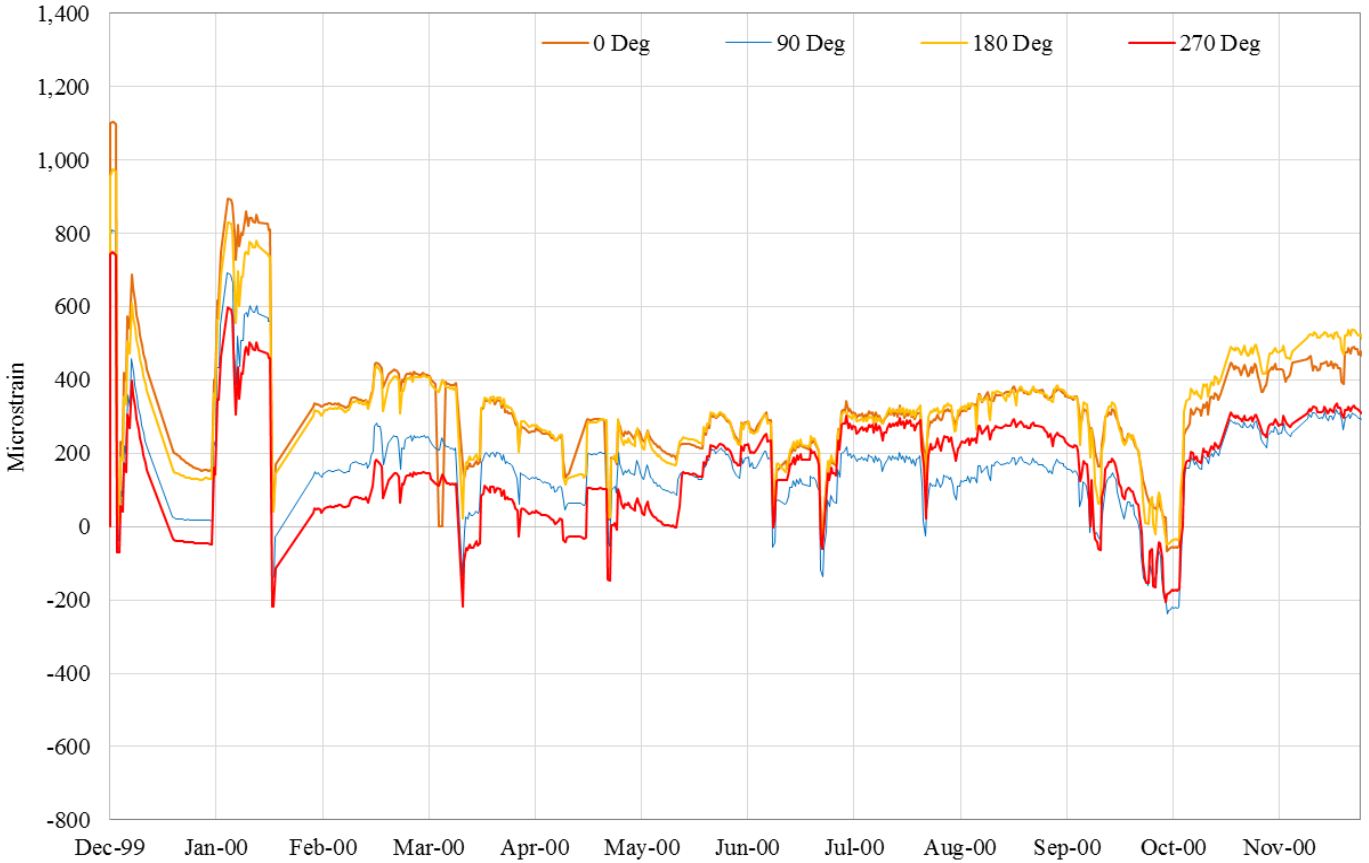

Figure 4.4 Circumferential Strain at SG-4 in the First Year of Pipeline Operation (Dec. 1999 – Nov. 2000)

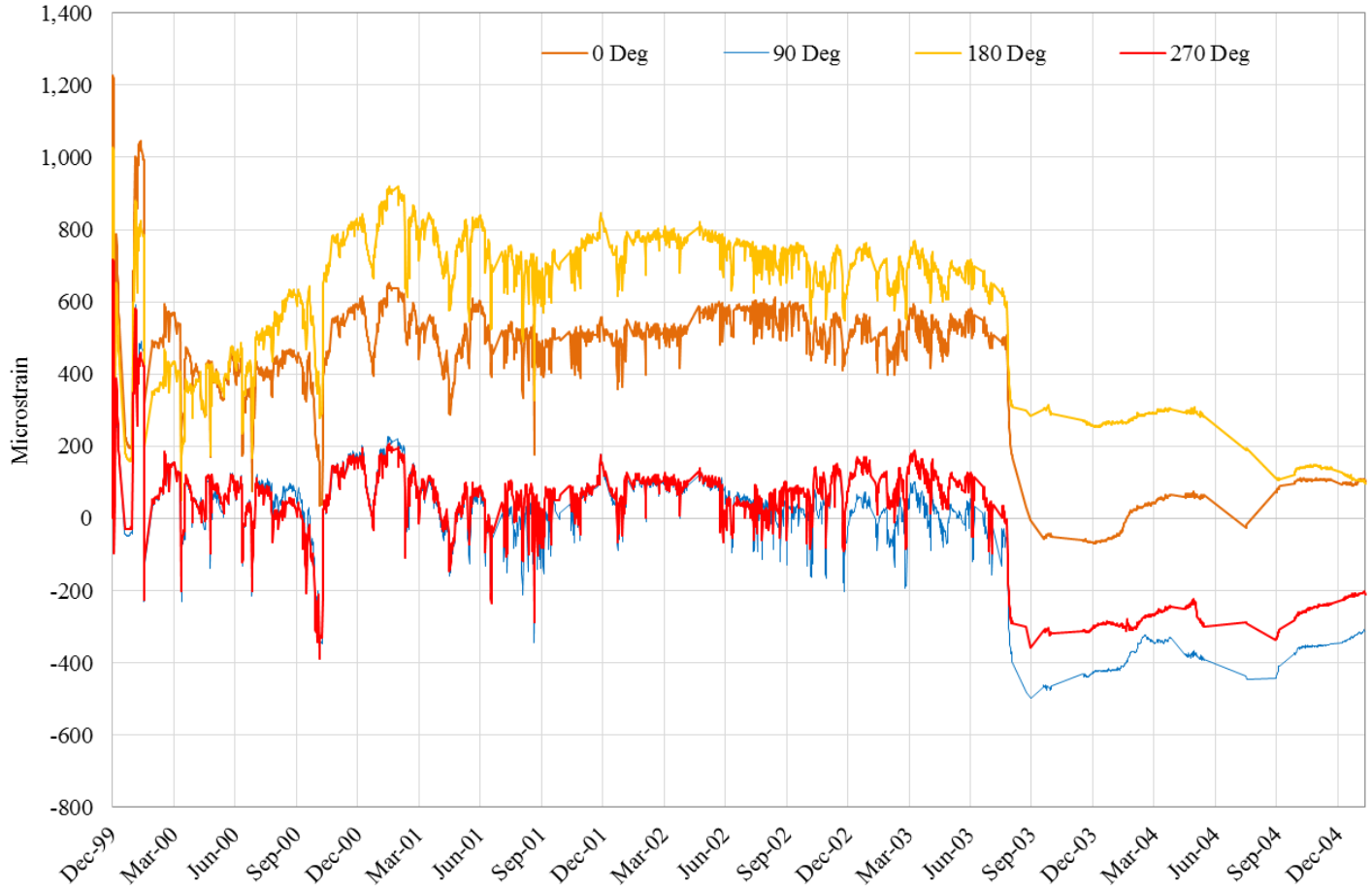

Figure 4.5 Circumferential Strain at SG-7 throughout Pipeline Operation Time

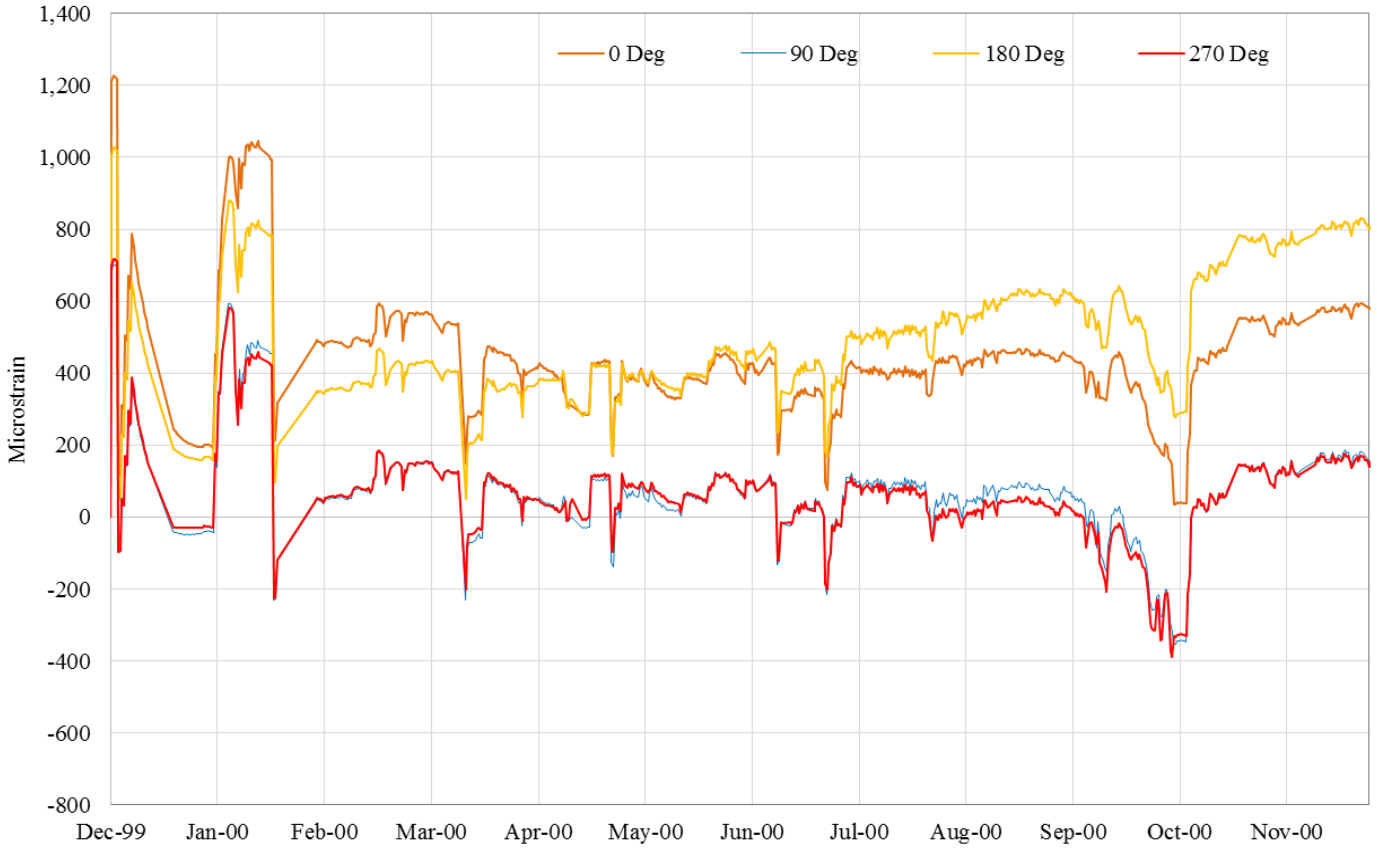

Figure 4.6 Circumferential Strain at SG-7 in the First Year of Pipeline Operation (Dec. 1999 – Nov. 2000)

4.2.2 Longitudinal strain

The development of longitudinal strain was also analyzed. The strain at the top of the pipeline (0^o) was measured from SG-1 to SG-11, the strain at the bottom (180^o) was measured from SG-2 to SG-10, and the strain on the left side of the pipeline (90^o) was measured from SG-3 to SG-8. The longitudinal strain at 270^o for SG-4 and SG-7 was also analyzed.

Figure 4.7 and Figure 4.8 illustrate the longitudinal strain measured at 0^o. Compared to circumferential strain, more noise was observed. As mentioned before, the effects of temperature on the pipeline and strain gauge were removed. However, the change of temperature also affected the heave and properties of surrounding soils, which dominated the stress state of the pipeline. After the chilled air was stopped, the vibration caused by the compressor was also stopped and the noise in the longitudinal strain disappeared. Each figure was divided into five sections with each representing year-long timespan. The strain recorded varied between approximately -400 and 400 με for SG-1 to SG-5 and between -100 and 700 με for SG-6 to SG-11. After chilled air circulation was stopped, the longitudinal strain of all stations became less noisy and about half of them changed direction from tension to compression.

Figure 4.9 and Figure 4.10 show the longitudinal strain at 0^o during the first year, and provide more details. Within the initial three days after installation, the strain jumped back and forth, albeit with less magnitude (i.e., <220 με) than the remaining monitoring period. This might have been caused by initial settlement of foundation soil and release of internal stress induced during construction. Then strain gradually increased and the measurements obtained from different stations were almost parallel to each other. The second strain peak was observed on January 17, 2000 when the strain reached 451 με. Strain at different stations began to separate into three groups starting from April 2000. Strain from SG-1 to SG-4 started to decrease, which indicated compressive strain

gradually built up for this portion of the pipeline. On the other hand, strain at SG-6 to SG-10 started to increase, which meant the increase of tension in the segment of pipe corresponding to those station locations. The strain at SG-5 and SG-11 was the most stable during this time.

Figure 4.11 and Figure 4.12 show the longitudinal strain at the bottom of the pipeline measured from SG-2 to SG-10 excluding SG-4. The strain was mostly developed in the initial 15 months. Generally speaking, after March 2001 the strain reached its maximum range as indicated in the figures.

The longitudinal strain at the bottom of the pipeline at SG-4 was considered as abnormal data, as illustrated in Figure 4.13. It can be seen that the strain remained at a high level of tension from August 2003 to May 2004, and then quickly became compressive. Finally, the strain returned to tension. Examining the data of heave gauges and heave rods, there was not any rapid change that could be found in the corresponding timeline. These abrupt changes of strain measured at SG-4 could not be interpreted with certainty. It might be caused by a defect in the strain gauge. The 180^{o} strain measured at SG-4 was considered abnormal and it was removed from Figure 4.11. For strain measured at the rest of the stations, higher tensile strain could be observed at SG-2 and SG-3. Compressive strain was found at SG-9. Compared to the strain on the top (i.e., 0^{o}) at all stations, the directions of strain was opposite with tensile strain at SG-9 and compressive strain at SG-2 and SG-3.

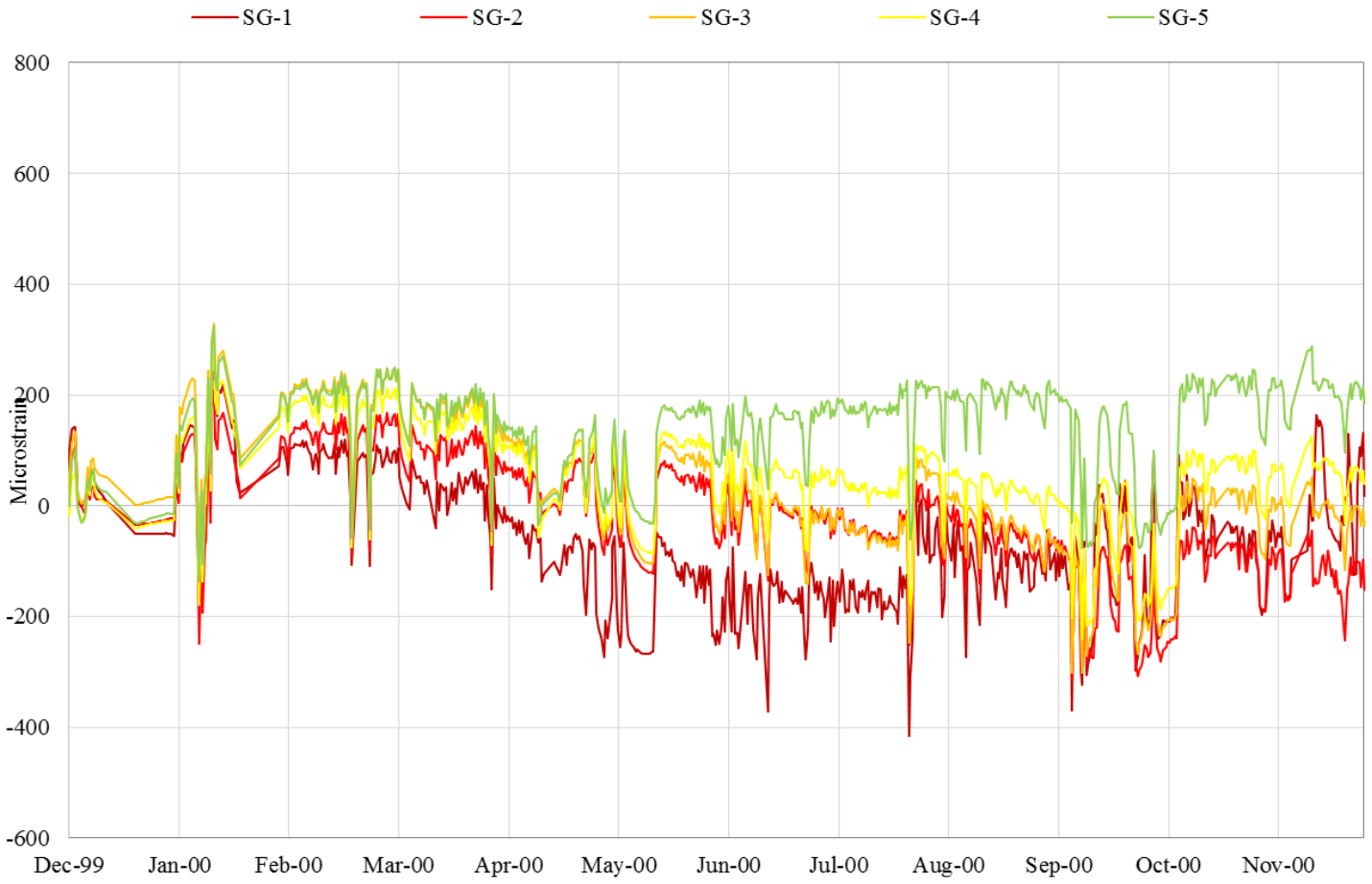

Figure 4.7 Longitudinal Strain at 0° throughout Pipeline Monitoring Time (SG-1 to SG-5)

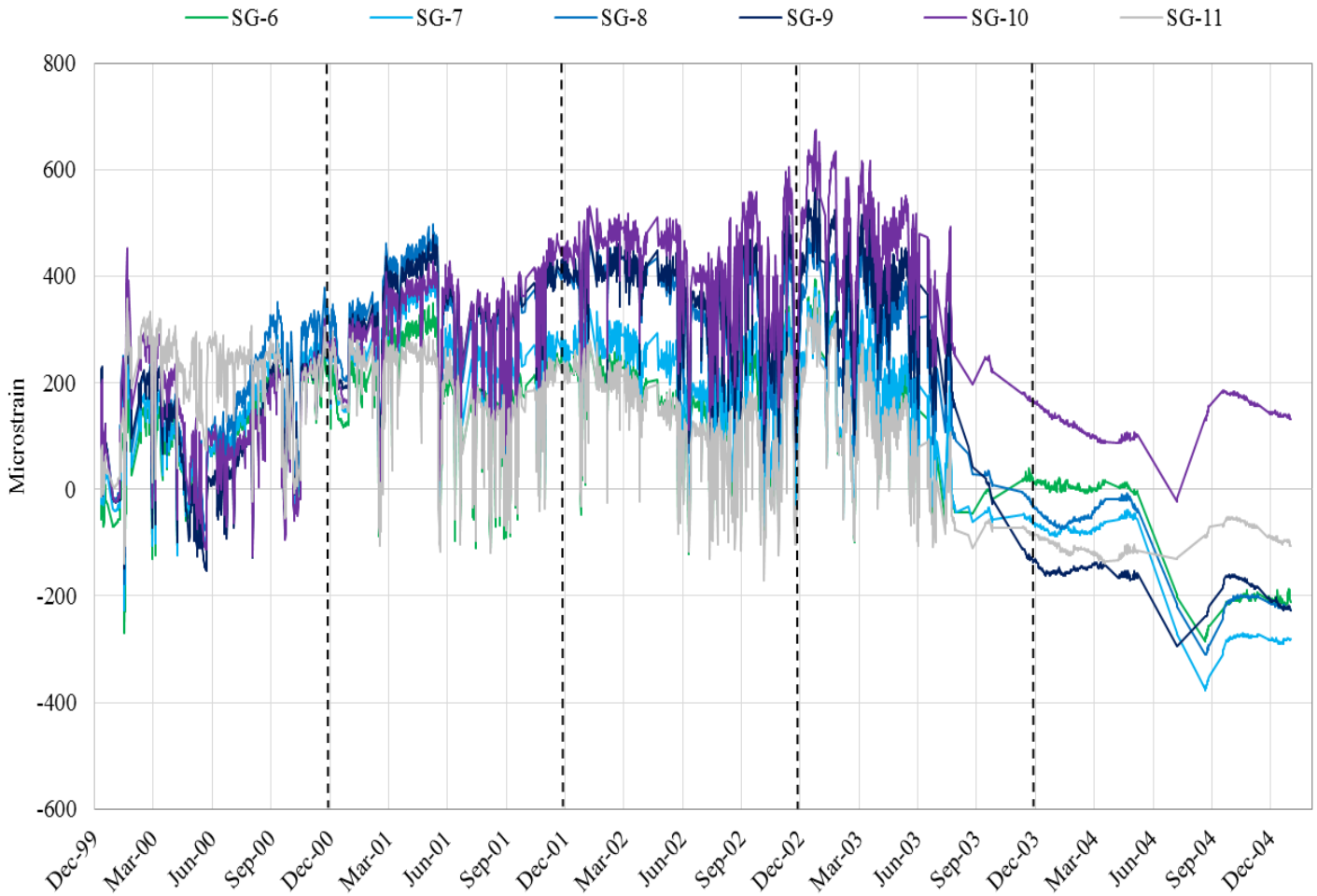

Figure 4.8 Longitudinal Strain at 0 ° throughout Pipeline Monitoring Time (SG-6 to SG-11)

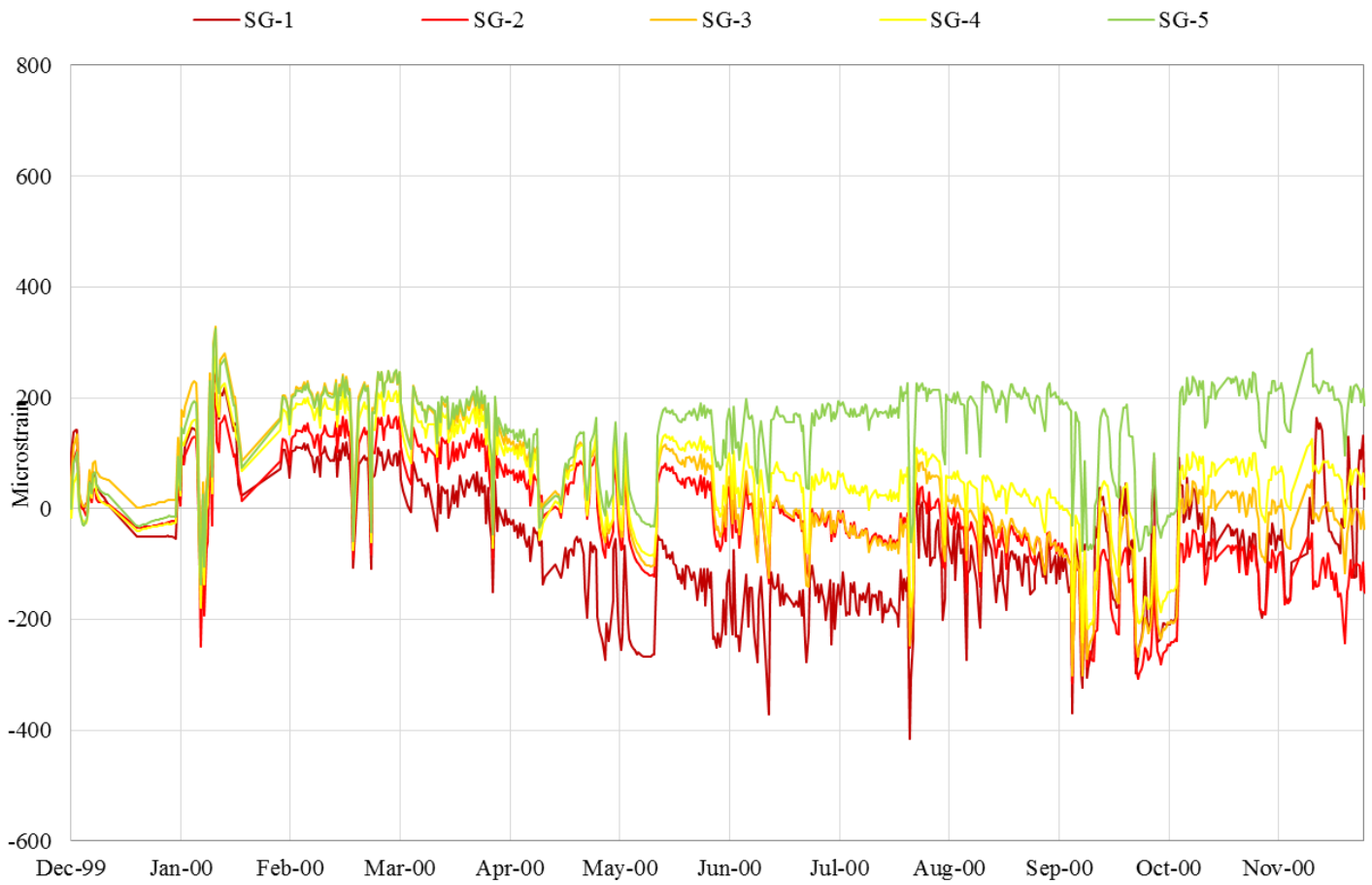

Figure 4.9 Longitudinal Strain at 0° in the First Year from Dec. 1999 to Nov. 2000 (SG-1 to SG-5)

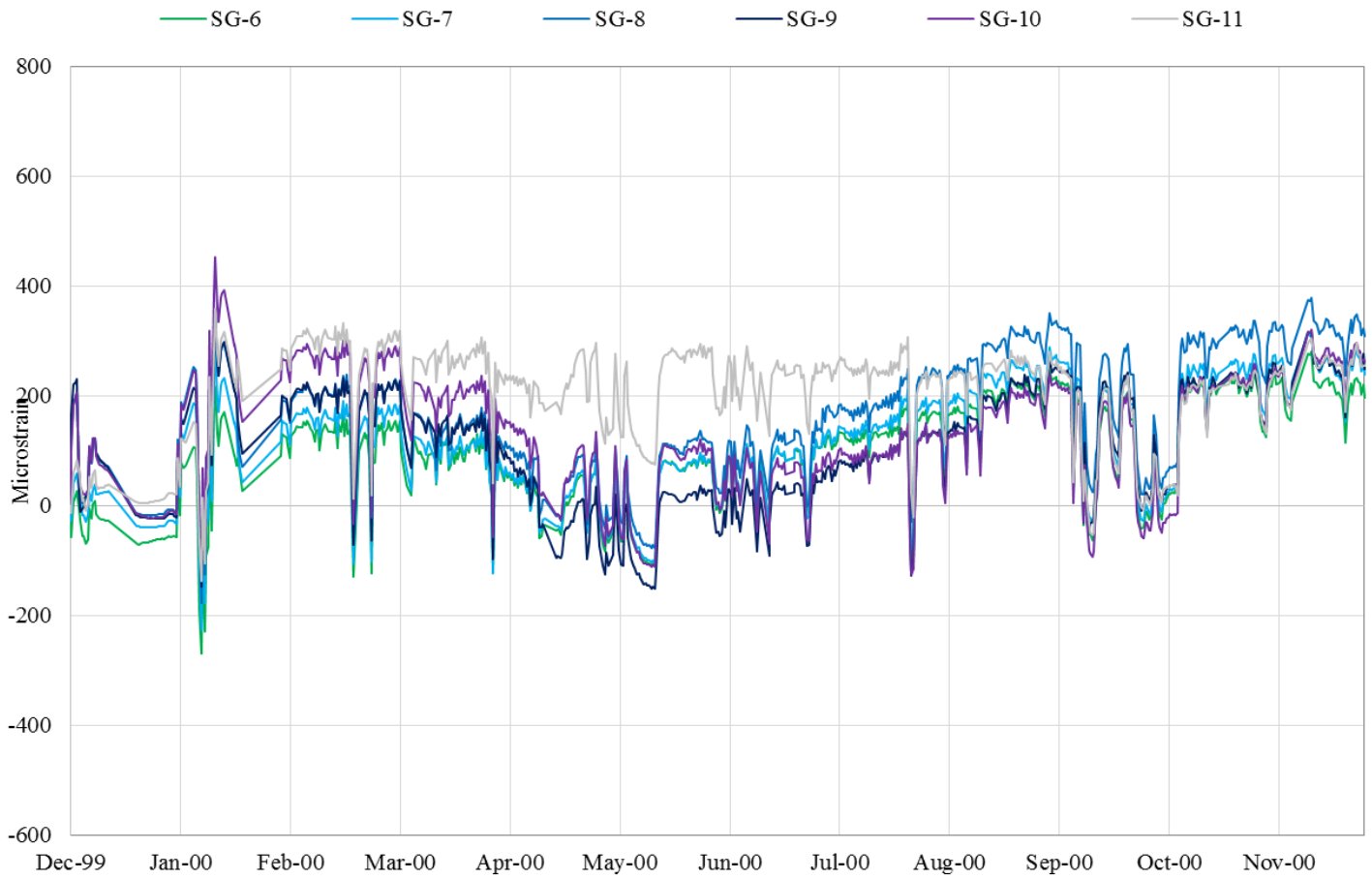

Figure 4.10 Longitudinal Strain at 0° in the First Year from Dec. 1999 to Nov. 2000 (SG-6 to SG-11)

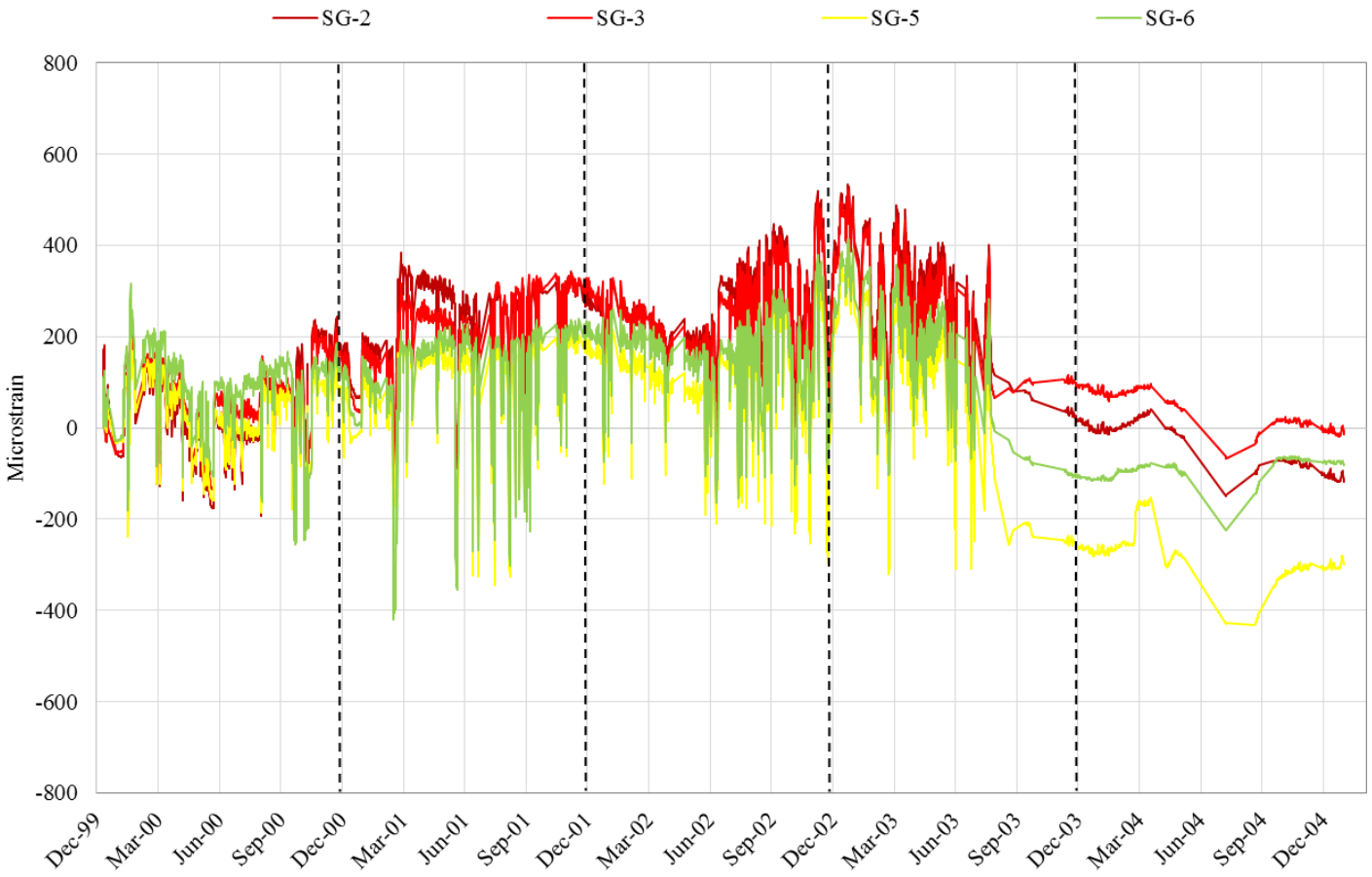

Figure 4.11 Longitudinal Strain at 180° throughout Pipeline Monitoring Time (SG-2 to SG-6)

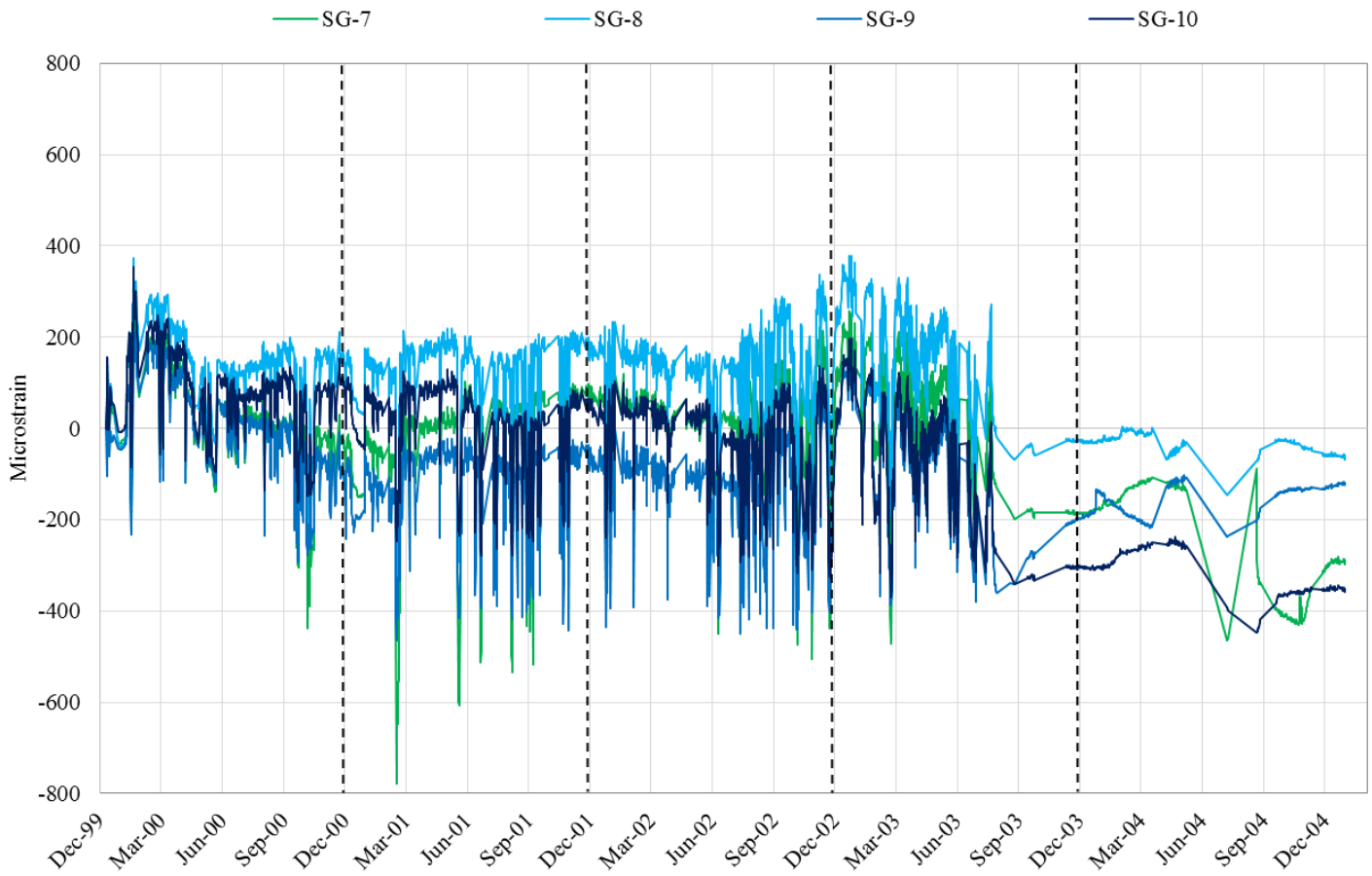

Figure 4.12 Longitudinal Strain at 180° throughout Pipeline Monitoring Time (SG-7 to SG-10)

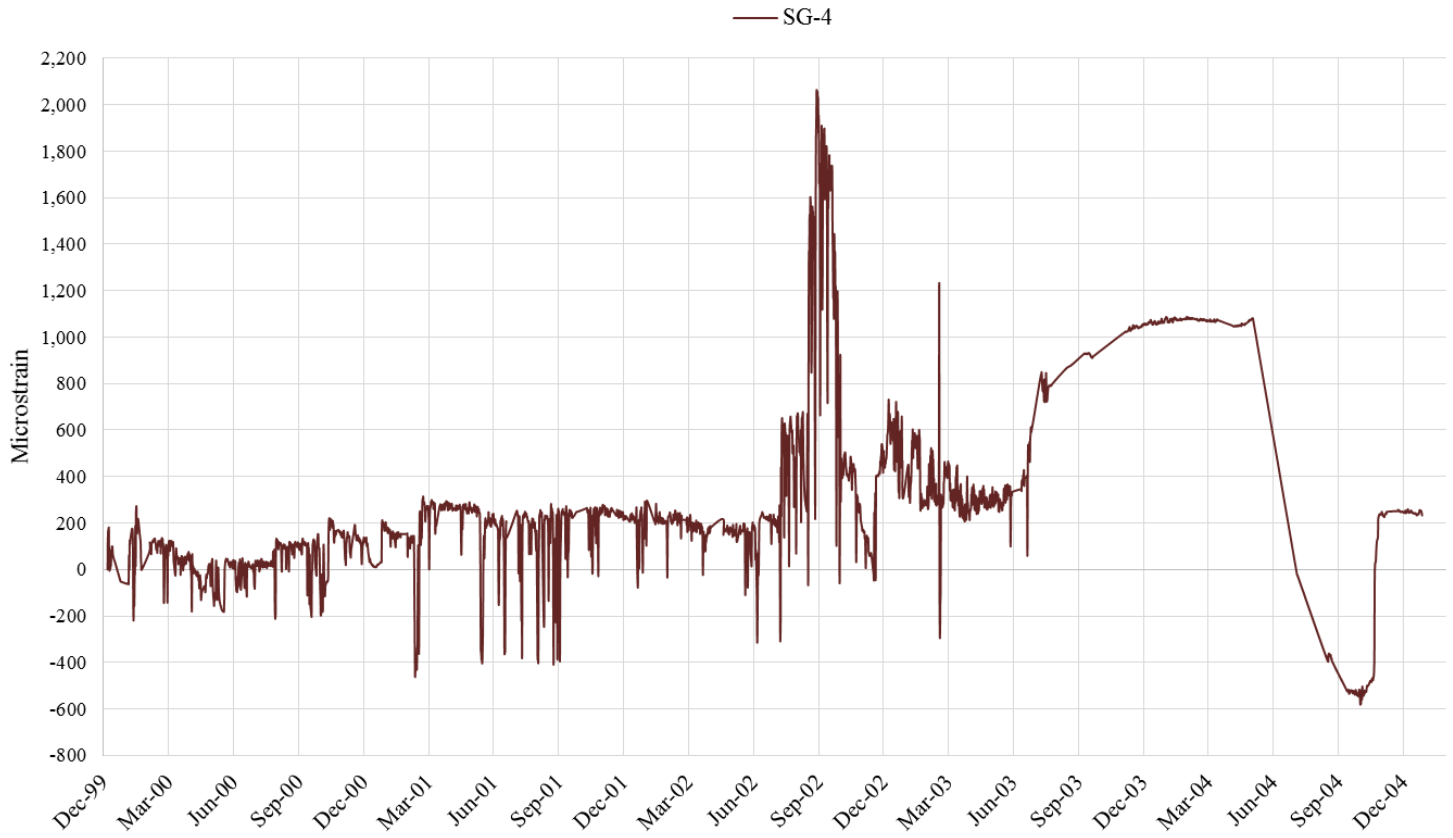

Figure 4.13 Longitudinal Strain at 180° for SG-4 throughout Pipeline Monitoring Time

Figure 4.14 and Figure 4.15 show the longitudinal strain at the bottom of the pipe in the first year of operation. Two peaks can be observed on December 12, 1999 and January 21, 2000. The strain was mostly stable from the end of January to mid-July. During this time, the strain curve of SG-8 had the highest tensile strain values, while SG-2, SG-3, and SG-4 had the lowest relative values. After mid-July, strain at SG-2, SG-3, and SG-4 started to increase slightly. During the time between September and October, the strain at all stations changed rapidly. At the end, strain at SG-2, SG-3, and SG-4 had the highest relative values.

Figure 4.16 and Figure 4.17 illustrate the longitudinal strain at 90^{o} from SG-3 to SG-8. Generally, the 90 ° strain was tensile among all stations excluding the noise. The trends were similar to the strain at the bottom of the pipe. The abrupt changes in strain similar to those observed at other positions (i.e., 180^{o}) were observed on December 13, 1999 and January 17, 2000. Prior to April 2000, the tensile strain among all stations ranked from the largest to the smallest in the order of SG-8, SG-7, SG-6, SG-5, SG-4, and SG-3. After May 2000, the tensile strain at SG-3 started to increase, while the strain at SG-8 started to decrease. At the end of the pipeline operation, the largest tensile strain was observed at SG-3 and the smallest strain was observed at SG-8.

Figure 4.14 Longitudinal Strain at 180° in the First Year from Dec. 1999 to Nov. 2000 (SG-2 to SG-6)

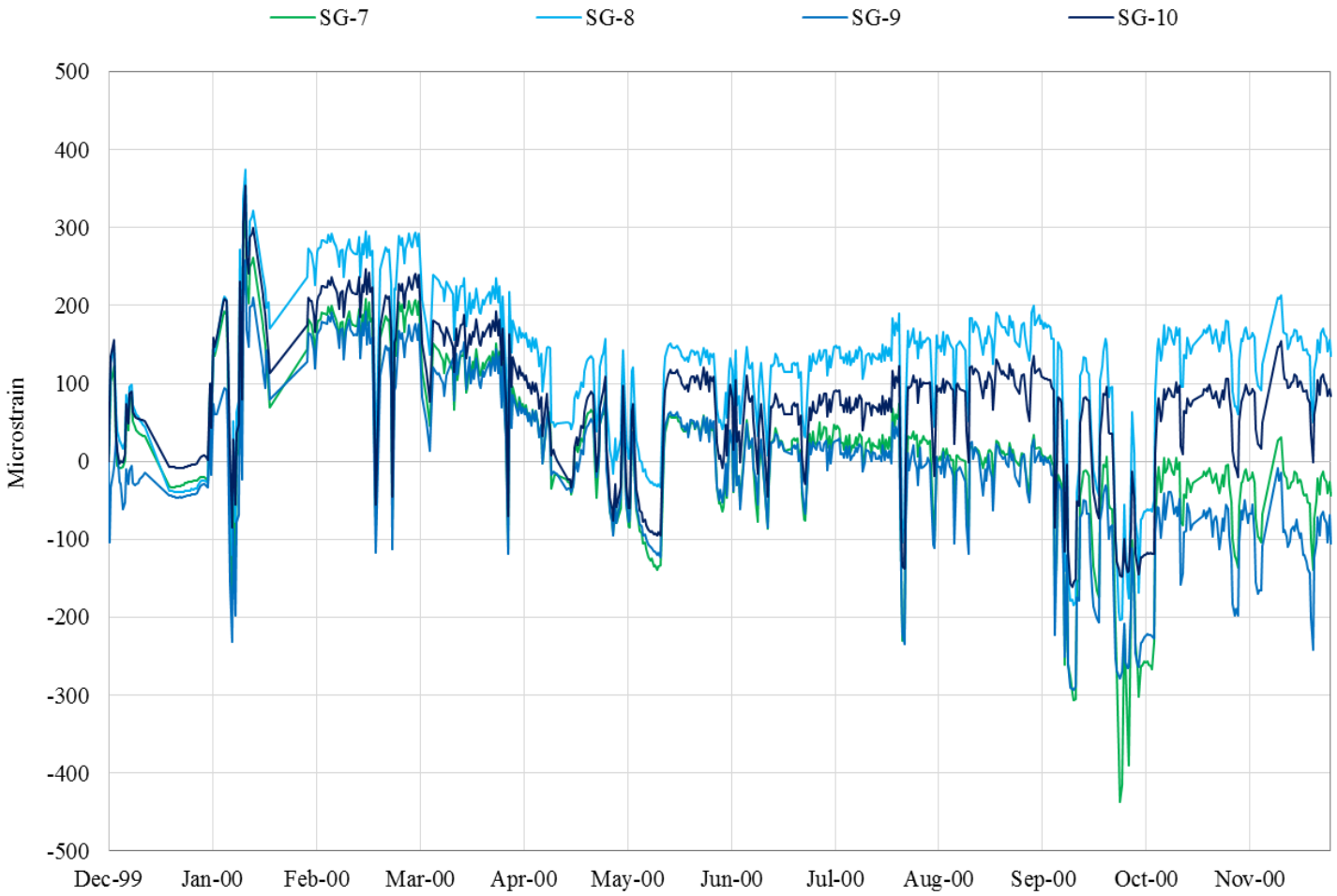

Figure 4.15 Longitudinal Strain at 180° in the First Year from Dec. 1999 to Nov. 2000 (SG-7 to SG-10)

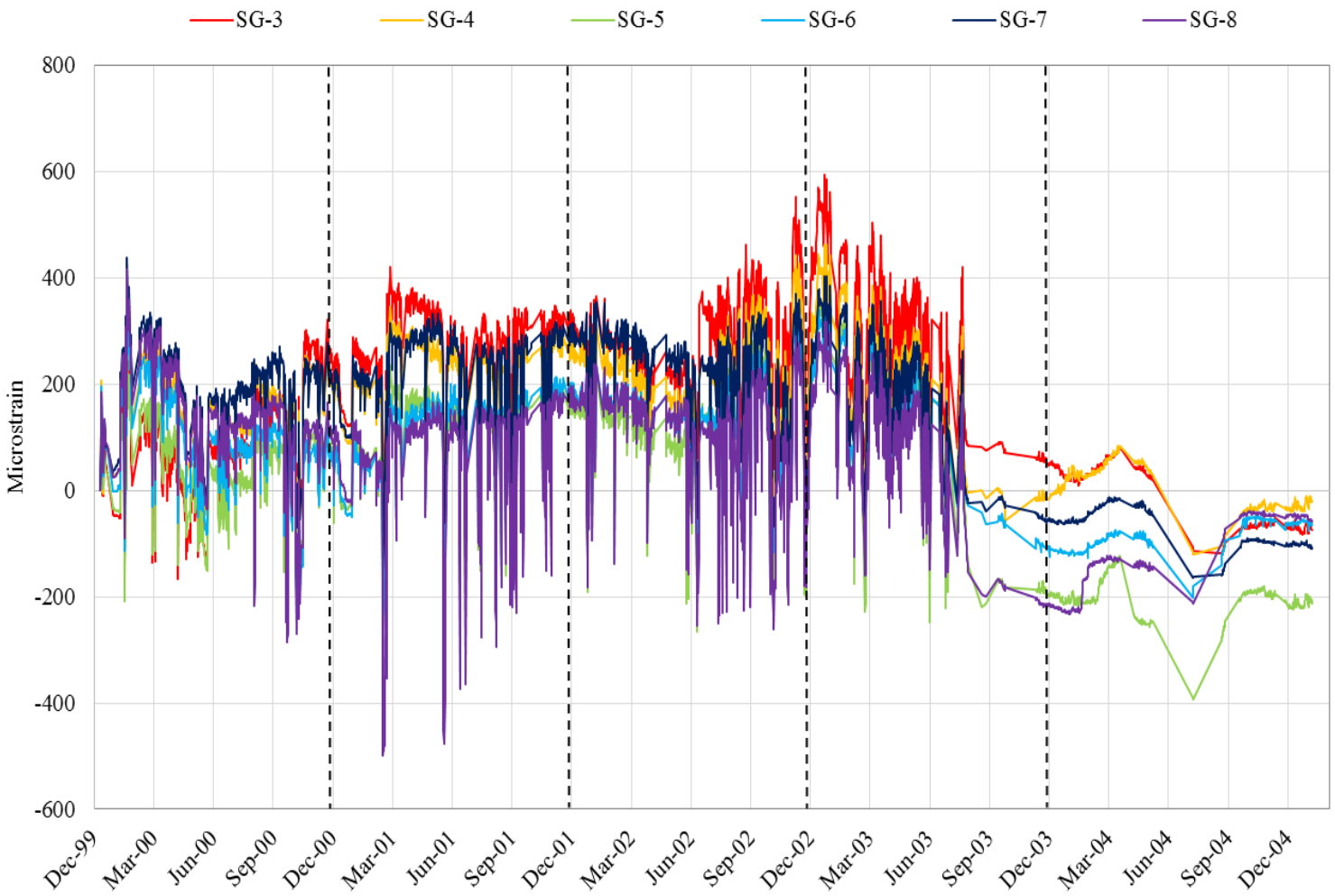

Figure 4.16 Longitudinal Strain at 90° throughout Pipeline Monitoring Time

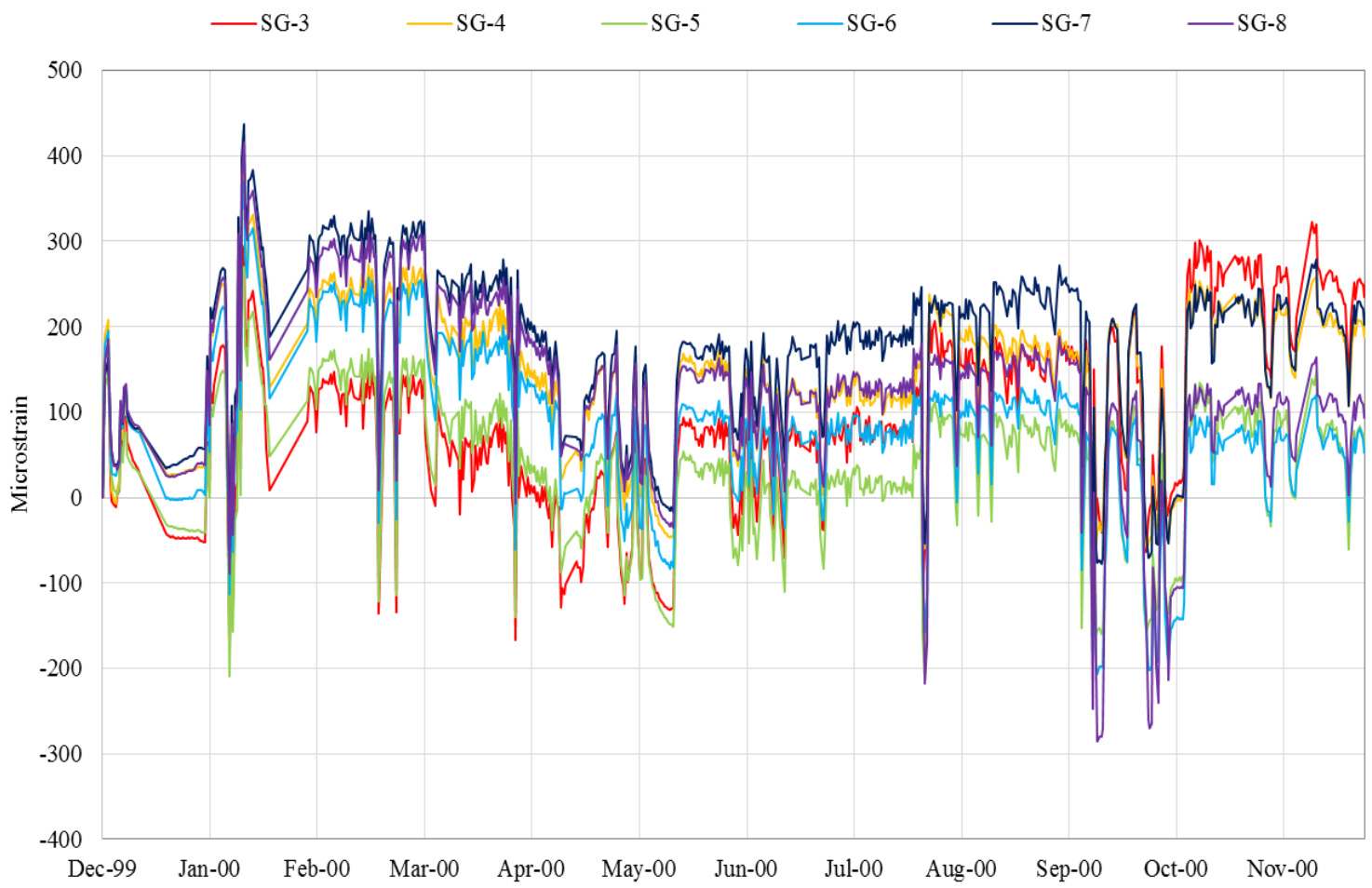

Figure 4.17 Longitudinal Strain at 90° in the First Year (Dec. 1999 Nov. 2000)

Figure 4.18 shows the longitudinal strain at SG-4 throughout the entire time. Generally, the longitudinal strains of the three orientations (0^o, 90^o, and 270^o) were in tension if the noise was excluded from consideration. From September 2000 to June 2002, the three strain curves had the same trend, and an inverse sawtooth pattern existed during this period. The similar trend continued until August 2003. After the chilled air was stopped in August 2003, the strain at 270^o dropped suddenly and returned to normal around December 2003. The 180^o strain measured at SG-4 was considered abnormal data and was not included.

Figure 4.19 shows the longitudinal strain at SG-7 throughout the entire time. The strain at the four orientations (0^o, 90^o, 180^o, and 270^o) was in tension except some portion of the strain curve at 180^o. The strain at 90^o and 270^o almost had nearly the same trend as SG-4. After the chilled air was ceased, the strain at all orientations dropped slowly until they returned to the general trend in May 2004, followed by an abrupt drop until September 2004. After that they remained stable to the end of monitoring.

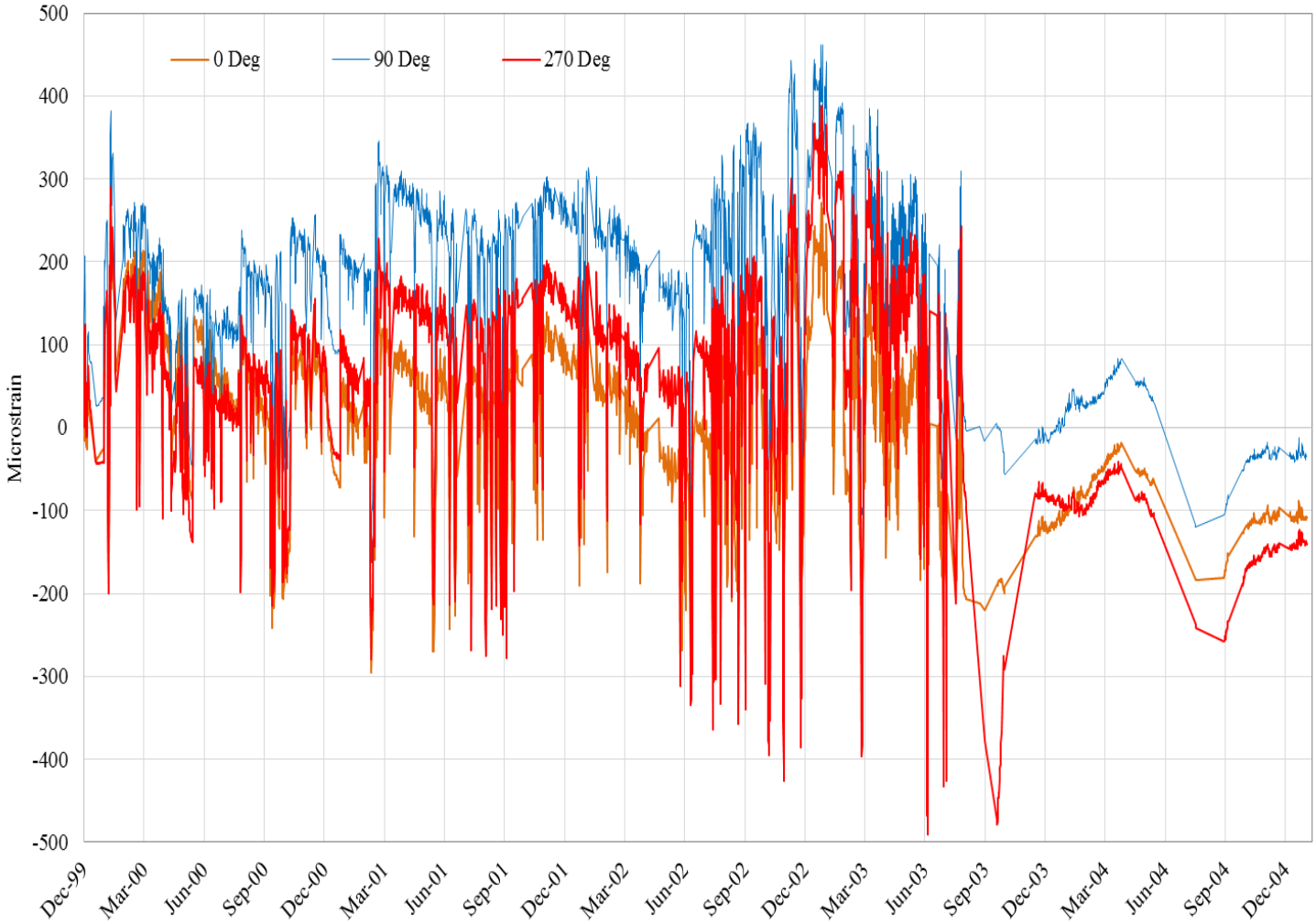

Figure 4.18 Longitudinal Strain at SG-4 throughout Pipeline Monitoring Time

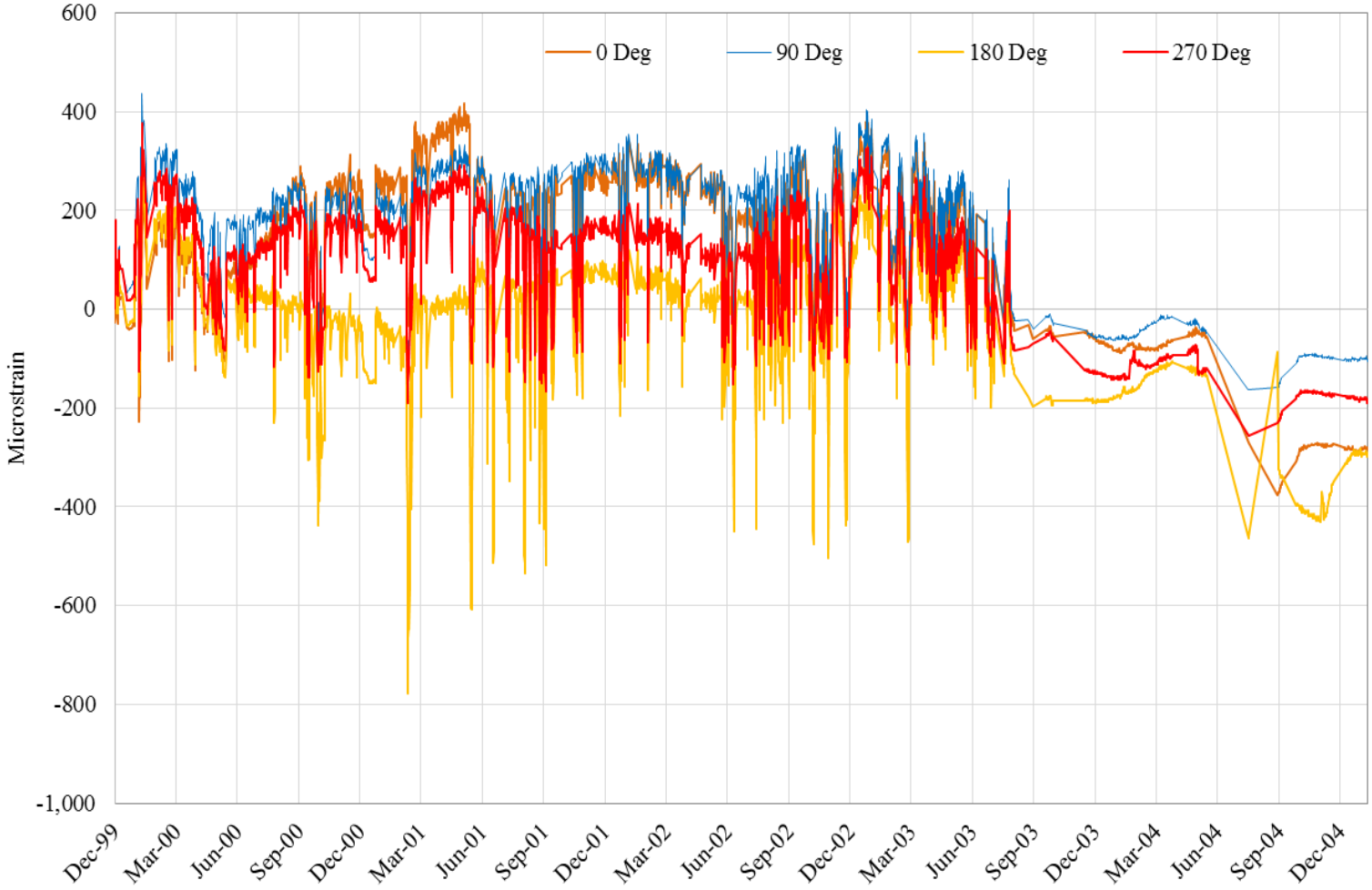

Figure 4.19 Longitudinal Strain at SG-7 throughout Pipeline Monitoring Time

4.3 Strain distribution

As discussed in the previous chapters, the primary objective of the full-scale experiment was to investigate the pipeline response due to differential heave. The differential heave in the transition zone imposes bending on the pipeline and causes relative axial movement (or potential movement) on the interface between the pipeline and the soil. In this section, the strain distributions on cross sections and along the longitudinal direction are analyzed.

4.3.1 Strain distribution on cross sections

It is commonly assumed that the strain of the pipeline is mainly caused by bending action. However, the real interaction between the soil and the pipeline can be very complicated. Miki et al. (2000) presented a study of a full-scale laboratory test to investigate the behavior of steel pipe subjected to bending. The laboratory test was well controlled and the corresponding stress/strain condition was relatively simple. The strain distribution presented by Miki was used as a reference. In a test, the bent pipe was pushed or pulled at both ends. The associated motions were denoted as "closing mode bending" or "opening mode bending", respectively. The strain distribution on the cross section due to closing mode bending is illustrated in Figure 4.20. Both longitudinal and circumferential strain are measured at the central section of pipe. The top of the pipe is designated as 0^o and the bottom is designated as 180^o. In theory, the bent pipe is symmetric to the vertical plane along the longitudinal direction. Miki's test results confirmed the theoretical analysis and showed that the strain distribution is symmetrical to the 0^o-180^o centerline. The maximum longitudinal tensile strain is along the springline, near 90^o and 270^o. The maximum longitudinal compressive strain is at 180^o. Meanwhile, the maximum circumferential tensile strain is on both sides of the pipe, (i.e., at 90^o and 270^o). The circumferential strain at 0^o and 180^o are approximately the same and are the maximum compressive strain.

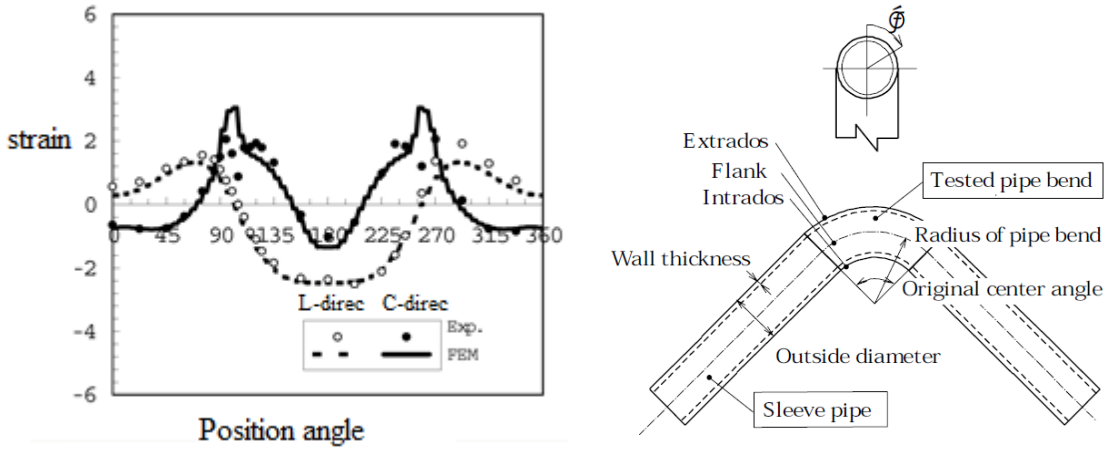

Figure 4.20 Strain Distribution on Pipeline Cross Section at Different Position Angles due to Closing Mode Bending (Miki et al., 2000)

At the Fairbanks, Alaska test facility, SG-4 and SG-7 were located at 24 m and 32.16 m from the inlet riser, respectively. This area was near the non-permafrost-permafrost boundary. Figure 4.21 illustrates the strain distribution on the cross section at different times based on the monthly average strain measured at SG-4. Both longitudinal and circumferential strain were included in the figures. Since Figure 4.21 was used to illustrate strain distribution on the cross section, for comparison purposes, the abnormal strain of SG-4 at 180^{o} was also included. The strain distribution was symmetric. The circumferential strain was in the range of 100 to 500 με before the chilled air was stopped. The maximum circumferential tensile strain was obtained at 0^{o}, followed by strain at 180^{o}. Circumferential compressive strain was not measured on this chilled pipeline. The lowest circumferential strain was obtained at 90^{o} and 270^{o}. As the chilled air was stopped after August 2003, the circumferential strain decreased dramatically (Figure 4.21h). Generally speaking, the distributions of both circumferential and longitudinal strain on the cross section at SG-4 were different from the findings reported by Miki et al. (2000). The reason could be that Miki investigated the strain distribution of pipe in the pure bending motion, while the pipeline in the Fairbanks test facility was subject to both bending and

interaction with the surrounding soil. In addition, the distribution reported by Miki was on the point where maximum bending accrued, but the location of SG-4 was not.

Figure 4.22 illustrates the distribution of monthly average strain on the cross section at SG-7. It can be seen that the distribution of longitudinal strain is similar to the one reported by Miki et al. (2000). The maximum longitudinal tensile strain was at the 270^{o} position and the maximum longitudinal compressive strain was at 180^{o}. Due the complicated stress conditions of the buried pipeline, the distribution was not exactly symmetric. Such findings indicated that bending was one of the primary loading conditions on the pipeline. The strain distribution of circumferential strain at SG-7 was similar to the conditions at SG-4, but was still different from the strain distribution reported by Miki et al. (2000).

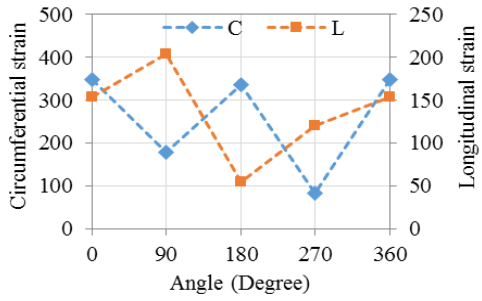

a) Mar. 2000

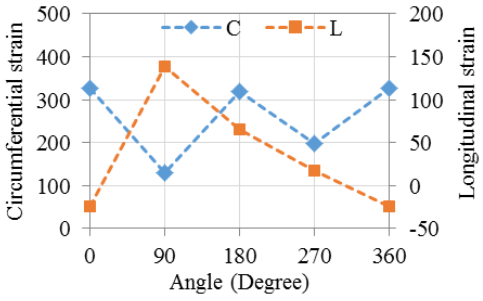

b) Sep. 2000

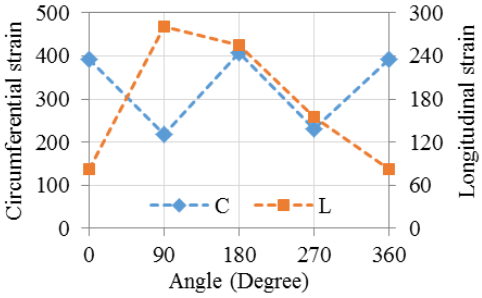

c) Mar. 2001

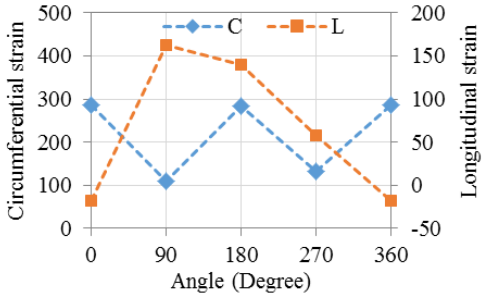

d) Sep. 2001

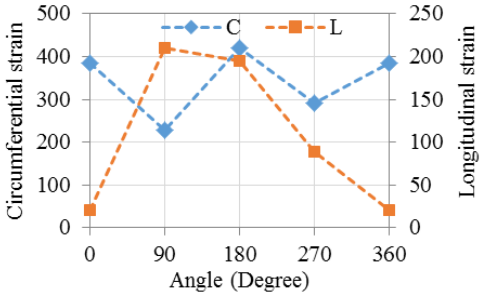

e) Mar. 2002

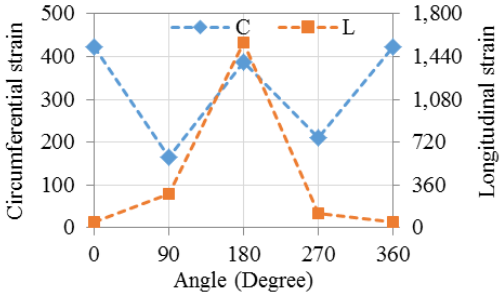

f) Sep. 2002

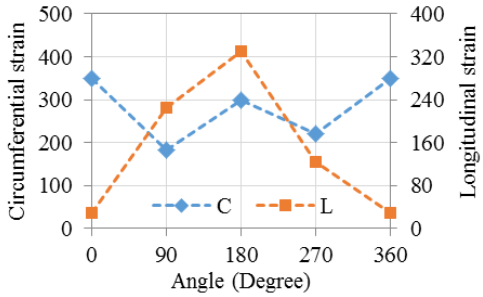

g) Mar. 2003

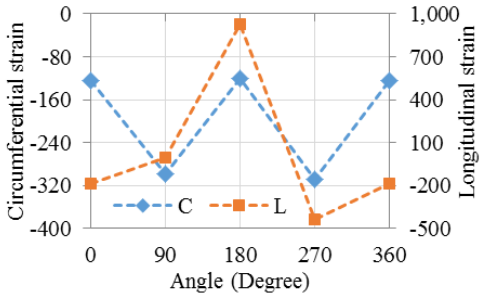

h) Sep. 2003

Figure 4.21 Distribution of Monthly Average Strain on Cross Section at Different Orientations (SG-4)

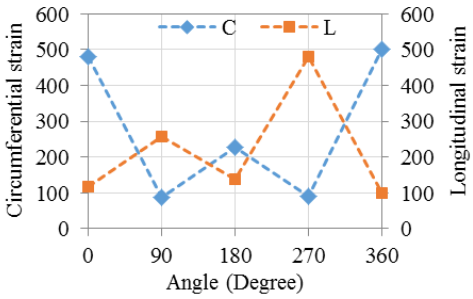

a) Mar. 2000

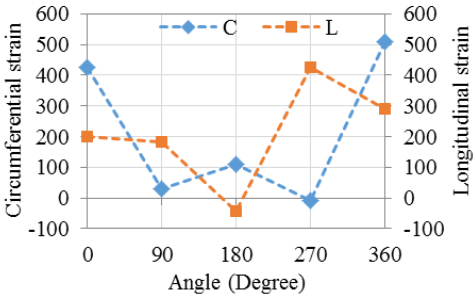

b) Sep. 2000

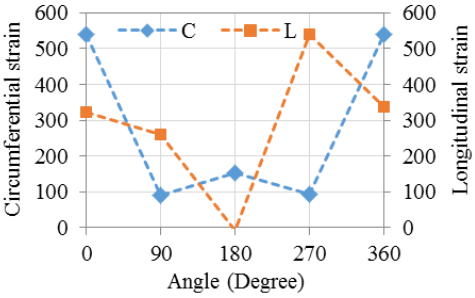

c) Mar. 2001

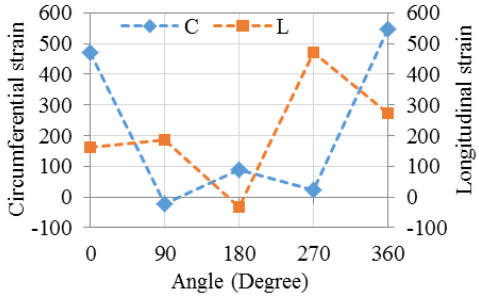

d) Sep. 2001

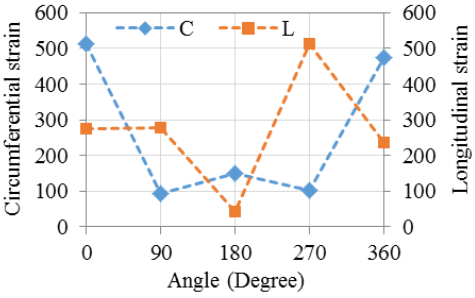

e) Mar. 2002

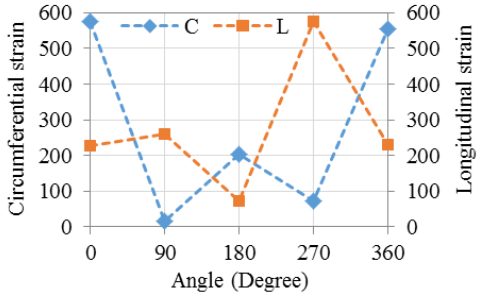

f) Sep. 2002

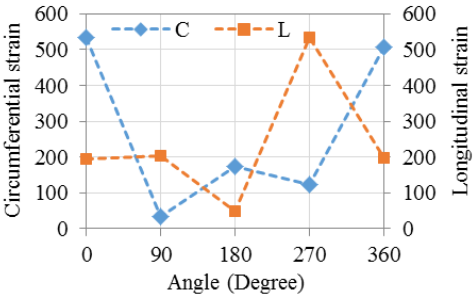

g) Mar. 2003

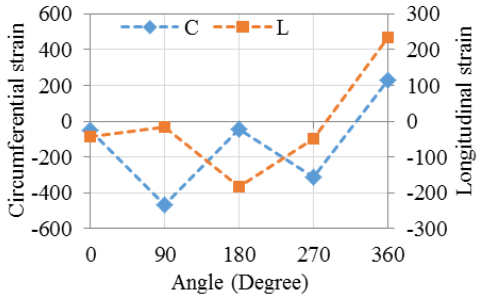

h) Sep. 2003

Figure 4.22 Distribution of Monthly Average Strain on Cross Section at Different Orientations (SG-7)

4.3.2 Distribution of strain in longitudinal direction

The distributions of strain in the longitudinal direction are presented in Figure 4.23 to Figure 4.26. Each figure shows the distribution of monthly average longitudinal strain along the pipe from 2000 to 2003. For each figure, the monthly average strain from March and September were used. They include the strains measured at 0^o, 90^o, and 180^o. Only a few strain gauges were also installed at 120^o, 240^o, and 270^o. As this limited data would not reveal a distribution of longitudinal strain at those orientations that could represent the real field conditions, they were not included in the diagrams.

As mentioned in the strain development, longitudinal strain due to differential heave began to develop in March 2000 and became relatively constant until the end of the first operational year. It can be seen from Figure 4.23 that in March 2000, the pipe segment between about 20 to 35 m experienced larger induced strain than pipe outside the permafrost-non-permafrost boundary; however, no particular trend of strain distribution was observed.

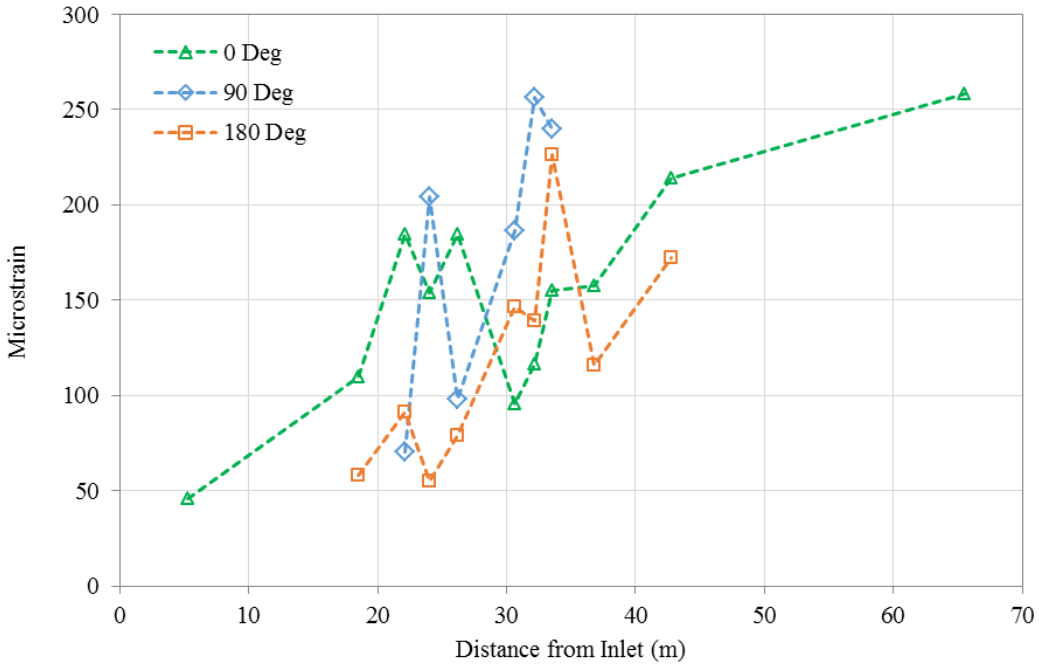

a) Mar. 2000

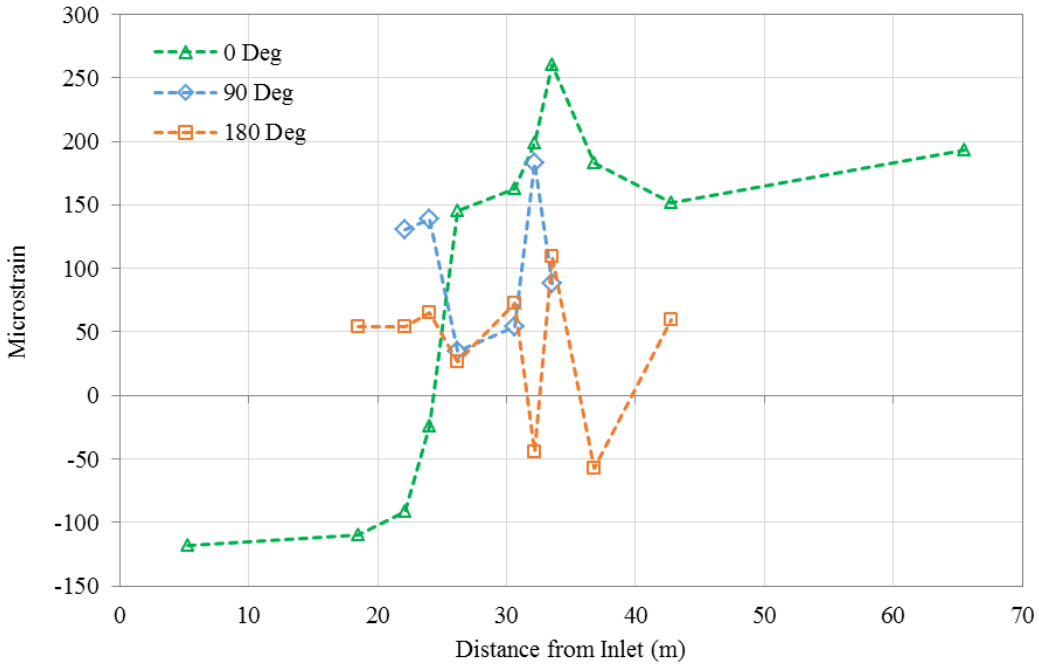

b) Sep. 2000

Figure 4.23 Distribution of Monthly Average Longitudinal Strain along Pipeline in 2000

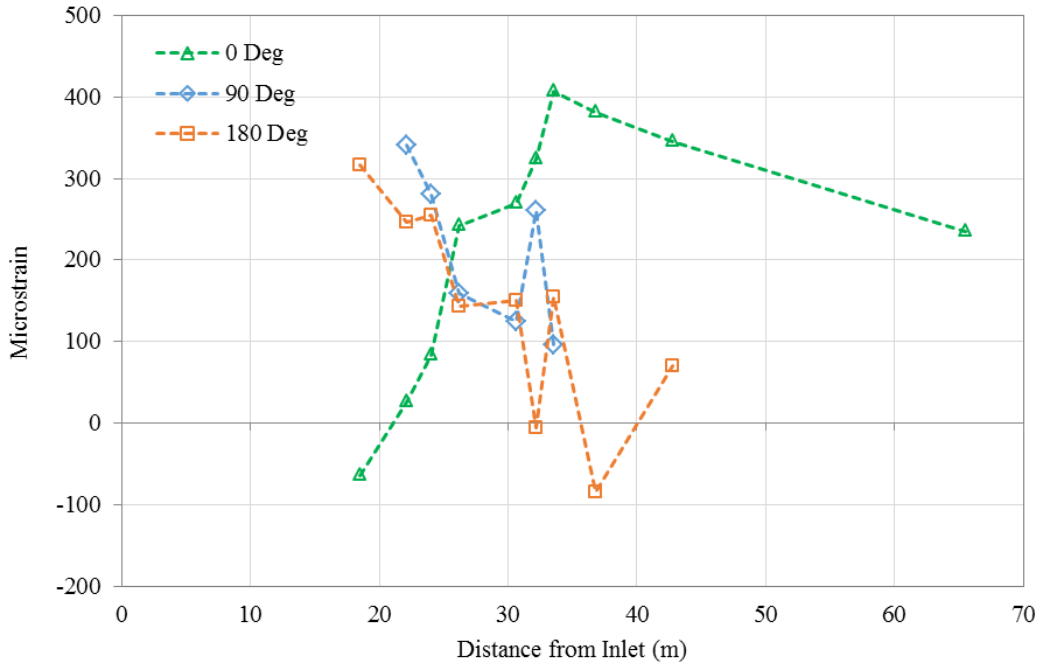

a) Mar. 2001

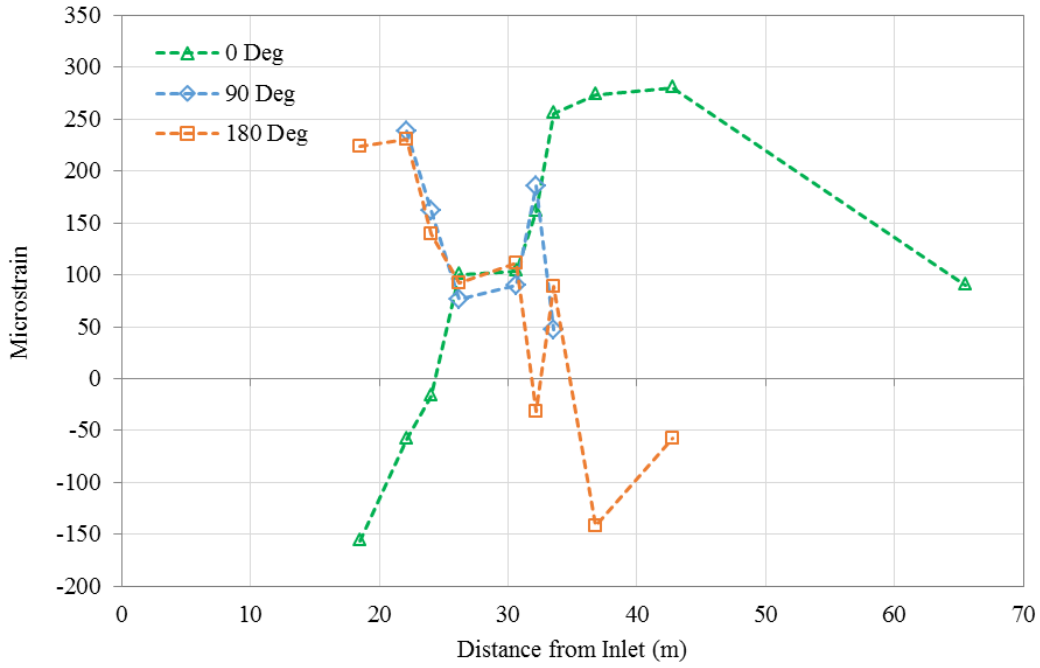

b) Sep. 2001

Figure 4.24 Distribution of Monthly Average Longitudinal Strain along Pipeline in 2001

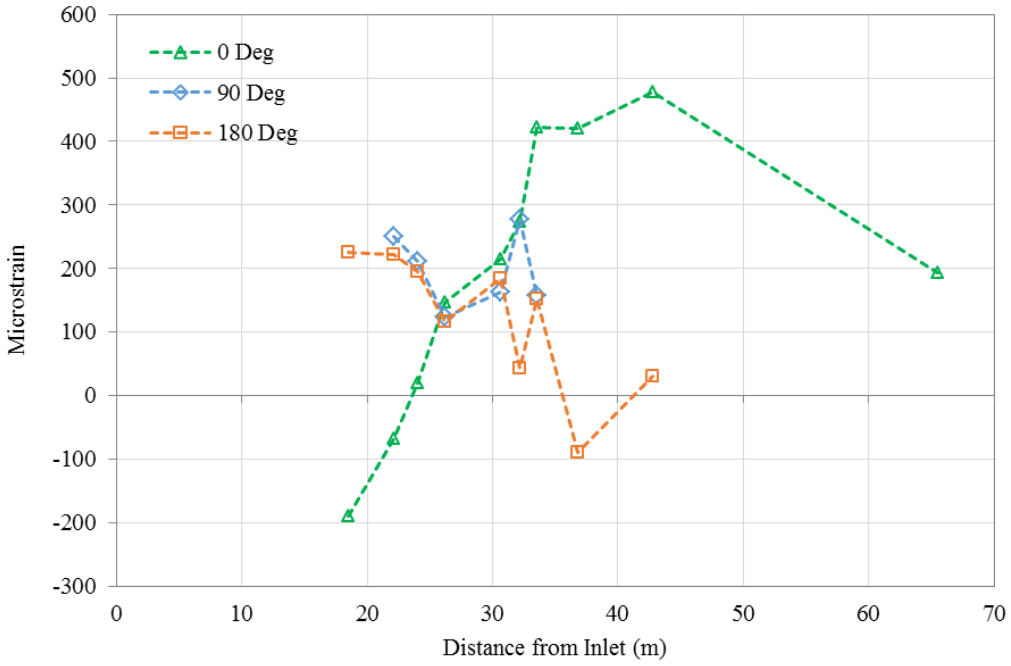

a) Mar. 2002

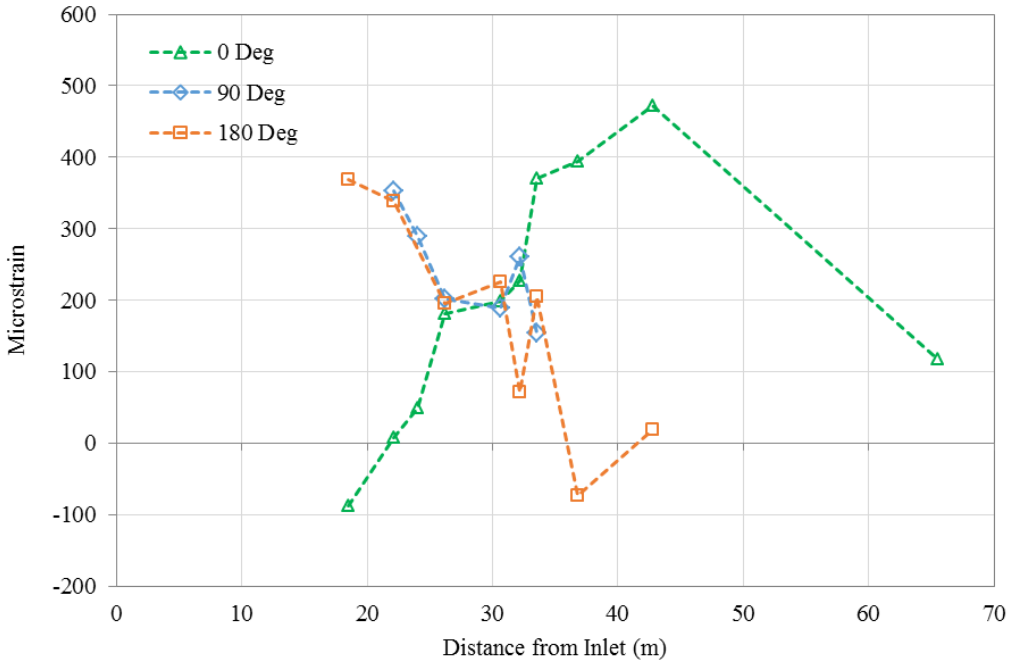

b) Sep. 2002

Figure 4.25 Distribution of Monthly Average Longitudinal Strain along Pipeline in 2002

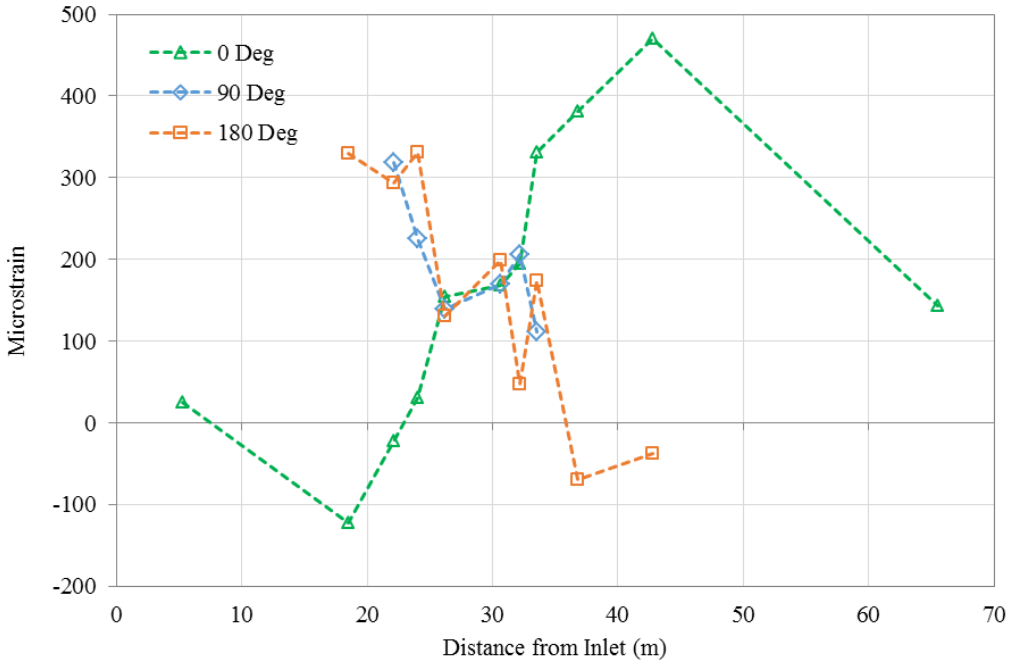

a) Mar. 2003

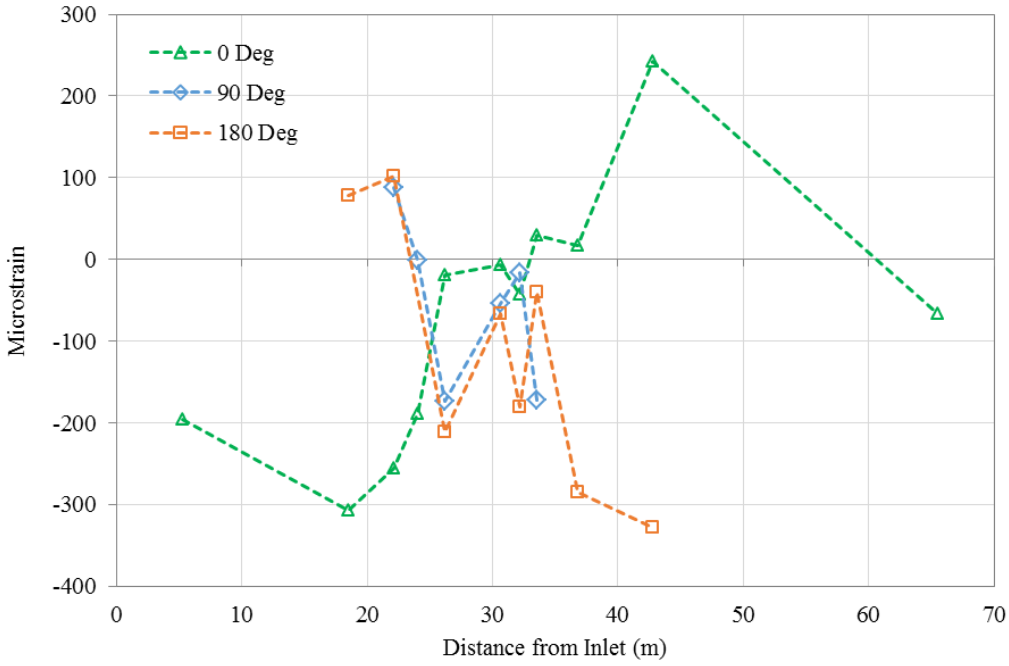

b) Sep. 2003

Figure 4.26 Distribution of Monthly Average Longitudinal Strain along Pipeline in 2003

In September 2000, the maximum tensile strain at 0^o was observed at 33 m from the inlet riser (Figure 4.23b), and at 18 m, the compressive strain at 0^o was close to the maximum value. The locations of maximum tensile and maximum compressive strain were located near the boundaries of the transition zone. As shown in Figure 4.24a, from SG-2 through SG-10, the 180^o strain of the pipeline decreased as the distance from the inlet riser increased. The maximum tensile strain at 180^o was at the same location as the maximum compressive strain at 0^o, and vice versa. The distribution of strain at 90^o was similar to the 180^o strain. As indicated in Figure 4.25 and Figure 4.26, the strain distribution at 0^o reached its maximum tensile strain value of 490 με in March 2002 and remained near this value until the end of pipeline operation.

The differential heave caused relative vertical movement of the foundation soil near the boundary between permafrost and non-permafrost, which imposed bending moment on the pipeline. Such bending moment was the primary loading condition for the pipeline at the test site and the dominant factor for the distribution of the longitudinal strain. After September 2000, the distribution of longitudinal strain along the pipeline could be simplified as an "X" pattern according to observations obtained from Figure 4.23 to Figure 4.26. As shown in Figure 4.27, the location of the maximum compressive strain at 180^o approximately aligned with the largest heave measured from the heave rods, which could be the maximum upward bending location. The corresponding point was designated as point A (see Figure 4.27b). In Figure 4.27b， the dash line passing the point B corresponds to the dash line on the left in Figure 4.27a, and the dash line passing point A corresponds to the dash line on the left in Figure 4.27a. At point A, as the pipeline was bent upwards, the top of the pipeline (0^o) was in the maximum tension and the bottom (180^o) was in the maximum compression.

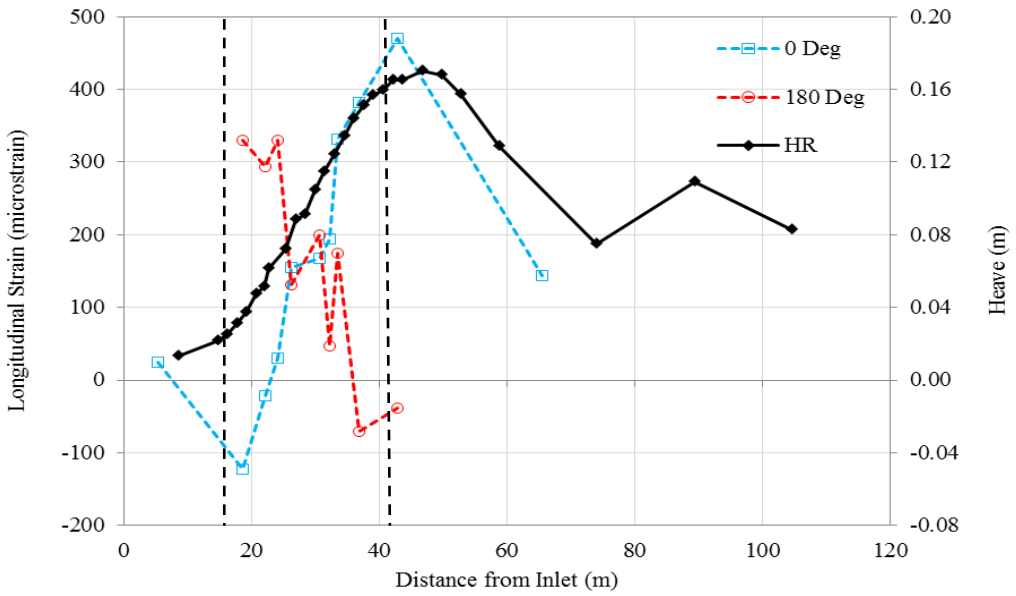

(a) Profiles of Strain and Heave along the Pipeline (March 2003)

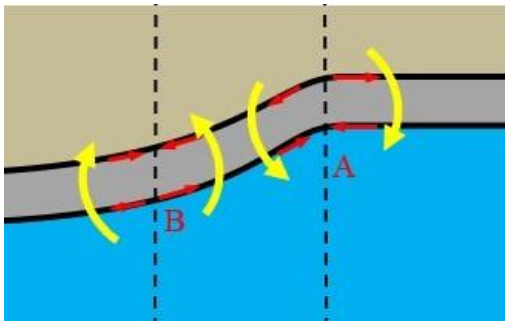

(b) Bended Pipeline Profile

Figure 4.27 Development of Longitudinal Strain

On the other hand, point B, where the maximum tensile strain at 180^{o} and the maximum compressive strain at 0^{o} was found, was the maximum downward bending location. At this point, the situation was opposite. As the pipeline bent downwards, the top of the pipeline was in the maximum compression and the bottom was in the maximum tension. In addition, the two ends of the pipeline were fixed. Due to differential heave, the length of the pipeline was extended. Therefore, the pipeline underwent additional tension, and the strain distribution curves for both 0^{o} and 180^{o} were shifted toward tension.

CHAPTER 5. CORRELATION BETWEEN STRAIN AND FROST HEAVE

This chapter analyzes the correlation between measured longitudinal strain and differential frost heave. The analysis was performed using a statistical regression approach. The equation that describes the heave profile within the transition zone was developed and the time factor was incorporated into the regression coefficients. The correlation between longitudinal strain and heave movement was established. The regression equations can be used to estimate the strain on the top and bottom of a chilled pipeline due to differential frost heave, where the site conditions are similar to the testing facility.

5.1 Regression equations for heave development

Figure 5.1 shows the distribution of strain at the top (0^o) and bottom (180^o) of the pipe along the entire length in March 2003, as well as the profile of frost heave indicated by heave rod (HR) measurements. The two vertical dash lines highlight the edges of the transition zone determined by the pipe's vertical movement. The interface between permafrost and non-permafrost was at 30 m from the inlet riser of the pipeline (Akagawa, 2012). The edges of the transition zone were about 20 m away from the interface on both sides. However, the exact boundaries of the transition zone were difficult to define. The regression analysis between heave movement and location of the heave rods was only performed on data collected in the transition zone (i.e., from HR-1 at 8.53 m to HR-22 at 46.6 m).

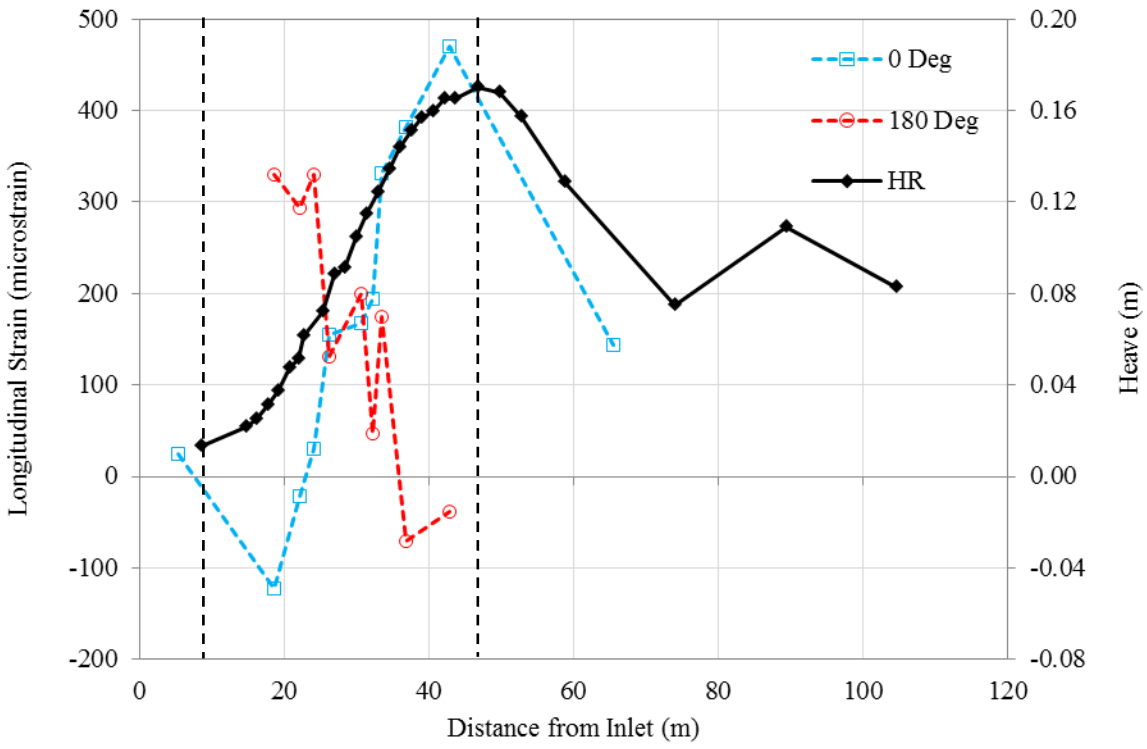

Figure 5.1 Profiles of Strain and Heave along the Pipeline (March 2003)

5.1.1 Multiple regression analyses for heave location and time

A third order polynomial function was used to fit the monthly average heave versus the distance from the inlet riser:

$$H = a_0 + a_1x + a_2x^2 + a_3x^3 \quad (5.1)$$

where

H = heave (m),

x = distance from the inlet riser (m), and

a_0, a_1, a_2, and a_3 = regression constants.

Figure 5.2 shows the monthly average heave in the transition zone fitted by the polynomial function. Six data series are included and each data series represents the heave profile along the pipeline at a specific time. Three years of measurements were included, and in each year the data sets in March and September were selected for illustration purposes. It can be seen that the third order polynomial function fits the heave data very well, except for the data series from March 2000. During the early days of the pipeline operation, the pipeline was still experiencing settlement and the general trend of a heave profile was not developed yet. As time elapsed, the trend of the heave profile gradually appeared. The rate and the cumulative amount of heave at the left boundary were also increasing through the monitoring time.

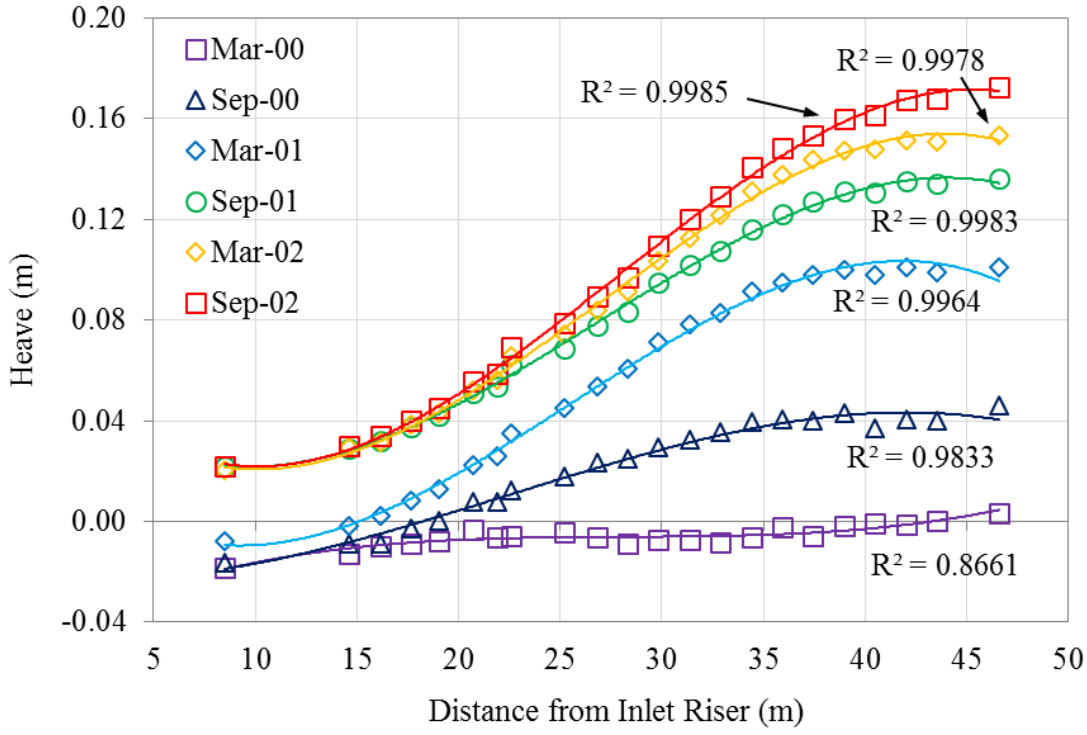

Figure 5.2 Third Order Polynomial Fit of Monthly Average Heave as a Function of Distance from the Inlet Riser from 2000 to 2002

The R^2 values of the regression, which account for the correlation between heave and distance, are plotted versus the operation date in Figure 5.3. The chart clearly shows that as operation time continued beyond the first nine months, the value of R^2 increased sharply. By June 2000, the R^2 increased to 0.9584. To exclude the transient heave behavior of the pipe during the early operation, the time factor was incorporated based on the data obtained from June 2000 onward.

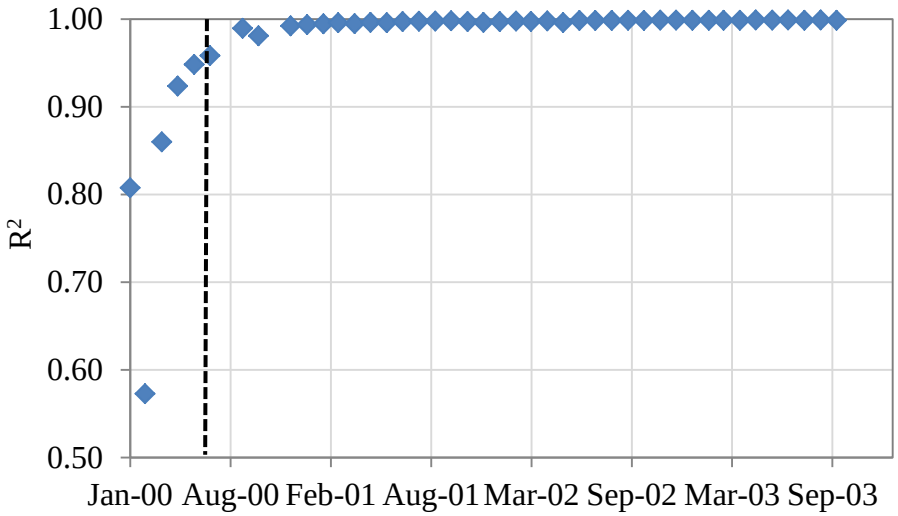

Figure 5.3 Summary of R^2 from January 2000 to September 2003

The maximum monthly average heave among all heave rods was calculated for each month from January 2000 to September 2003. The data is plotted as shown in Figure 5.4. The data shows that the heave peaked in November 2002, at about the time the 2002 Denali Fault earthquake stuck, as indicated by the dash line in the figure. From December 2002 until May 2003, the heave started to decrease. The maximum heave was not reached again, even though the chilled air was provided for additional months of cooling. In this study, the time factor was incorporated in the analysis based on heave data obtained from June 2000 to November 2002.

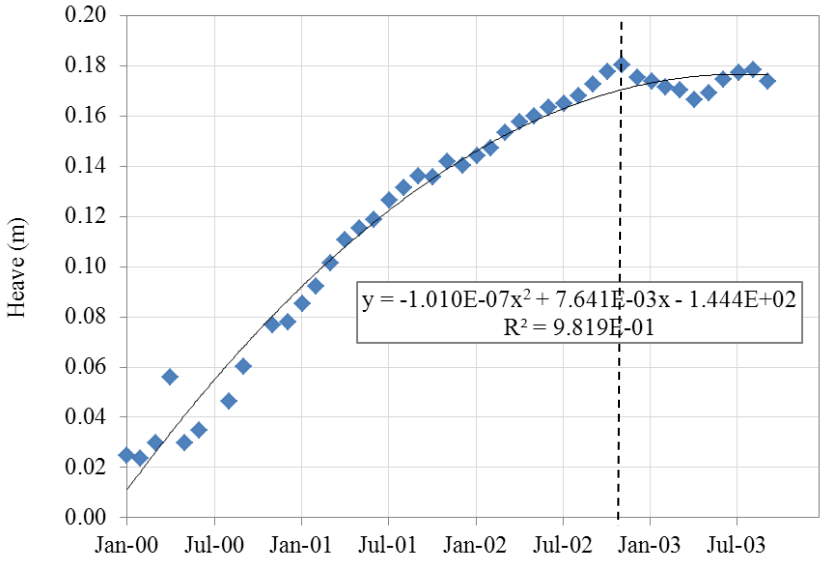

Figure 5.4 Summary of Maximum Monthly Heave along the Pipeline from January 2000 to September 2003

The time factor of frost heave was incorporated based on the correlations between time and regression constants: a_0, a_1, a_2, and a_3. The correlations coefficients are presented in Figure 5.5 to Figure 5.8. In these figures, Day 1 was the beginning of operation on December 11, 1999. As shown in these charts, a_0 and a_2 increase with time. Near the end of the selected time, the regression constants level off and reach their maximum values. Meanwhile, a_1 and a_3 decrease with time. A second order polynomial function was used to fit the data for each correlation coefficient. The R^2 values were 0.9770, 0.9299, 0.9033 and 0.8487 for a_0, a_1, a_2, and a_3, respectively. The regression equations for each correlation coefficient are:

$$a_0 = -1.488 \times 10^{-7}t^2 + 2.958 \times 10^{-4}t - 1.01 \times 10^{-1} \quad (5.2)$$

$$a_1 = 1.663 \times 10^{-8}t^2 - 2.963 \times 10^{-5}t + 7.893 \times 10^{-3} \quad (5.3)$$

$$a_2 = -7.076 \times 10^{-10}t^2 + 1.245 \times 10^{-6}t - 2.417 \times 10^{-4} \quad (5.4)$$

$$a_3 = 1.588 \times 10^{-13}t^2 - 2.624 \times 10^{-10}t + 4.362 \times 10^{-8} \quad (5.5)$$

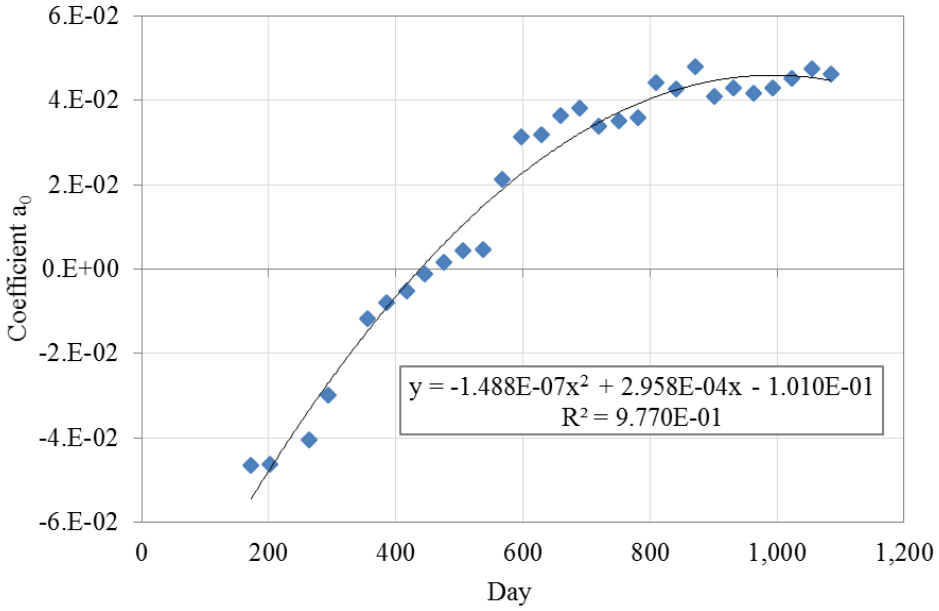

Figure 5.5 Relationship between a_0 and Pipeline Operation Time

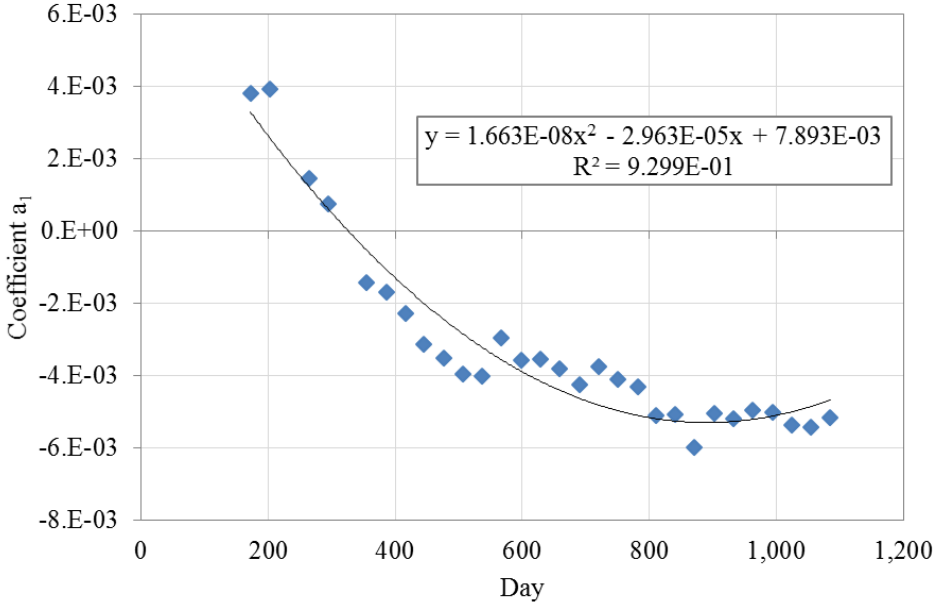

Figure 5.6 Relationship between a_1 and Pipeline Operation Time

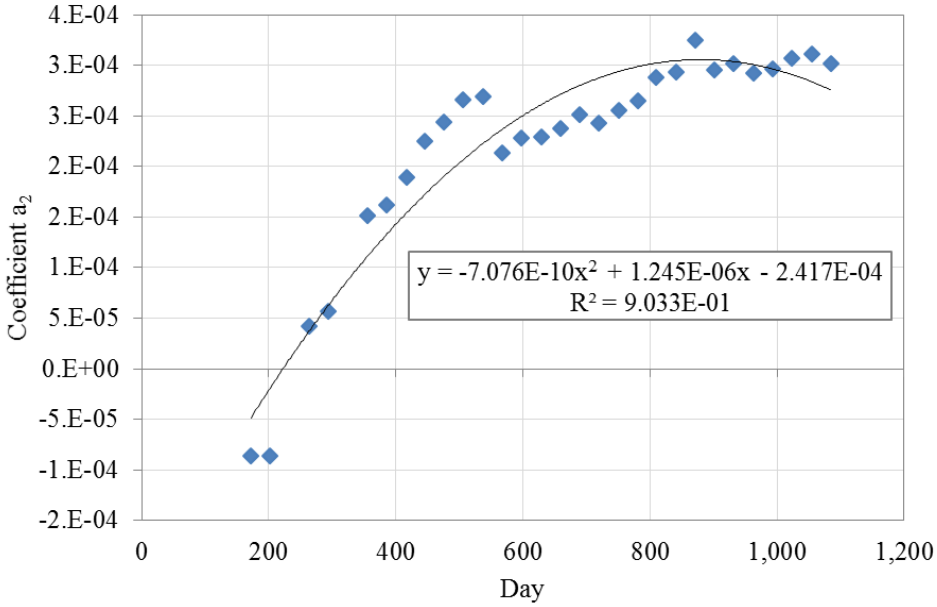

Figure 5.7 Relationship between a_2 and Pipeline Operation Time

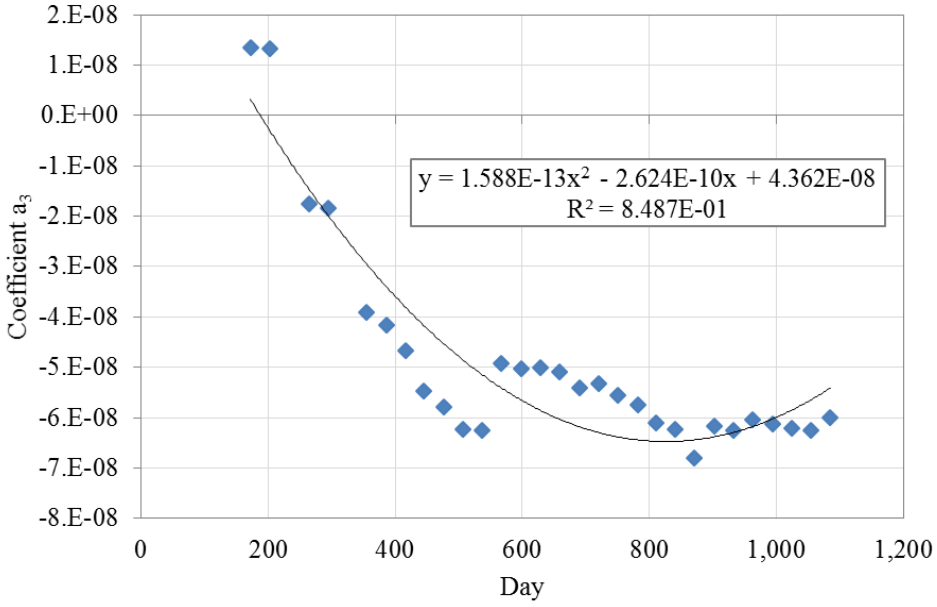

Figure 5.8 Relationship between a_3 and Pipeline Operation Time

5.1.2 One regression analysis for heave location and time

By substituting Eq. 5.2 to Eq. 5.5 into Eq. 5.1, a general relationship was obtained to estimate pipeline heave based on the distance from the inlet riser and time. The overall regression equation is:

$$H = (i_0 + i_1 t + i_2 t^2) + (j_0 + j_1 t + j_2 t^2)x + (k_0 + k_1 t + k_2 t^2)x^2 + (n_0 + n_1 t + n_2 t^2)x^3 \quad (5.6)$$

where

H = heave (m),

x = distance from the inlet riser (m),

i, j, k, and n = regression constants, and

t = time in days of operation starting with December 11, 1999 as Day 1.

The coefficients of Eq. 5.6 were recalculated for one step regression based on the data collected from 22 heave rods from June 2000 to November 2002. Figure 5.9 shows the predicted versus measured heave. The predictive equation has an R^2 of 0.9892. Each coefficient of the predictive equation is summarized in Table 5.1.

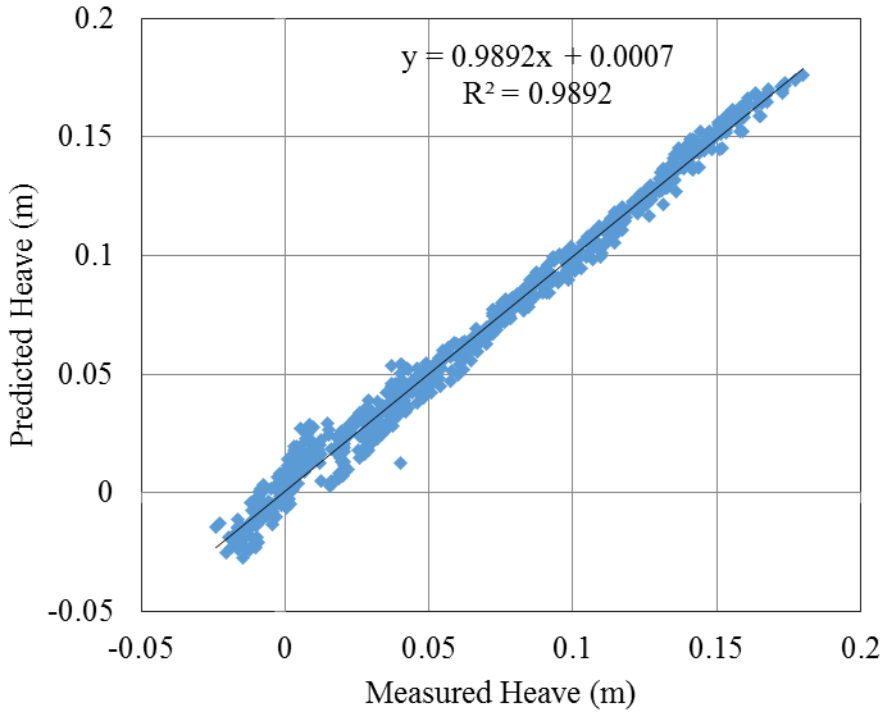

Figure 5.9 Predicted vs. Measured Heave

Table 5.1 Coefficients of Predictive Equation for Pipeline Heave

Terms	$\mathbf{i_0}$	$\mathbf{i_1}$	$\mathbf{i_2}$
Coefficients	-6.8879×10^{-02}	2.3903×10^{-04}	-1.01343×10^{-07}
Terms	$\mathbf{j_0}$	$\mathbf{j_1}$	$\mathbf{j_2}$
Coefficients	6.7739×10^{-03}	-3.4650×10^{-05}	1.8590×10^{-08}
Terms	$\mathbf{k_0}$	$\mathbf{k_1}$	$\mathbf{k_2}$
Coefficients	-3.0364×10^{-04}	1.9832×10^{-06}	-1.1218×10^{-09}
Terms	$\mathbf{n_0}$	$\mathbf{n_1}$	$\mathbf{n_2}$
Coefficients	3.7919×10^{-06}	-2.5903×10^{-08}	1.5411×10^{-11}

5.2 Correlation between longitudinal strain at 0^o and heave

The correlation between longitudinal strain at 0^o and frost heave was also analyzed. As shown in Figure 2.3 and Figure 5.1, SG-2 to SG-10 were in the transition zone and the strain measured at top of the pipeline at these locations was used for analysis. Since the locations of the strain gauges and the heave rods were not exactly the same, the

corresponding frost heave at each strain gauge location was calculated using Eq. 5.6. Analysis indicated a linear trend between strain and heave, with an R^2 of 0.6977. Frost heave at each strain gauge location also was calculated using the interpolation method based on the measurements of two adjacent heave rods. The regression was based on the monthly average strain and the monthly average heave. A new database was developed including all longitudinal strain at 0^o and heave from SG-2 to SG-10. The time domain was from June 2000 to November 2002. The data is plotted in Figure 5.10. The linear regression has an R^2 of 0.6977. The measured strain is within ±203.2 με of the estimated value, as shown by the 95% confidence intervals in Figure 5.10. Eq. 5.7 can be used to estimate the longitudinal strain at 0^o after heave is measured:

$$S_{0^\circ} = 4162.6H - 218.62 \tag{5.7}$$

where

S_{0° = longitudinal strain at 0^o (με), and

H = heave (m).

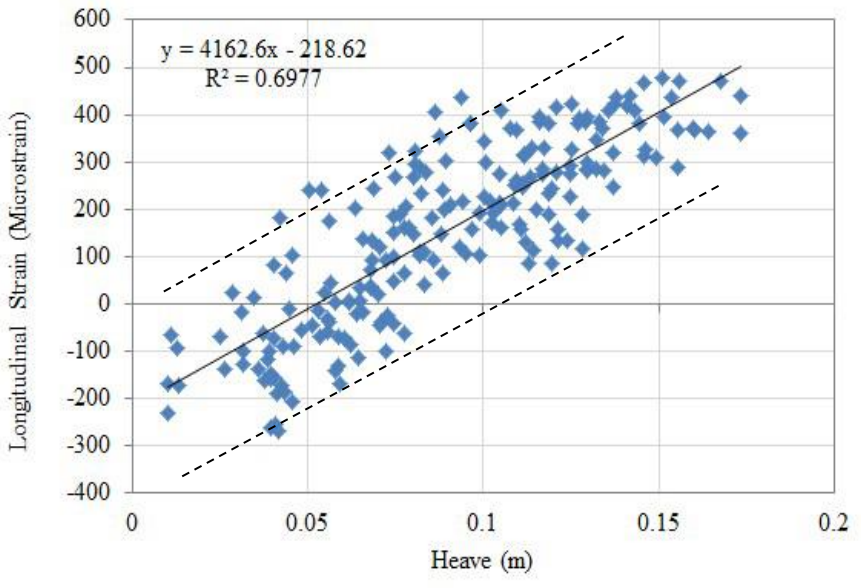

Figure 5.10 Correlation between Longitudinal Strain at 0^o and Heave

5.3 Correlation between longitudinal strain at 180^o and heave

Following the same approach, the correlation between longitudinal strain at 180^o and heave was also analyzed. Due to the abnormal strain measured at SG-4, the longitudinal strain at this station was removed entirely. The data is plotted in Figure 5.11, which indicates that as heave increases, the longitudinal strain at the bottom of the pipe decreases. Generally, a linear trend line can be fitted, but the associated R^2 of 0.4244 is not as high as that calculated for longitudinal strain at 0^o. The measured strain is within ±191.4 με of the estimated value, as indicated by the 95% confidence intervals. Eq. 5.8 can be used to estimate the longitudinal strain at 180^o when heave is measured:

$$S_{180^\circ} = 291.28 - 2170.4H \tag{5.8}$$

where

S_{180° = longitudinal strain at 180^o (με), and

H = heave (m).

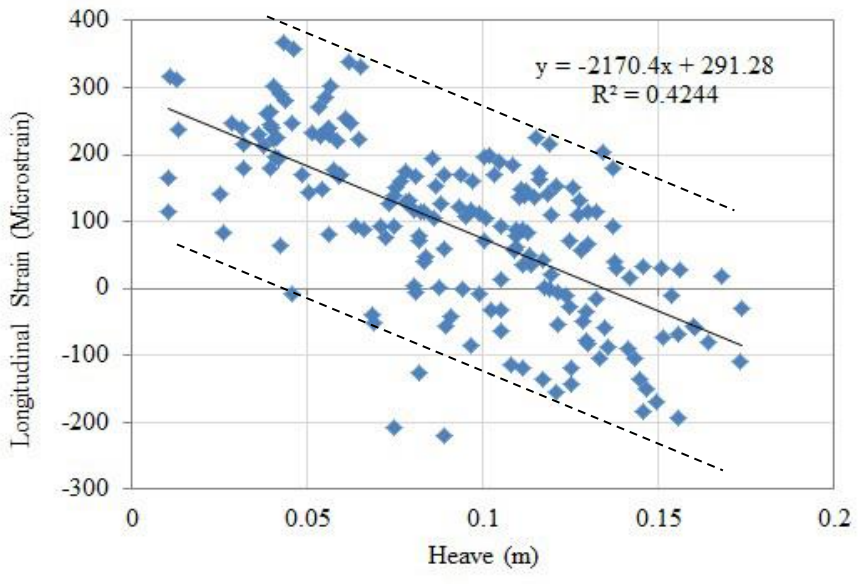

Figure 5.11 Correlation between Longitudinal Strain at 180^o and Heave

5.4 Correlation between longitudinal strain and time

In order to analyze the strain development over time and explore the likelihood of a predictive model, longitudinal strain at the bottom of the pipeline measured at SG-3 is plotted against operation time (Figure 5.12). The monthly average strain was used. It can be seen that the strain gradually increased during the pipeline operation, demonstrating a cyclic pattern. The length of a cycle was approximately 365 days, which indicated that the cyclic pattern was likely related to the air temperature change throughout the year. Based on the above observations and properties of mathematical functions, Eq. 5.9 is proposed as the predictive model of strain development:

$$S = a_0 + a_1 \times t + a_2 \times {a_3}^t \times \sin\left(\frac{2\pi}{365}(t + a_4)\right) \quad (5.9)$$

where,

S = longitudinal strain at the bottom of the pipeline (με),

t = time (days), and,

a_0, a_1, a_2, a_3, a_4 = constants.

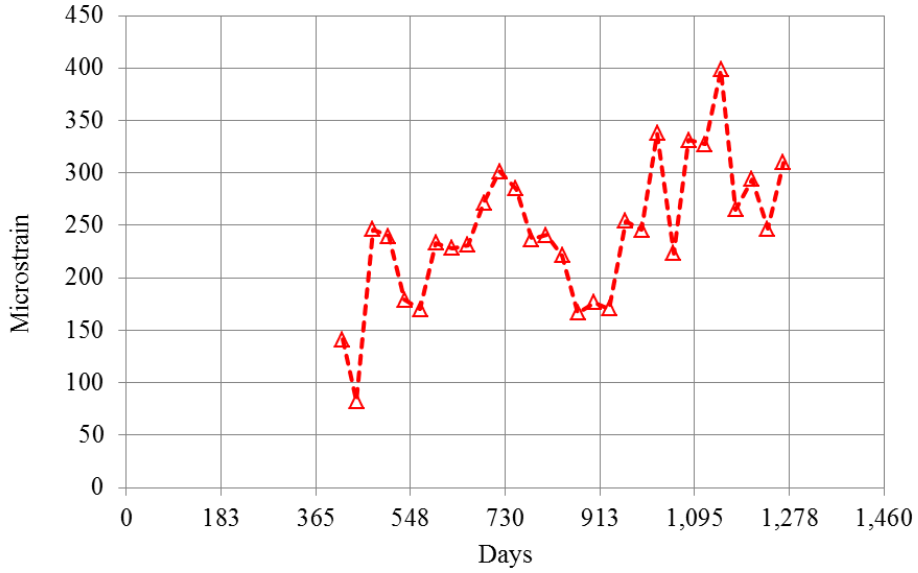

Figure 5.12 180° Strain Development over Time at SG-3

The proposed model contains two parts: $(a_0 + a_1 \times t)$ and $[a_2 \times {a_3}^t \times \sin\left(\frac{2\pi}{365}(t + a_4)\right)]$. The first part is a linear function, which is used to fit the general trend of a gradual strain increase during the pipeline operation. The second part is used to account for the cyclic pattern of strain, in which $\sin\left(\frac{2\pi}{365}(t + a_4)\right)$ represents the length and offset of the cyclic pattern. Since Figure 5.12 shows that the amplitude of the cyclic pattern decreases over time, instead of using a fixed value, $a_2 \times {a_3}^t$ is used to control the amplitude of the sinusoidal function, which is a power function with a_3 less than 1 to form a decreasing function.

The process of determining the values of constants is illustrated in Figure 5.13 and Figure 5.14. In Figure 5.13a, a linear trend line is fitted to the strain curve, which corresponds to $(a_0 + a_1 \times t)$. From this plot, the values of constants a_0 and a_1 were calculated as 113.87 and 0.154, respectively. The residuals between measured strain and fitted values calculated based on the linear trend line are plotted in Figure 5.13b. The cyclic pattern can be easily identified. Based on this observation, the sinusoidal function with the period length of 365 days can be used to fit the pattern with a maximum magnitude of 90 (Figure 5.13c). Accordingly, the value of a_2 was determined to be 80. The offset of sinusoidal function was determined by observing the difference between peaks of residual strain and the fitted sinusoidal function. The value of offset, a_4, was chosen as 110. The results are illustrated in Figure 5.13d.

So far, the only unknown value of a constant was a_3, which controlled the reduction of magnitude of the sinusoidal function. Based on a trial and error process, it was found that the value of a_3 needed to be greater than 0.999 and less than 1. Therefore, to accurately determine its value, six values of a_3, 0.999, 0.9992, 0.9994, 0.9996 and 1, were used in Eq. 5.9, and correlations between fitted and measured data set were plotted against trial values of a_3 (Figure 5.14). A second polynomial function was fitted and the maximum value of the function was reached when a_3 was equal to 0.9994.

As illustrated in Figure 5.15, the proposed model fits measured longitudinal strain well. In addition, measured versus fitted strain is plotted in Figure 5.16. The R^2 was 0.4943.

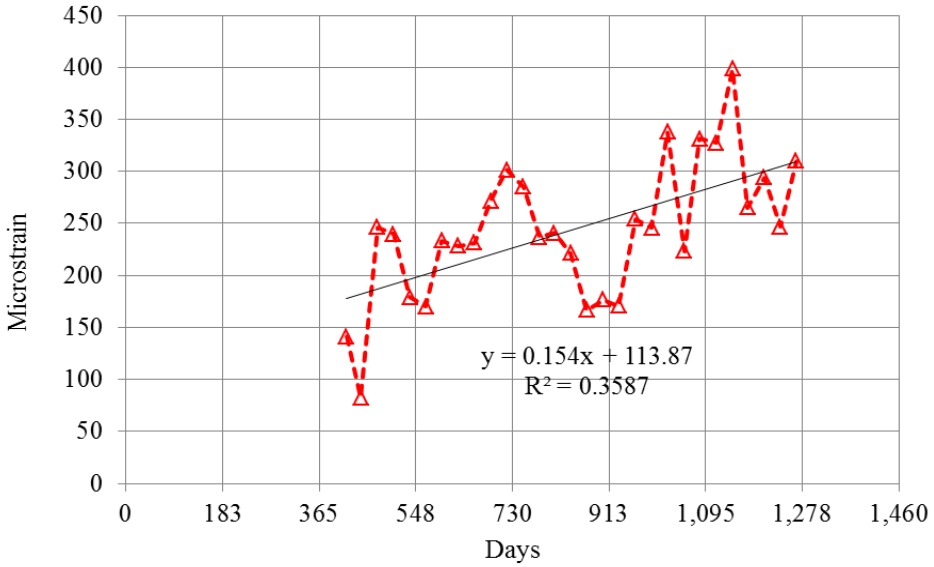

a) Linear function fitted to the strain curve

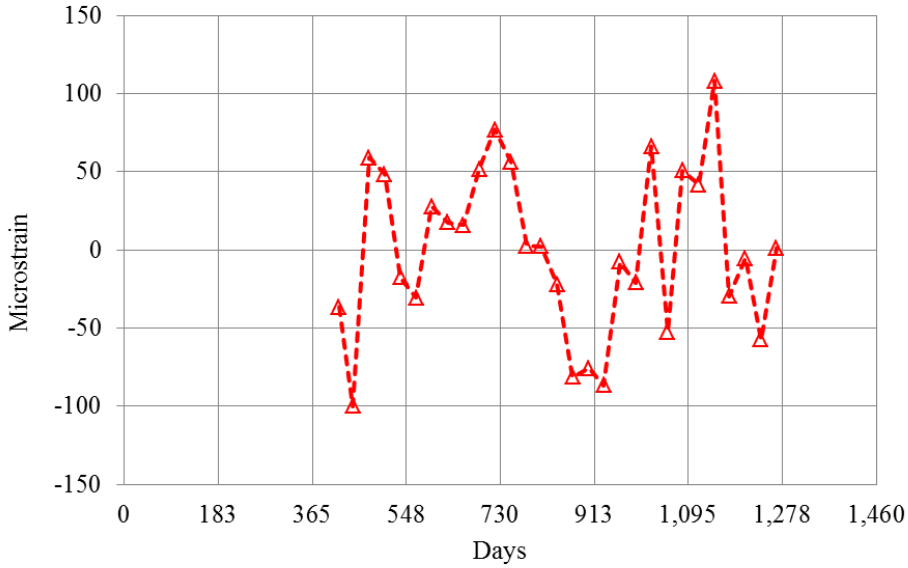

b) Residual between measured strain and fitted values
Calculated based on the linear trend line

Figure 5.13 The Process to Determine the Value of Constants in the Predictive Model for 180^o Strain at SG-3

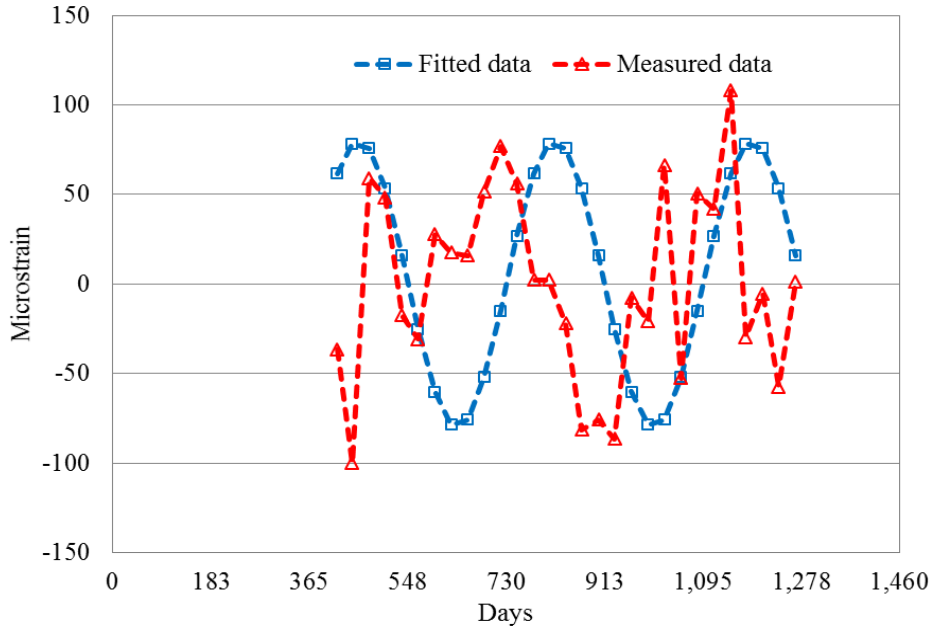

c) Sinusoidal function to fit the cyclic pattern

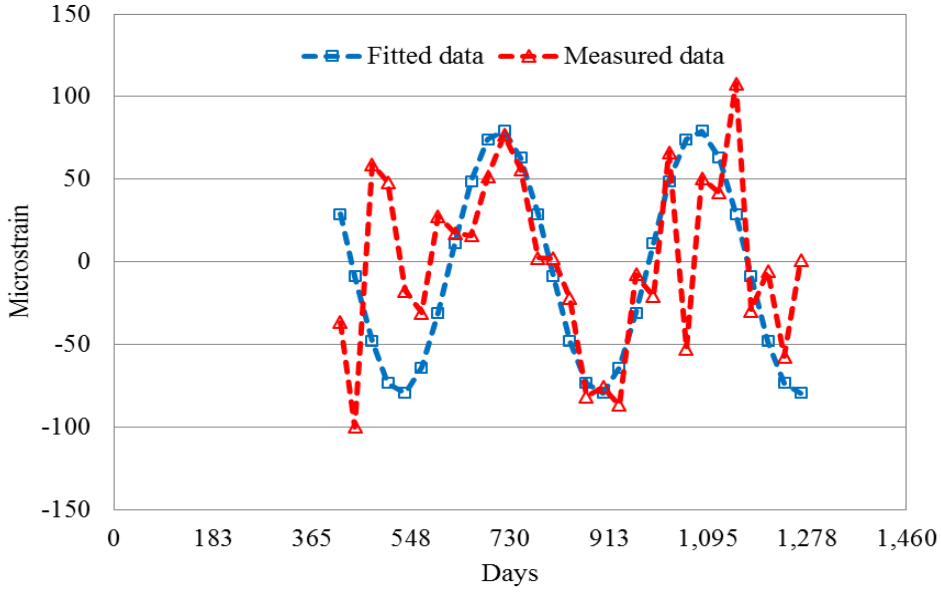

d) Adjusting the offset

Figure 5.13 Continued…

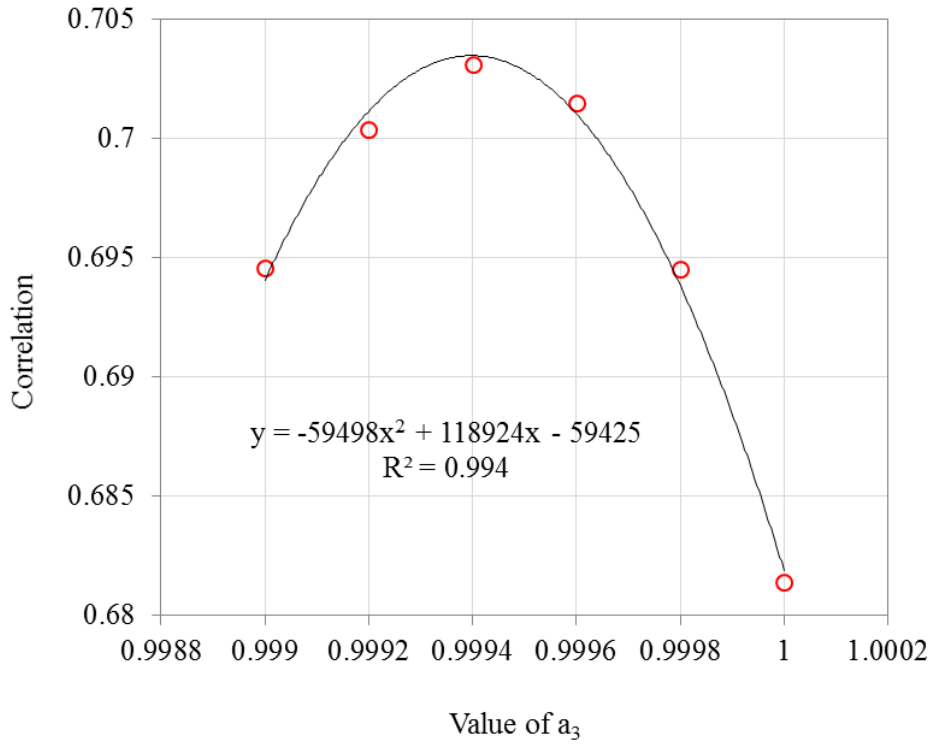

Figure 5.14 Data used to Determine the Value of a_3

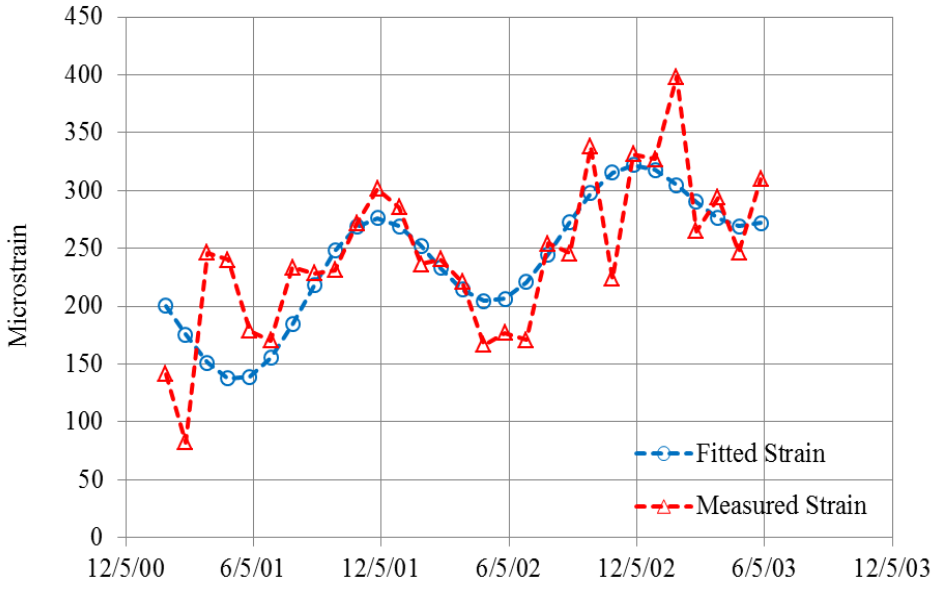

Figure 5.15 Fitted Curve of Strain Development for 180° Strain at SG-3

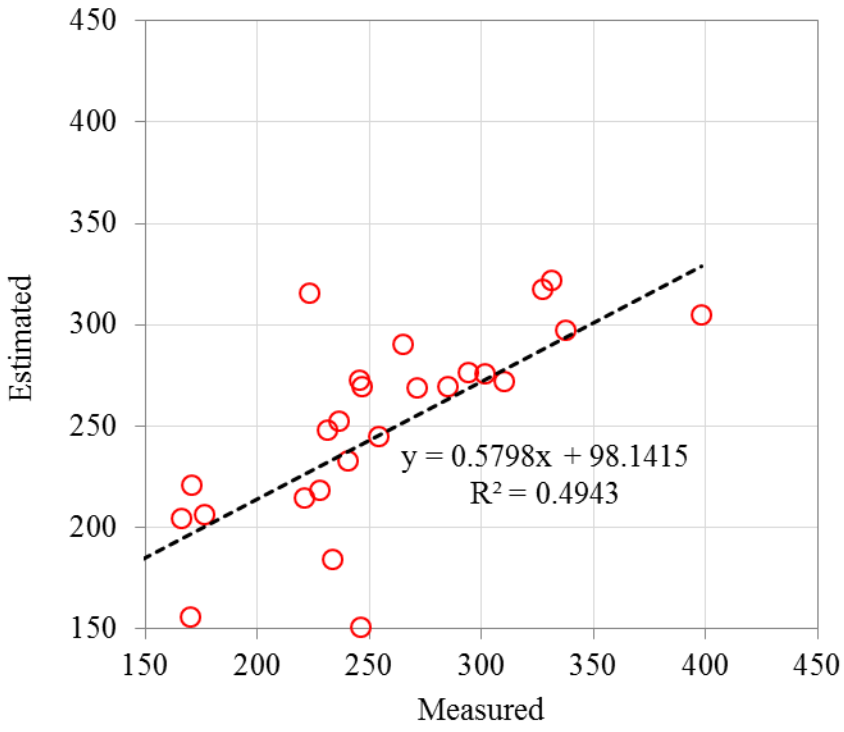

Figure 5.16 Measured vs. Fitted Strain for 180^{o} Strain at SG-3

An attempt was made to identify the correlation between longitudinal strain at 180^{o} and air temperature. As shown in Figure 5.17, there appears to be no detectable correlation between longitudinal strain at 180^{o} and air temperature, even though both longitudinal strain and temperature correlated well with time.

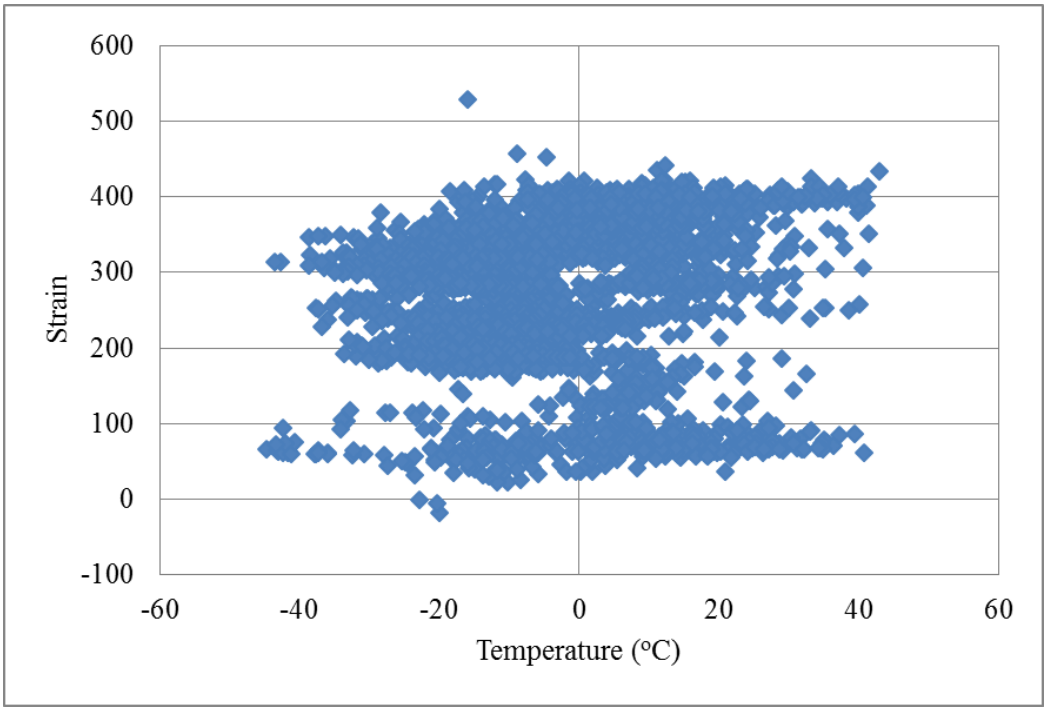

Figure 5.17 Correlation between 180° Longitudinal Strain at SG-2 and Air Temperature

CHAPTER 6. CONCLUSIONS

The objective of this research was to analyze the pipe strain characteristics due to frost heave of a full-scale buried chilled gas pipeline near Fairbanks, Alaska. The key findings of this research are summarized below.

The strain of the buried pipe appeared to be caused by a combined effect of the frost bulb surrounding the pipe and frost heave of the foundation soil. The differential heave near the permafrost-non-permafrost boundary imposed bending action on the pipe and caused relative axial movement on the pipe-soil interface. Regarding longitudinal strain and circumferential strain of the pipe, several conclusions are summarized below.

1. Strain distribution on the cross section of the pipe: The result of the monthly average strain on cross sections at SG-4 and SG-7 indicated that bending was one of the primary loading conditions on the pipeline. Generally speaking, the values of circumferential strain ranged from about 100 to 500 με before chilled air was stopped. After the chilled air was ceased in August 2003, the circumferential strain decreased quickly.

2. Strain distribution in longitudinal direction: After analyzing the monthly average longitudinal strain along the pipeline from 2000 to 2003, the longitudinal strain due to differential heave began to develop after March 2000 and became relatively constant at the end of the first year of operation. The maximum tensile and maximum compressive strains were approximately located at the edges of the transition zone. The differential heave caused relative vertical movement of the foundation near the boundary between permafrost and non-permafrost, which imposed a bending moment on the pipeline. Such bending moment was the primary loading condition for the pipeline and the dominant factor for the distribution of the longitudinal strain.

3. In order to study the relationship between pipe strain and frost heave, a statistical regression approach was used to study the correlation between measured monthly average longitudinal strain and monthly average heave. The correlations between longitudinal strain at 0^o and 180^o, and frost heave were analyzed, and two linear trends were developed as listed below:

$$S_{0^\circ} = 4162.6H - 218.62 \quad (6.1)$$

$$S_{180^\circ} = 291.28 - 2170.4H \quad (6.2)$$

where

S_{0° = longitudinal strain at 0^o ($\mu\varepsilon$)

S_{180° = longitudinal strain at 180^o ($\mu\varepsilon$) and

H = heave (m).

In future work, the two regression equations can be used to determine the strain at the top and bottom of a pipeline caused by differential frost heave, where the site conditions are similar to those of the test facility.

For the strain development over time, the longitudinal strain at the bottom of the pipeline measured at SG-3 was analyzed as an example. An equation was proposed as the predictive model of strain development over time:

$$S = 113.87 + 0.154 \times t + 80 \times 0.9994^t \times \sin(\frac{2\pi}{365}(t + 110)) \quad (6.3)$$

where

S = longitudinal strain at the bottom of the pipeline ($\mu\varepsilon$), and

t = time (days).

During analysis of this data, several limitations came to light, which inspired the recommendations for future work listed below:

1. For this experiment, the pipe strain was mainly caused by interaction between the pipe and the soil, so it is important to monitor the soil movement along the pipe. However, there were only five heave gauges installed for the experiment, which were not sufficient to compare the data obtained from strain gauges and heave gauges. In the future research, the situation can be improved with heave gauges installed at the same locations as the strain gauges.

2. As discussed in Chapter 4, bending action was one of the primary loading conditions on the pipeline. However, the magnitude and the shape of pipe cross section corresponding to bending are unknown. In future work, more analysis is needed to better understand the bending effect on a pipe near the permafrost-non-permafrost boundary.

3. After processing the measured strain gauge data in Chapter 4, noise was amplified and varied over a big range. The noise may be related to air pressure fluctuation inside the pipe and/or mechanical vibration caused by compressor. In future analysis, the fast Fourier Transform (FFT) method will be needed to filter out the noises first.

REFERENCES

Akagawa, S., Huang, S.L., Kanie, S. and Fukuda, M. (2012). "Movement due to Heave and Thaw Settlement of A Full-Scale Test Chilled Gas Pipeline Constructed in Fairbanks Alaska." *OTC Arctic Technology Conference*, Houston, TX.

Beskow, G. (1935). "Soil Freezing and Frost Heaving with Special Application to Roads and Railroads." Swedish Geological Society Series C, 375, 145.

Bray, M.T. (2003). "Field Observations of a Large Diameter Chilled Pipeline Experiment, Fairbanks, Alaska." M.S. thesis, University of Alaska Fairbanks., Fairbanks, AK.

Chong, P. (1999). *Long-Term Strain Gauge Installation on the 36 inch Diameter Pipeline at Frost-Heave Test Station in Fairbanks Alaska, AGRA Earth & Environmental Ltd.* Vancouver, Canada.

Dallimore, S.R. (1985). "Observations and Predictions of Frost Heave around a Chilled Pipeline." M.A. thesis, Carleton University., Ottawa, Canada.

Dallimore, S.R. and Williams, P.J. (1984). "Pipelines and Frost Heave." *Permafrost seminar*, Caen, France.

Darrow, M.M. (2009). "Active Layer and Frost Bulb Interaction for a full-scale, Buried Chilled Gas Pipeline." *14th Conference on Cold Regions Engineering*, ASCE, Duluth, MN.

Huang, S.L., Bray, M.T., Akagawa, S. and Fukuda, M. (2004). "Field Investigation of Soil Heave by A Large Diameter Chilled Gas Pipeline Experiment; Fairbanks, Alaska," *Journal of Cold Regions Engineering*, 18(1), 2-34.

Jorgenson, T., Yoshikawa, K., Kanevskiy, M., Shur, Y., Romanovsky, V., Marchenko, S., Grosse, G., Brown, J. and Jones, B. (2008). "Permafrost Characteristics of Alaska - A New Permafrost Map of Alaska." *Ninth International Conference on Permafrost*, Fairbanks, AK.

Kanie, S., Sato, M. and Akagawa, S. (2010). "Adfreeze Behavior between Chilled Gas Pipeline and Surrounding Frost Bulb." *Proc., Pipelines 2010*, ASCE, Keystone, CO, 1350-1359.

Klein, R.M., Lyle, W.M., Dobey, P.L. and O'Connor, K.M., (1974). "Estimated Speculative Recoverable Resources of Oil and Natural Gas in Alaska." Division of Geological & Geophysical Surveys. Department of Natural Resources. State of Alaska.

Konrad, J.M. and Morgenstern, N. R. (1984), "Frost Heave Prediction of Chilled Pipelines Buried in Unfrozen Soils." *Canadian Geotechnical Journal*, 21, 100-115.

Kim, K., Zhou, W. and Huang, S.L. (2008). "Frost Heave Predictions of Buried Chilled Gas Pipelines with the Effect of Permafrost." *Cold regions science and technology*, 53(3), 382-396.

Miki, C., Kobayashi, T., Oguchi, N., Uchida, T., Suganuma, A. and Katoh, A. (2000) "Deformation and Fracture Properties of Steel Pipe Bend with Internal Pressure Subjected to In-Plane Bending." *12th World Conference on Earthquake Engineering*, Auckland, New Zealand.

National Energy Board, (2011). "Mackenzie Gas Project - Reasons for Decision." Calgary, Canada.

Nixon, J.F. (1983). "Frost Heave-Pipeline Interaction Using Continuum Mechanics." *Canadian Geotechnical Journal*, 20(2), 251-261.

O'Neill, K. and Miller, R.D. (1982). "Exploration of a Rigid Ice Model of Frost Heave." Water Resour. Res., 82-13, 21(3), 281-296.

Razaqpur, A.G. and Wang, D. (1996). "Frost-Heave Deformations and Stresses in Pipelines." *International Journal of Pressure Vessels and Piping*, 69(2), 105-118.

Selvadurai, A.P.S. and Shinde, S.B. (1993). "Frost Heave Induced Mechanics of Buried Pipeline." ASCE, *Journal of Geotechnical Engineering*. Proc, ASCE. 119(12), 1929-1952.

Selvadurai, A.P.S., Hu, J. and Konuk, I. (1999a) "Computational Modelling of Frost Heave Induced Soil-Pipeline Interaction. I. Modelling of Frost Heave." *Cold Regions Science and Technology*, 29, 215-228.

Selvadurai, A.P.S., Hu, J. and Konuk, I. (1999b) "Computational Modelling of Frost Heave Induced Soil-Pipeline Interaction. II. Modelling of Experiments at the Caen Test Facility." *Cold Regions Science and Technology*, 29, 229-257.

Shah, K.R. (1990). "Deformations and Stresses in Pipelines Buried in Freezing Ground." M. E. Thesis, Carieton University. Ottawa, Canada.

Shah, K.R. and Razaqpur, A.G. (1993). "A Two-Dimensional Frost Heave Model for Buried Pipelines." *Int. J. For Num. Meth in Eng.*, 36(15), 2545-2567.

Taber, S., (1929). “Frost Heaving.” *Journal of Geology*, 37(1), 428-461.

Taylor, G.S. and Luthin, J.N. (1978). “A Model for Coupled Heat and Moisture Transfer during Soil Freezing.” *Canadian Geotechnical Journal*, 15, 548-555.

Tsytovich, N.A. (1975). “The Mechanics of Frozen Ground.” McGraw-Hill, New York.

White, T.L. (2006). “Pipelines in Permafrost and Freezing Ground; Engineering Resource Library and Database Indexes.” *Permafrost Environmental Consulting*, Incorporated, Ottawa, Canada.